The PHILOSOPHICAL MAGAZINE

FIRST PUBLISHED IN 1798

. 1 Eighth Series No. 4 April 1956

A Journal of Theoretical Experimental and Applied Physics

PRICE 15s. 0d.
Annual Subscription £8 0s. 0d. payable in advance

ALERE FLAMMAM.
Printed and Published by
TAYLOR & FRANCIS LTD.
RED LION COURT, FLEET STREET, LONDON, E.C.4

CONTENTS OF No. 4.

*** All communications for the Philosophical Magazine should be addressed, post-paid, to the Editors, c/o Messrs. Taylor and Francis, Ltd., Red Lion Court, Fleet Street, London, England.

XXVIII. *The Propagation of Heat in Liquid Helium at Temperatures below* 0·6°K

By D. V. Osborne†
Royal Society Mond Laboratory, University of Cambridge‡

[Received August 10, 1955 ; revised November 15, 1955]

Abstract

Experiments are described in which sine waves of heat are propagated in liquid helium at temperatures between 0·25°K and 0·6°K. Although propagation takes place in a closed tube, resonance does not occur, but, by measuring the phase and amplitude of the temperature waves, values are deduced for the velocity and attenuation of the waves at frequencies between 60 c/s and 2 kc/s. The velocity increases with frequency ; at 0·5°K it tends to a limit of about 133 m sec^{-1} at high frequencies, but at 0·25°K it reaches about 190 m sec^{-1} at 2 kc/s and is still increasing. The attenuation per wavelength decreases with increasing frequency being nearly 2π at the lowest frequencies.

At temperatures up to 0·4°K it is shown that the mean free path of the phonons must be greater than the tube diameter (2 cm) and that their reflection at the wall must be partly diffuse. The data are quantitatively explained if about one-third of the phonons suffer diffuse reflection and the remainder suffer specular reflection.

Above 0·5°K the mean free path is found to be smaller than the tube diameter, being about 0·08 cm at 0·54°K and about 0·04 cm at 0·58°K.

§ 1. Introduction

Since the original prediction of Landau (1941) that the velocity of second sound in liquid helium II would rise to $1/\sqrt{3}$ of the velocity of ordinary sound as the temperature approached absolute zero, several experimental investigations have been carried out to test his theory (Peshkov 1948 b, Maurer and Herlin 1949, Pellam and Scott 1949, Atkins and Osborne 1950, Mayper and Herlin 1953, Kramers, van den Burg and Gorter 1953, de Klerk, Hudson and Pellam 1953, 1954, Kramers, van Peski-Tinbergen, Wiebes, van den Burg and Gorter 1954). In all this work (except that of Peshkov whose measurements extended down only to 1·03°K) the pulse method has been used and two main results have emerged : that at temperatures below 0·6°K the received

† Now at the Department of Natural Philosophy, St. Salvator's College, University of St. Andrews.

‡ Communicated by Professor N. F. Mott.

pulse is greatly rounded and lengthened compared with the input pulse, and that the time of arrival of the beginning of the received pulse corresponds to a velocity of propagation of 130 to 200 m sec^{-1}. Since the probable velocity of ordinary sound at absolute zero is 239 m sec^{-1} (Chase 1953, Chase and Herlin 1955), while the velocity of second sound at 1°K is only about 20 m sec^{-1}, Landau's prediction is qualitatively verified and with it the hypothesis that phonons are the dominant excitations in liquid helium at temperatures below 0·6°K. It remains to explain the elongation of the received pulse and to explain why the velocity of propagation tends to exceed the Landau value of 138 m sec^{-1} at the lowest temperatures. Discussions of these phenomena in terms of the behaviour of the liquid have been given by Dingle (1952), Osborne (1952), Gorter (1952), Atkins (1953), Mayper and Herlin (1953), and Kramers *et al.* (1954), the last of these papers containing also some discussion of the behaviour of the heater and thermometer.

In the present experiment sine waves are used so that the pulse distortion previously observed appears as measurable dispersion and attenuation. Moreover the method is such that the velocity and attenuation measurements do not involve any assumption concerning the behaviour of the heater and thermometer at high frequencies.

The sine waves are emitted by a plane heater at one end of a closed cylindrical tube and detected by a plane thermometer at the other end. This technique was first used by Peshkov (1948 a), who observed resonance in the tube and so deduced the velocity of the waves at temperatures above 1°K. It is now found that no resonance can be observed at temperatures below 0·7°K, but that it is still possible to estimate the velocity and attenuation of the waves by measuring the phase and amplitude of the sine waves received at the thermometer. The use of sine waves means that a detector of very narrow bandwidth and correspondingly low noise level can be used, and this facilitates the measurement of the very small signals obtained in the absence of resonance.

Since the thermometer has an unknown frequency response and phase lag, experiments are carried out with several different lengths of tube using the same heater and thermometer each time. A final run, using the first tube length again, is necessary to verify that the thermometer behaviour does not change with time. The velocity and attenuation at any given frequency are then obtained by comparing observations made at that frequency during each of the five runs. The experiments are described in §§ 2 to 5 and their interpretation in §§ 6 to 9.

§ 2. The Cryostat

The problem of cooling liquid helium by adiabatic demagnetization is complicated by the two opposing requirements that it must be easy to dispose of the heat of magnetization, but that the heat leak to the helium, once cold, must be as small as possible. The device used for solving this problem in the present cryostat is due to Dr. J. Ashmead

and one use of it has already been reported by Herlin and Chase (1955); it is illustrated in fig. 1. The experimental chamber A is surrounded by a vacuum space and is connected to the helium bath B by a conical German silver tube C of length 6 cm, wall thickness 0·3 mm, diameter at the larger end 1·6 cm and diameter at the smaller end 1·0 cm. Into this tube fits a plug D consisting of a similar cone closed at both ends

Fig. 1

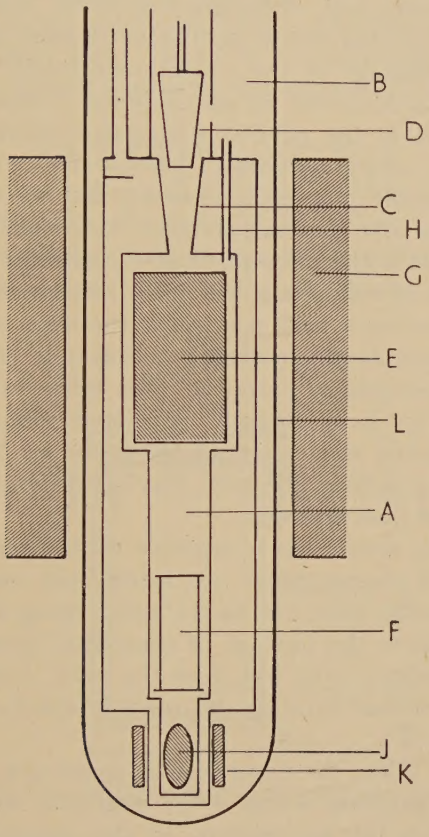

The cryostat. L, helium dewar and liquid air shield; for remaining key see § 2.

and evacuated. The plug may be raised or lowered by a control rod projecting out of the top of the cryostat. The experimental chamber contains the paramagnetic salt E, which acts as the refrigerant, and the experimental apparatus F, both immersed in liquid helium. Initially the plug is raised so that there is direct communication between the experimental chamber and the main helium bath at 1·2°K and with the apparatus in this condition a magnetic field is applied to the salt by means of the magnet G, an armoured water-cooled solenoid with its axis vertical. The heat of magnetization is led away at once by the

helium in the conical tube to the helium bath and, on account of the excellent thermal conductivity of liquid helium at 1·2°K, temperature equilibrium is reached in a few seconds. The plug is now lowered so as to fit tightly in the conical tube, and the magnetic field is reduced to zero. The experimental chamber cools, in the present instance to 0·2°K, and may take between 20 and 40 minutes to return as far as 0·7°K, the warming rate depending partly upon the amount of power supplied during the actual measurements. The conical plug and tube have well-machined surfaces and, although it is easily possible for superflow to take place past the plug, the fit is sufficiently good to offer considerable resistance to the passage of the normal component of liquid helium, the flow of which is hindered by an ordinary viscosity of the order of 20μpoise. Since it is the normal component which carries heat, the heat leak is by this means reduced to quite a small value.

The use of a movable plunger in this way has the advantage over the more usual capillary tube that large heats of magnetization can be quickly conducted away. It is therefore particularly suitable for experiments in which a large mass of refrigerant salt has to be used, a condition which obtains in this experiment both because of the large volume of helium to be cooled and because of the occasional necessity of using relatively large heat inputs for experimental purposes. The refrigerant E in the present work consists of 200 g of coarsely powdered manganous ammonium sulphate placed above the experimental space so that it may absorb the residual heat input from the cone, leaving the region below relatively free from unwanted heat currents.

The experimental space has a capacity of 150 cm^3. Electrical leads for the heater and thermometer are introduced via two 1 mm tubes packed with petroleum jelly, one of the tubes being shown at H. These almost certainly allow the passage of superfluid from the experimental chamber to the helium bath but, like the cone, they do not permit a sufficient flow of normal fluid in the reverse direction to constitute an appreciable heat leak.

In an appendix below the experimental space is a small ellipsoid J of copper potassium sulphate which is the core of a mutual inductance K and thereby enables the temperature in the chamber to be measured. This ellipsoid is never magnetized and is cooled solely by thermal contact with the helium surrounding it, so that it cannot attain a temperature lower than that of the helium. In fact it always responds within two or three seconds to any change of temperature produced by changing the power dissipated in the second sound apparatus. Since the rate of warming is not more than 0·01 deg. min^{-1}, this means that the thermometer gives a faithful indication of the helium temperature. The salt J is that originally used by Garrett (1950), and the absolute temperature is deduced as indicated in his paper, due allowance being made for the magnetic behaviour of the German silver tubes. The necessary correction was estimated in some auxiliary experiments.

About 6 litres of liquid helium are required to cool the cryostat from liquid air temperatures down to 4·2°K and to fill it. The length of run is then about five hours of which one hour is taken up in calibrating the measuring salt J at liquid helium temperatures. During the remaining time, four or five demagnetizations are carried out, the actual process of demagnetization taking about five minutes and the warming time between 0·2°K and 0·7°K being about forty minutes. In a trial run it was established that the natural heat leak was of the order of 600 erg sec^{-1} and that the rate of rise of temperature varied from about 2 m deg. min^{-1} at 0·25°K to about 7 m deg. min^{-1} at 0·5°K. The thermal capacity which may be deduced from these values is in reasonable accord with that estimated from the known masses of salt and helium.

§ 3. The Propagation Tube

That part of the second sound apparatus which is in the cryostat is shown in fig. 2. The tube A defining the separation between the heater and thermometer is of silica and has an inside diameter of 2·02 cm and a wall thickness of 2 mm. The heater B consists of some 70 cm of

Fig. 2

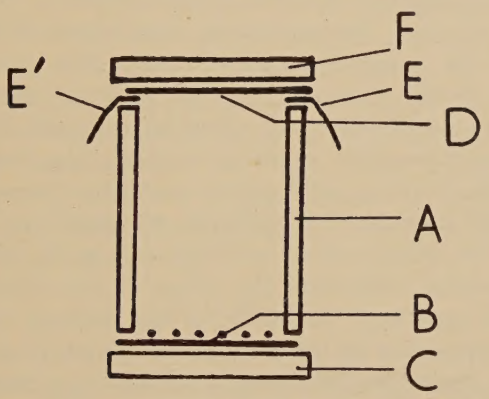

The propagation tube. For key see § 3.

46 s.w.g. Eureka wire wound zig-zag on a thin paxolin former and backed by a glass disc C 3 mm thick. The thermometer D is a thin strip of mica, 2 cm × 2 mm × 20 μ painted over with Aquadag and silvered at the two ends for better electrical contact. It is laid across a diameter of the tube with its coated side facing the heater, and the silvered ends press against copper contacts EE′ stuck to the silica with Sellotape. It is backed by a second glass disc F. The whole was held together with Sellotape during assembly and was finally clamped together by a light copper frame. There are sufficient slight gaps at the ends to admit helium freely and to maintain temperature equilibrium with the rest of the inner chamber. Current and potential leads for the

heater and thermometer are led up the two tubes H (fig. 1) to the helium bath, the heater leads being kept separate from the thermometer leads to reduce the coupling between them when using sine waves.

When the heater is switched on to generate second sound, the temperature in the tube rises with a time constant of about two seconds to a value slightly higher than the temperature measured by the salt. The effect is negligible except at the lowest temperatures when using the highest powers. In these circumstances an appropriate correction has been applied to give the temperature inside the chamber from the measured temperature of the salt J. The final accuracy of the temperature assigned to any given phase and amplitude measurement is $\pm 10^{-2}$ deg.

§ 4. The Electrical Equipment

Outside the cryostat are the oscillator which supplies sine waves to the heater, and the amplifier and cathode-ray tube which amplify and display the signals from the thermometer. The amplifier incorporates a phase sensitive detector which makes the bandwidth of the system about 0·2 c/s and the resulting noise level is sufficiently low for input signals of the order of 0·1 μv to be detected. The cathode-ray tube is so connected that the polar coordinates (v, ϵ) of its spot give a direct measure of the amplitude and phase angle of the amplifier output.

In order to calculate the amplitude and phase of the thermometer waveform from the observed values of v and ϵ, the gain and phase shift of the amplifier system have been measured at all relevant frequencies. The temperature amplitude may then be calculated by dividing the amplitude of the fluctuation of thermometer resistance by the slope of the resistance–temperature calibration curve but, except at the lowest frequencies, this procedure is unlikely to give the correct absolute values because the steady state calibration is unlikely to be applicable at audio frequencies. Similarly the phase of the observed fluctuations of thermometer resistance is likely to lag behind the phase of the temperature fluctuations in the helium except at very low frequencies. Since, however, the same thermometer was always used, it is legitimate to compare the effective amplitudes and phases obtained in this way at one given frequency and temperature for different lengths of propagation tube.

The accuracy of phase measurement is better than ± 2 degrees for sufficiently large signals but for very small signals (particularly at high frequencies, at higher temperatures and with long tubes) the accuracy falls in some cases to ± 5 degrees. Fortunately it is in these circumstances that the phase shift is large and the accuracy less important.

§ 5. Experimental Results

The whole experiment consisted in carrying out four successful runs, each with a different tube length but with the same heater and thermometer, and then repeating the first run to check the stability of the thermometer. The tube lengths used were 0·38 cm, 3·16 cm, 9·26 cm

and 12·35 cm. In order that the readings of different runs might be compared, observations in each run were made at fifteen fixed frequencies (f) between 60 c/s and 2 kc/s. For each frequency the polar coordinates (v, ϵ) of the cathode-ray tube spot were plotted against temperature and the readings corresponding to six fixed temperatures between 0·25°K and 0·58°K were read from each curve. Readings at a given frequency and temperature could then be compared for different runs, i.e. for different tube lengths. A representative selection of the readings is shown in figs. 3 and 4.

In fig. 3, where phase, ϕ, is given as a function of tube length, L, for the various frequencies, ϕ has been obtained by subtracting the known phase shift of the amplifier from the observed phase, ϵ. There remains the unknown phase lag of the thermometer, a correction for which would decrease the values of ϕ particularly at the higher frequencies (see § 8). Points in fig. 3 corresponding to a given frequency have been joined by straight lines merely to facilitate identification.

The observed amplitude, v, is proportional to θ, the temperature amplitude of the received signal and θ is calculated from v using the known gain of the amplifier and the known sensitivity of the thermometer. That this sensitivity is strictly applicable only to steady temperatures means that the values of θ so calculated will in general be smaller than the true temperature amplitude in the helium, especially at the higher frequencies (see § 8). The values of θ are divided by the amplitude, W, of the power flow per unit area and it is found that for the given values of frequency and tube length, all the values of θ/W fall on a smooth curve if plotted against temperature, i.e. that under fixed conditions of temperature, frequency and tube length, θ must be proportional to W. In presenting the amplitude data, therefore, it has been found convenient to give the quantity A, defined by

$$A=\theta/W\gamma_0.$$

γ_0 is here the characteristic impedance of liquid helium for second sound waves (Osborne 1948) and it serves both to relate the values of A obtained at different temperatures and also to render A dimensionless. γ_0 is equal to $(\rho c_2 C)^{-1}$ where ρC is the specific heat per unit volume and c_2 is the velocity of second sound. Since the latter quantity is under discussion, the value of γ_0 actually used has been that based strictly on Landau's theory, using the single experimental datum that the extrapolated velocity c of ordinary sound in helium at the absolute zero is 239 m sec^{-1} (Chase 1953). From Landau's theory

$$c_2=c/\sqrt{3}$$

and

$$\rho C=\frac{16\pi^5 \boldsymbol{k}^4 T^3}{15\boldsymbol{h}^3 c^3}$$

at sufficiently low temperatures, whence we find

$$\gamma_0=2{\cdot}42\times 10^{-2}T^{-3} \text{ deg. } W^{-1} \text{ cm}^2.$$

Fig. 3

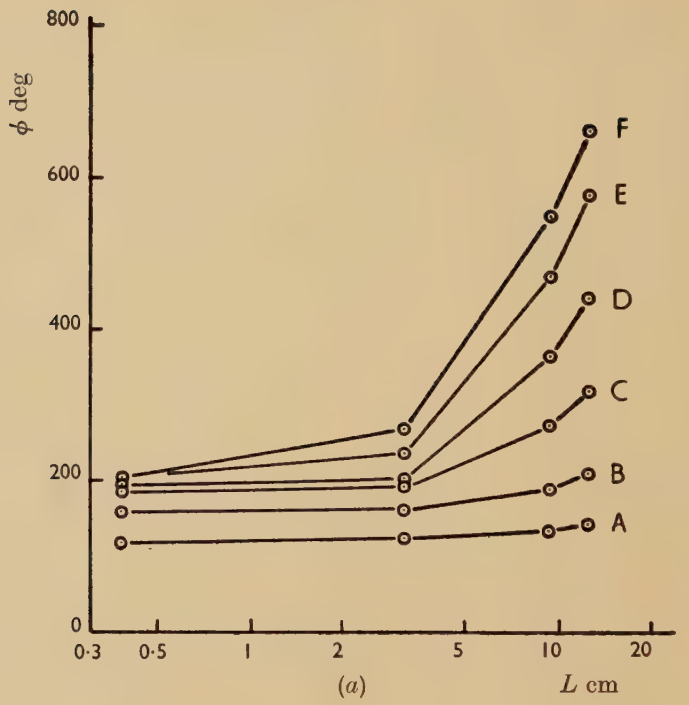

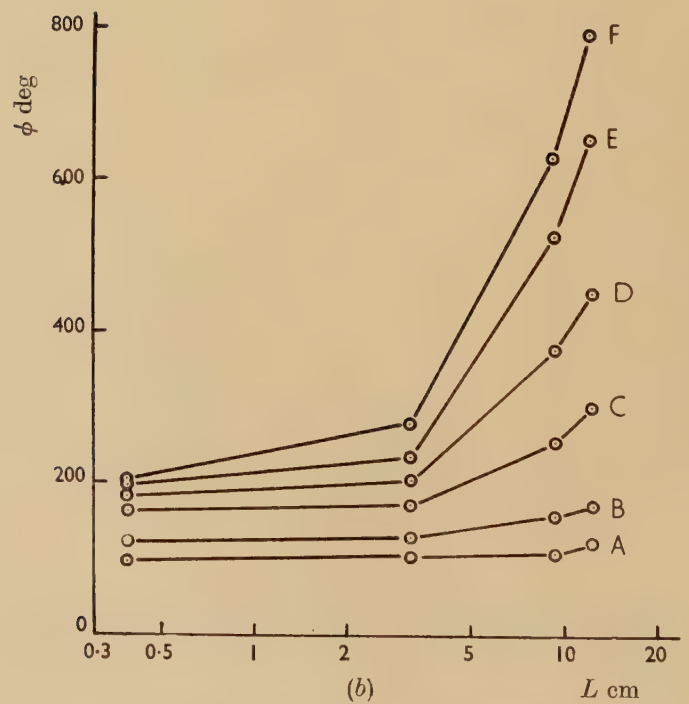

Phase lag as a function of tube length.

A, 80 c/s ; B, 237 c/s ; C, 576 c/s ; D, 1000 c/s ; E, 1595 c/s ; F, 1995 c/s.

(*a*) $T=0{\cdot}3^{\circ}\text{K}$; (*b*) $T=0{\cdot}5^{\circ}\text{K}$.

Fig. 4

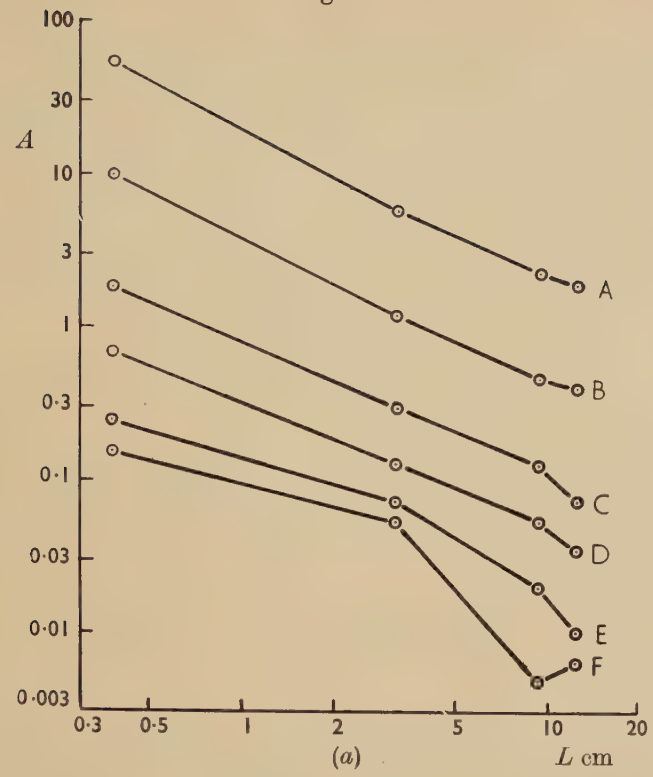

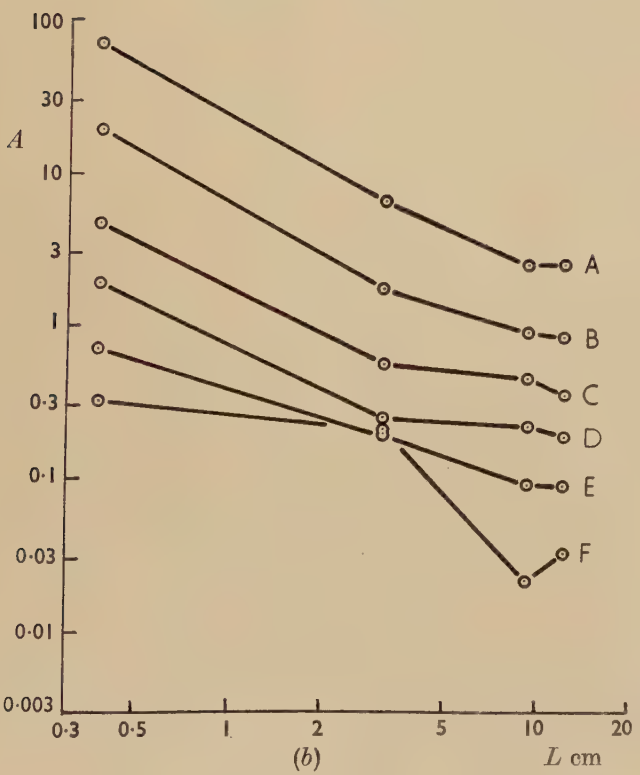

Normalized amplitude as a function of tube length.
80 c/s ; B, 237 c/s ; C, 576 c/s ; D, 1000 c/s ; E, 1595 c/s ; F, 1995 c/s.
(*a*) $T=0{\cdot}3^{\circ}\text{K}$; (*b*) $T=0{\cdot}5^{\circ}\text{K}$.

The experimental value of C (Kramers *et al.* 1952) is about 10% higher than the Landau value, and the experimental values of c_2 so far published range from about $c/\sqrt{3}$ to c.

The first and fifth runs, both with $L=0{\cdot}38$ cm, give phases which agree to within ± 3 degrees. The amplitudes obtained in the fifth run are systematically about 15% less than those of the first run but in view of the very wide range of amplitudes used this error is not regarded as very serious. The phase shown in fig. 3 for this tube is the mean of the two runs ; the amplitude shown in fig. 4 is that obtained during the first run.

Table 1. Typical Signal Sizes

Length L cm	Frequency f c/s	Temperature T°K	Power $W\,\mu W$ cm^{-2}	Signal amplitude θ μdeg.
0·38	60	0·25	1·0	110
0·38	60	0·5	2·9	53
0·38	2000	0·25	22	3·7
0·38	2000	0·5	22	1·4
12·35	60	0·25	5·3	19
12·35	2000	0·5	49	0·27

Table 1 gives some idea of the orders of magnitude used. For a given power the received signal decreased with increasing length, with increasing frequency and with increasing temperature. The signal amplitudes quoted are those recorded by the thermometer. At 60 c/s these will be about the same as the amplitudes in the helium but at 2000 c/s the amplitude in the helium may be several times larger than that recorded by the thermometer (see § 8).

At temperatures between 0·2°K, the lowest reached, and 0·3°K the measured phases depend a little on the power used. At the lower frequencies an increase of power by a factor of ten can produce a phase advance up to 15 degrees. The phenomenon suggests that second order effects of two kinds may become important ; the amplitude of the normal fluid velocity may become comparable with the wave velocity (Osborne 1951, Temperley 1951, Khalatnikov 1952), and the average normal fluid velocity due to the mean flow of heat along the tube may become comparable with the wave velocity. It may be shown, however, that both of these effects might be expected to change the velocity of second sound by a fraction of the order of magnitude of $3\theta/T$, and reference to table 1 shows that this fraction is in all circumstances very small compared with unity. The observations, therefore, remain at present unexplained.

§ 6. The Continuum Theory

If the phonons have very short mean free paths, the fluid may be treated as a continuum, and the observed amplitudes and phases will be explicable in terms of the propagation of waves having a definite velocity c',

attenuation α, and characteristic impedance γ. The observations will be treated on the basis of this assumption and it will be shown that the result is satisfactory only at temperatures above 0·5°K. It will therefore be inferred that below 0·5°K the mean free paths are no longer short, and an alternative interpretation of the low temperature data will be given in § 7.

If the characteristic impedance γ of the helium for a travelling wave propagated in the tube is defined by

$$\gamma = \frac{\text{temperature amplitude}}{\text{heat flow amplitude per unit area}}$$

and if the thermal penetration impedance ζ of the two end walls is given by

$$\zeta\gamma = \frac{\text{temperature amplitude at end wall}}{\text{heat flow amplitude into end wall per unit area}},$$

then the usual methods of transmission line theory may be used to show that the temperature amplitude θ at the thermometer will be given by

$$\frac{\theta}{\gamma W} = \frac{\zeta}{\cosh \beta L + (\zeta + 1/\zeta)\sinh \beta L}, \qquad \ldots \quad (1)$$

where W=heat flow amplitude per unit area given out by heater, L=length of tube, $\beta=\alpha+ik$, α=attenuation constant per unit length, $k=2\pi/\lambda$ and λ=wavelength. γ and ζ will in general be complex.

If the reflection coefficient is very nearly unity ($|\zeta| \gg 1$) we shall expect θ to be inversely proportional to L, at least for the two shorter tubes, and this is in fact observed at the lower frequencies, as may be verified by reference to fig. 4.

The very high value of $|\zeta|$ arises partly because the end plates are of thermally insulating material, and partly because of the Kapitza (1941) boundary resistance which impedes the flow of heat from the helium into the solid.

At the higher frequencies, where even the 3·16 cm tube becomes a considerable fraction of a wavelength, L will no longer be sufficiently small for this approximation to hold, and it is indeed observed (e.g. fig. 4(*b*), curve F) that the inverse proportionality breaks down. At these frequencies no simple argument is possible to show that $|\zeta| \gg 1$, but the assumption that this is so is justified on the one hand by the fact that ζ would not be expected to vary very rapidly with frequency and on the other hand by the fact that the interpretation of the high frequency results is relatively insensitive to the value of ζ.

Upon making the assumption $|\zeta| \gg 1$, we find from eqn. (1) a theoretical amplitude A' and phase lag ϕ' given by

$$A' = \left|\frac{\theta}{\gamma W}\right| = \left\{\sin^2\psi + \sinh^2\left(\frac{\alpha}{k}\psi\right)\right\}^{-1/2} \qquad \ldots \quad (2)$$

and

$$\tan\phi' = \tan\psi \coth\left(\frac{\alpha}{k}\psi\right), \qquad \ldots \quad (3)$$

where

$$\psi = kL = 2\pi f L/c',$$

$\phi'(\psi)$ and $A'(\psi)$ for a few representative values of α/k are shown in figs. 5 and 6 respectively. For convenience in the use of tables, α/k has been expressed in radian deg.$^{-1}$.

Fig. 5

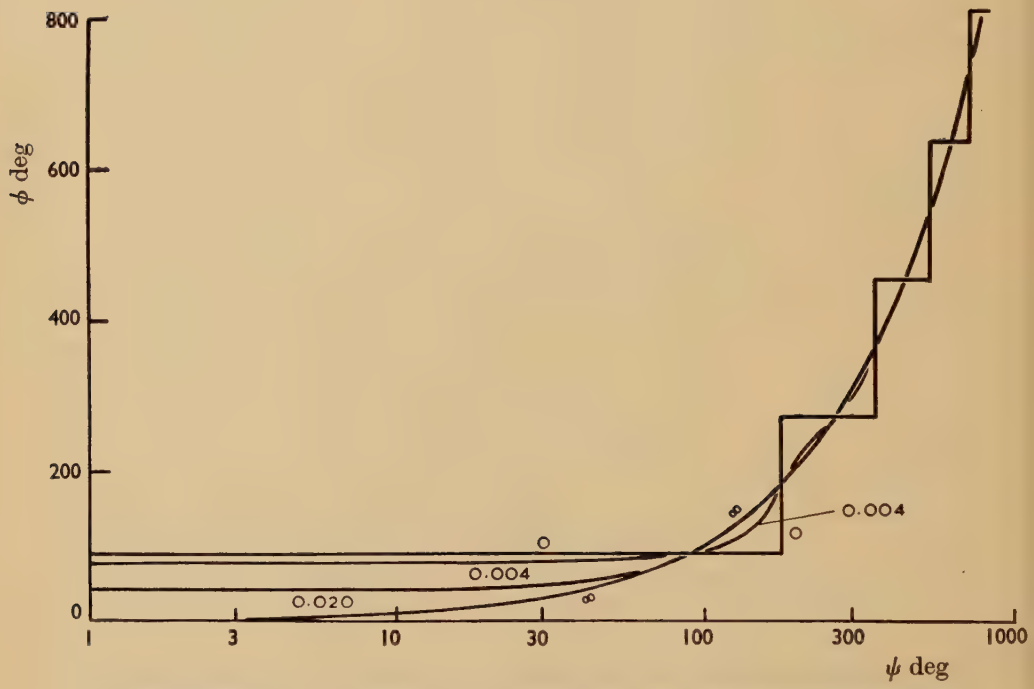

Theoretical phase lag. Values of α/k in radian deg.$^{-1}$ are indicated for each curve.

The experimental points $\phi(L)$ and $A(L)$ (figs. 3 and 4) are fitted to these curves by plotting $\phi(L)$, $A(L)$, $\phi'(\psi)$ and $A'(\psi)$ on transparent logarithmic graph paper and superposing each set of experimental points in turn on the appropriate theoretical curve. α/k is determined by selecting that theoretical curve which fits the experimental points best, and the relative position of the abscissae ψ and L is adjusted for the best fit. This adjustment determines the constant of proportionality relating ψ to L and hence gives the velocity c'. In order to allow for the unknown phase lag and efficiency of the thermometer, the relative position of the ordinates is also adjusted for the best fit. At any given temperature and frequency the same pair of values of α/k and c' must, of course, be used to fit both the phase and the amplitude data. It proves possible to carry out this fitting process within the limits of experimental error for all frequencies and for all temperatures, except for one or two individual points which seem rather far out,

The results are given in figs. 7 and 8 where the wave velocity c' and the attenuation per wavelength $\alpha\lambda$ ($=360\alpha/k$ if α/k is in radian deg.$^{-1}$) are given as functions of frequency at various temperatures. The accuracy of the velocity determinations improves with increasing frequency, the values being accurate to within about $\pm 20\%$ at 60 c/s, $\pm 5\%$ at 480 c/s and $\pm 3\%$ at 2 kc/s. The attenuations are probably accurate to within

Fig. 6

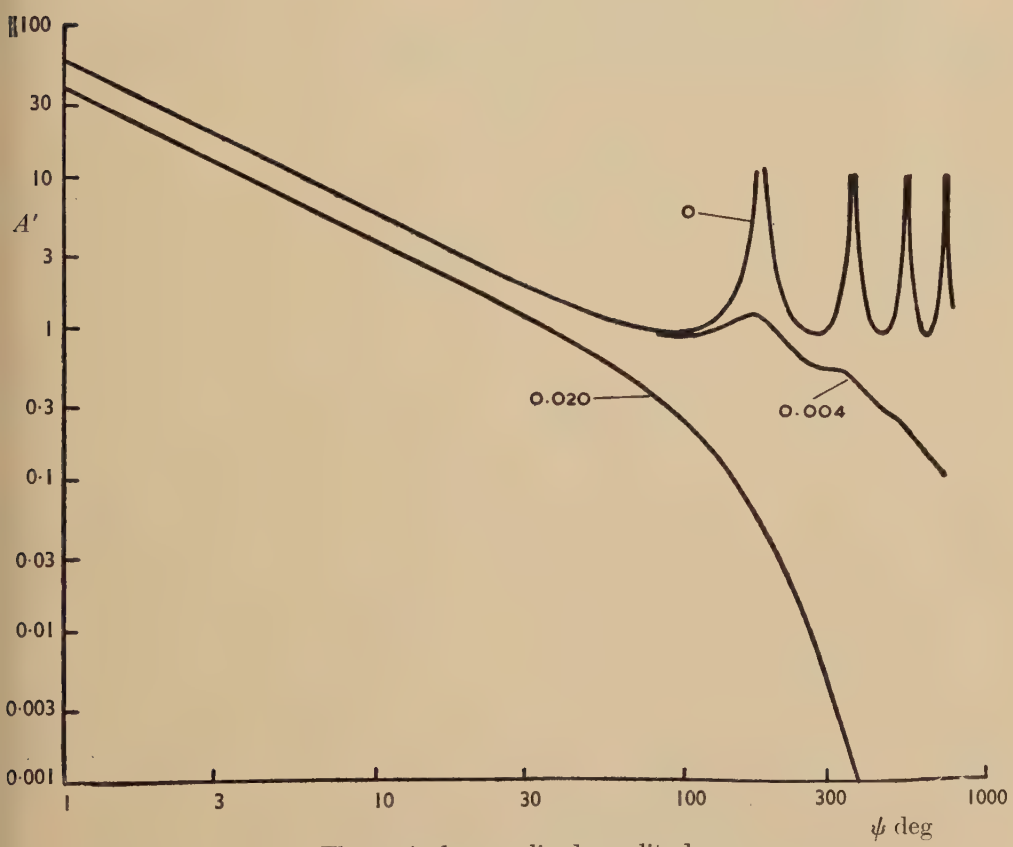

Theoretical normalized amplitude.

Values of α/k in radian deg.$^{-1}$ are indicated for each curve.

$\pm 20\%$ at all frequencies. The chief source of error at low frequencies is the possibility of fitting the data over rather a large range of values of α/k and the chief source of error at high frequencies is the smallness of the signals.

We now interpret these velocities and attenuations by treating the normal component of liquid helium II as a continuous medium with a definite shear viscosity, second viscosity, and thermal conductivity.

We have then the following equations of motion for the normal component and for the superfluid:

$$\frac{\partial \mathbf{v}_n}{\partial t}+\frac{1}{\rho}\nabla p+\frac{\rho_s}{\rho_n}S\nabla T-\frac{\mu}{\rho_n}(\nabla^2\mathbf{v}_n+\tfrac{1}{3}\nabla(\nabla\,.\,\mathbf{v}_n))-\frac{\mu_2}{\rho_n}\nabla(\nabla\,.\,\mathbf{v}_n)=0 \quad . \quad (4)$$

and

$$\frac{\partial \mathbf{v}_s}{\partial t}+\frac{1}{\rho}\nabla p-S\nabla T=0, \quad . \quad . \quad . \quad . \quad . \quad . \quad . \quad (5)$$

where $\mathbf{v}_n$ and $\mathbf{v}_s$ are the velocities of the two components, ρ_n and ρ_s are their densities, μ is the viscosity of the normal component as measured,

Fig. 7

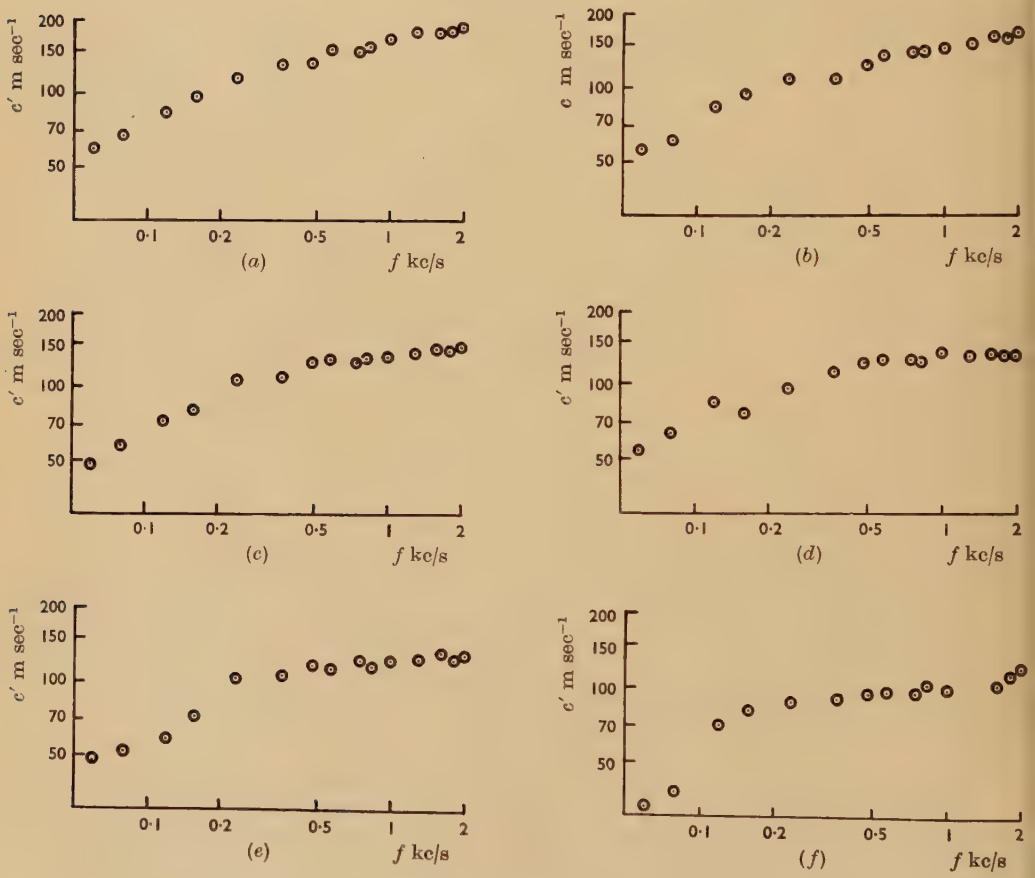

Wave velocity c' as a function of frequency.

(*a*) $T=0{\cdot}25°\text{K}$, (*b*) $T=0{\cdot}3°\text{K}$, (*c*) $T=0{\cdot}4°\text{K}$,

(*d*) $T=0{\cdot}5°\text{K}$, (*e*) $T=0{\cdot}54°\text{K}$, (*f*) $T=0{\cdot}58°\text{K}$,

Fig. 8

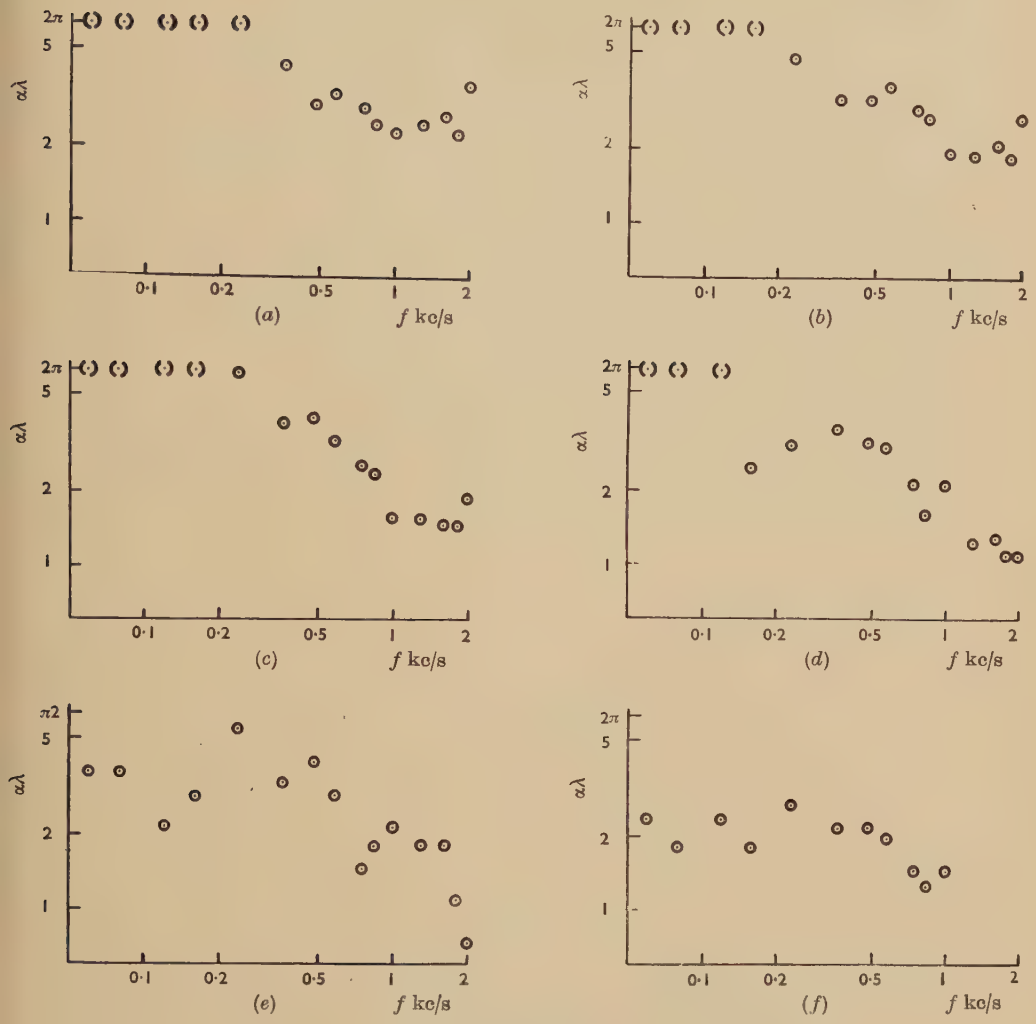

Attenuation per wavelength as a function of frequency.

⊙ experimental points ; ( ) $\alpha\lambda$ uncertain, 2π a possible value.

(*a*) T=0·25°K, (*b*) T=0·3°K, (*c*) T=0·4°K,

(*d*) T=0·5°K, (*e*) T=0·54°K, (*f*) T=0·58°K.

for example, in a rotating cylinder viscometer, μ_2 is the second viscosity of the normal component and S is the entropy per unit mass of helium. The equations are valid only for $\mathbf{v}_n$ and $\mathbf{v}_s$ small compared with the velocity of sound, and for small excursions of p, ρ and T from their mean values.

The equations of continuity of matter and continuity of entropy are

$$\frac{\partial \rho}{\partial t}+\nabla \cdot (\rho_n \mathbf{v}_n+\rho_s \mathbf{v}_s)=0 \quad . \quad . \quad . \quad . \quad . \quad . \quad (6)$$

and

$$\frac{\partial(\rho S)}{\partial t}+\rho S \nabla \cdot \mathbf{v}_n-\frac{K}{T}\nabla^2 T=0 \quad . \quad . \quad . \quad . \quad . \quad . \quad (7)$$

to the same approximation, where K is the thermal conductivity of the normal fluid. We shall assume that the thermal expansion coefficient (Atkins and Edwards 1954, 1955) is very small so that ρ may be taken as a function of p only, and S as a function of T only. For second sound above 1°K where dissipative processes are usually unimportant, the net flow of matter is zero, i.e. $\rho_n \mathbf{v}_n+\rho_s \mathbf{v}_s=0$. This is not necessarily true when dissipative forces are acting, but we shall assume that $\rho_n v_n$ and $\rho_s v_s$ are of the same order of magnitude and accordingly, since $\rho_s \gg \rho_n$ we have $v_s \ll v_n$. This is equivalent to considering the behaviour of a phonon gas in a fixed medium (see Ward and Wilks 1952). Equations (4) and (7) may then be treated by the method of Kirchhoff (1868) (see also Rayleigh 1896, Weston 1953). (For an alternative treatment following Helmholtz 1863, see Dingle 1950.)

Table 2. The Continuum Theory

	$x \ll$ 'Narrow tube'	$x \gg$ 'Wide tube'
$\frac{c'}{c_2}$	$\frac{\sqrt{x}}{2}\left(1-\frac{x}{12}+\frac{7x^2}{2304}\right)$	$\left(1-\frac{1}{\sqrt{(2x)}}+\frac{1}{(2x)}-\frac{19}{4(2x)^{3/2}}\right)$
$\alpha\lambda$	$2\pi\left(1-\frac{x}{6}+\frac{x^2}{72}\right)$	$\frac{2\pi}{\sqrt{(2x)}}\left(1+\frac{1}{\sqrt{(2x)}}+\frac{11}{4(2x)}\right)$
$\frac{\bar{\gamma}}{\gamma_0}$	$\frac{1-i}{\sqrt{x}}$	$1+\frac{1-i}{\sqrt{(2x)}}\left(1+\frac{\mu' x^2}{12 c_2 a}\right)$

Two approximate solutions emerge, depending upon the ratio of δ to a, where δ is the penetration depth of viscous waves given by $\delta^2=\mu/\pi\rho_n f$ and a is the radius of the tube. If $\delta/a \ll 1$ only a thin layer of the medium near the wall is affected by viscosity, and the attenuation and change of velocity are small; but if $\delta/a \gg 1$ the flow reduces to an alternating Poiseuille flow, and the propagation characteristics are profoundly modified. The condition for the validity of the calculations is that the mean free path l shall be short compared with each of the four lengths δ, a, λ and L, the last two being the wavelength and the length of the tube respectively. It is assumed, in accordance with the usual results of kinetic theory, that the thermal diffusivity ($K/\rho C$), kinematic viscosity (μ/ρ_n) and kinematic second viscosity (μ_2/ρ_n) are all of the order of magnitude cl where c is the velocity of phonons. With these approximations and assumptions, thermal conduction and second viscosity disappear from the final expressions,

The results for velocity and attenuation, given in table 2, are expressed in terms of the dimensionless parameter $x=2\pi fa^2/\mu'$, where μ' is the kinematic viscosity, μ/ρ_n. $x \gg 1$ corresponds to $\delta \ll a$ and $x \ll 1$ corresponds to $\delta \gg a$. The velocity c' is given in terms of the velocity c_2 of second sound in the free liquid in the absence of dissipative effects. $\bar{\gamma}$ is the effective value of thermal impedance defined by $\bar{\gamma}=\bar{\theta}/\overline{W}$. $\overline{W}$ is the heat flow amplitude averaged across the whole area of the tube on the assumption that the heater is a uniform plane source. $\bar{\theta}$ is the temperature amplitude and this is averaged along a diameter of the tube to correspond with the fact that the thermometer is a thin strip across one end. γ_0 is defined as $(\rho C c_2)^{-1}$ where ρC is the specific heat per unit volume, and is therefore the thermal impedance of the free liquid in the absence of dissipation. The expressions for c'/c_2 and for $\alpha\lambda$ contain higher order terms in x and these have been obtained by following Weston's (1953) extension of Kirchhoff's treatment for ordinary sound.

Fig. 9

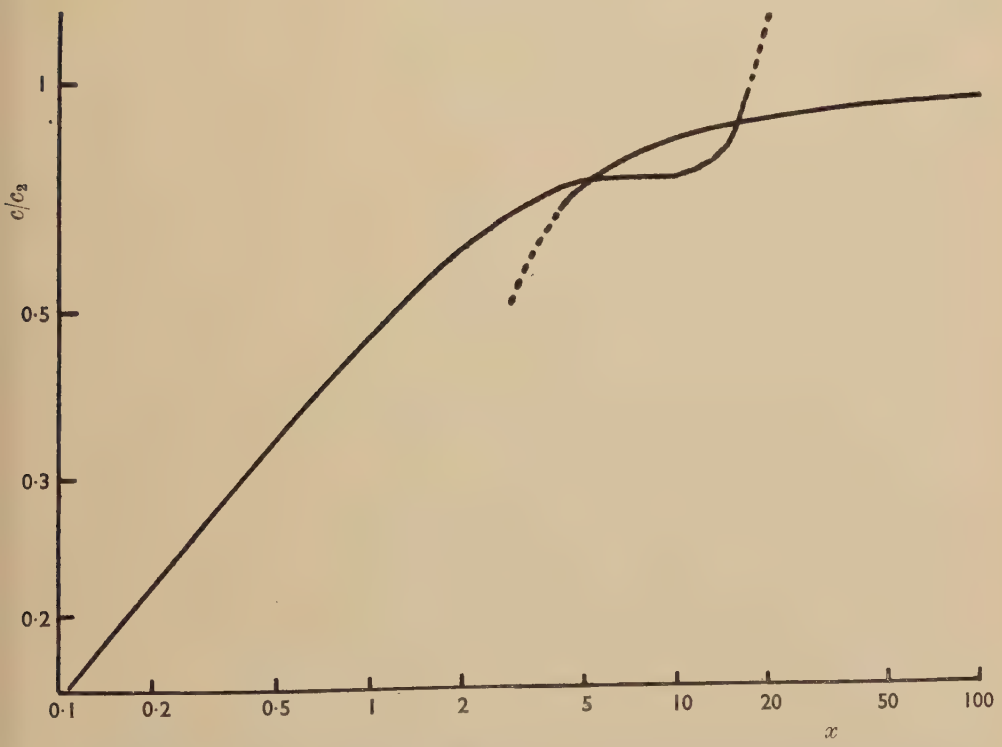

Theoretical curves of velocity against x. The two parts of this curve represent the approximate formulae of table 2 for small x and for large x.

Logarithmic graphs of the functions c'/c_2 and $\alpha\lambda$ are given in figs. 9 and 10. Since x is proportional to frequency these curves may be compared

with the logarithmic curves of c' and $\alpha\lambda$ against f (figs. 7 and 8) it and will be seen that they are of the same general form. In order to make a detailed comparison the method of superposing logarithmic graphs is again used, the values of $\alpha\lambda$ as a function of frequency (fig. 8) being first superposed on the theoretical curve of $\alpha\lambda$ versus x (fig. 10). The theoretical and experimental values of the ordinate $\alpha\lambda$ have to agree without any adjustable constant of proportionality, and the theory must therefore be made to fit by adjusting the relation between the abscissae. This process determines the ratio of x to f, i.e. it determines the quantity $2\pi a^2/\mu'$ and hence

Fig. 10

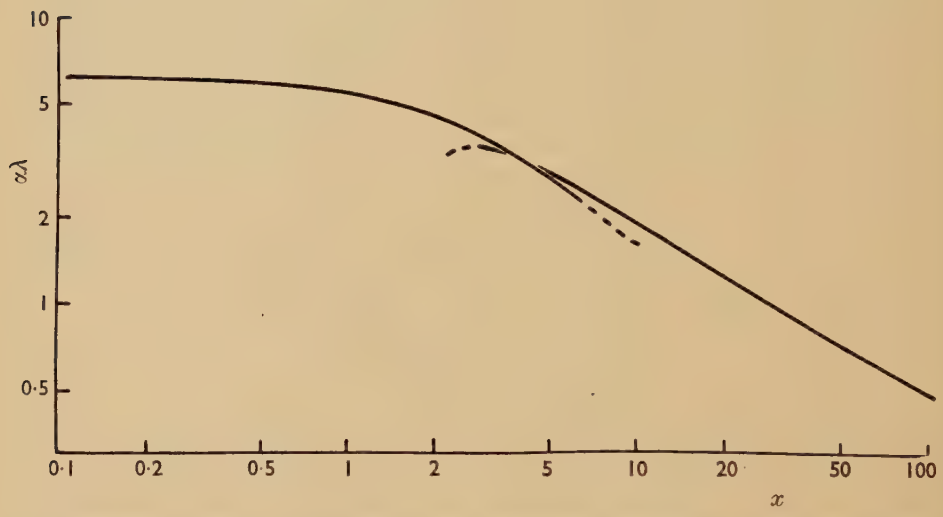

Theoretical curves of attenuation per wavelength against x. The two parts of this curve represent the approximate formulae of table 2 for small x and for large x.

determines μ'. It is found that a tolerable fit can be obtained at all six temperatures by the choice of an appropriate value of f/x at each temperature ; the high frequency results are used to determine f/x and the low frequency results are, within rather large experimental errors, also consistent with the theory. The values of μ' obtained in this way (using the fact that $a=1{\cdot}01$ cm) are shown in table 3. In order to determine c_2, the experimental curve of c' versus f is superposed on the theoretical curve of c'/c_2 versus x, making use of the relation between f and x already found. When the ordinates are suitably adjusted it is found that a good fit can be obtained, again within rather large experimental errors at the low frequency end. The value of c' on the experimental graph which coincides with the ordinate $c'/c_2=1$ on the theoretical graph is taken as the value of c_2 and is given in table 3,

The actual viscosity μ may be obtained from the kinematic viscosity μ' if ρ_n is known. ρ_n may be obtained from the Landau theory using the extrapolated velocity c of ordinary sound for the velocity of phonons; this procedure gives

$$\rho_n = \tfrac{1}{3}\rho TC/c^2 = 1{\cdot}78 \times 10^{-5} T^4 \text{ g cm}^{-3}.$$

We may also make use of the relation derived from elementary kinetic theory,

$$\mu' = \tfrac{1}{3}cl,$$

to calculate formally a kind of mean free path l for the phonons. Values of ρ_n, μ and l are given in table 3. If the continuum theory is to be self-consistent, this mean free path must be shorter than each of the four lengths δ, a, λ and L. We note from table 3 that l is always less than these lengths, and in most cases less by a considerable factor.

Table 3. Results according to the Continuum Theory

Temp. T°K	Kinematic viscosity μ' cm^2 sec^{-1}	Velocity c_2 m sec^{-1}	Normal fluid density ρ_n g cm^{-3}	Viscosity μ μpoise	Mean free path l cm	Penetration depth at 2 kc/s δ cm
0·25	1025	210	$6{\cdot}95 \times 10^{-8}$	71	0·13	0·40
0·3	830	180	$14{\cdot}4 \times 10^{-8}$	119	0·11	0·36
0·4	740	160	$44{\cdot}5 \times 10^{-8}$	320	0·092	0·34
0·5	545	140	111×10^{-8}	600	0·068	0·30
0·54	640	145	151×10^{-8}	970	0·080	0·32
0·58	320	115	202×10^{-8}	650	0·040	0·23

The continuum theory, then, appears to offer a self-consistent description of the experimental facts at all temperatures from 0·25°K to 0·58°K. It has however two major shortcomings at the lower temperatures: it demands the assumption that c_2 increases to as much as 210 m sec^{-1} at 0·25°K, and it gives a viscosity which increases with increasing temperature between 0·25°K and 0·54°K. These two results are in serious conflict with the theoretic expectations of Landau (1941) and of Landau and Khalatnikov (1949) respectively. It is perhaps particularly noticeable that the mean free path l given in table 3 diminishes by less than a factor of 2 when the temperature rises from 0·25°K to 0·5°K, a rather improbable situation.

It is therefore believed that the continuum theory may be legitimately applied only at the two highest temperatures used here, i.e. 0·54°K and 0·58°K. The conclusions summarized in table 3 are believed to be valid only for these two temperatures, and the figures shown for lower temperatures are without real physical significance, except that the mean

free paths at lower temperatures are probably related to the tube diameter and to the degree of specular reflection of phonons at the walls. This is discussed in § 7.

§ 7. The Long Mean Free Path Theory

It remains to show that the observations at temperatures below 0·5°K may be explained by assuming the mean free path of the phonons to be long compared with the tube diameter. Ziman (1954) has treated the problem of the propagation of a pulse of heat along a cylindrical tube, assuming a mean free path long compared with the diameter of the tube and diffuse reflection of phonons at the walls. His treatment gives a correct description of the general shape of the received pulse but it cannot claim to give a valid description of the beginning of the pulse because it depends on the assumption that every phonon makes many collisions with the wall during its journey from heater to thermometer. This leads to a diffusion equation which in turn predicts that the thermometer temperature will start to change immediately the heat pulse is applied. In practice, the earliest phonons to arrive at the thermometer will do so after a time of the order of L/c by taking comparatively direct paths and will not fall within the scope of the above assumption. Moreover, in terms of sine waves, this theory is not applicable at high frequencies where the periodic time is short compared with the time taken for a phonon to travel from one collision with the wall to another. In the absence of a treatment valid for all frequencies, however, we shall in the first place adapt Ziman's treatment for use with sine waves and apply it to the low frequency results.

In the steady state the heat flow F along a cylinder whose radius is small compared with the phonon mean free path is

$$F=\tfrac{2}{3}\pi a^3\rho C c\frac{dT}{dz} \quad . \quad . \quad . \quad . \quad . \quad . \quad . \quad . \quad (8)$$

(Casimir 1938, with the correction pointed out by Berman, Simon and Ziman 1953), implying an effective thermal conductivity which may be written in the form

$$K_{\text{eff}}=\tfrac{1}{3}\rho C c(2a), \quad . \quad . \quad . \quad . \quad . \quad . \quad . \quad . \quad (9)$$

where the diameter $2a$ acts as the mean free path.

For subsequent comparison with the continuum theory we note that a flow of heat in liquid helium II corresponds to a flow of normal fluid and that a temperature gradient corresponds, by virtue of the fountain effect, to a pressure gradient. Using the standard formulae of the two fluid theory, Landau's formula for the phonon contribution to ρ_{n}, and the fact that the specific heat is proportional to T^3, eqn. (8) can be transformed to

$$Q=\frac{2\pi a^3}{\rho_{\text{n}}c}\frac{dp}{dz}, \quad . \quad . \quad . \quad . \quad . \quad . \quad . \quad . \quad (10)$$

where Q is the volume flow of normal fluid. This relation may be compared with Poiseuille's formula for flow through a tube and it suggests an effective viscosity

$$\mu_{\text{eff}} = \frac{1}{32}\rho_{\text{n}} c(2a), \quad \ldots\ldots\ldots \quad (11)$$

where the effective mean free path is now $3/32(2a)$.

At this point we introduce a coefficient ξ, being that fraction of the phonons which are scattered diffusely at the walls, the remaining $1-\xi$ suffering specular reflection. We also introduce a factor to allow for the fact that the tube is not infinitely long and that there is some probability of a phonon travelling straight from one end of the tube to the other without colliding with the wall. For steady flow these two factors appear in eqn. (8) in the form

$$F = \tfrac{2}{3}\pi a^3 \rho C c \frac{3L}{8a} W\left(\frac{L'}{a}\right), \quad \ldots\ldots\ldots \quad (12)$$

where $L' = \xi L/(2-\xi)$. W has been the subject of analysis by Clausing (1928) and it is discussed by Kennard (1938) ; it takes the value (Clausing 1928, p. 103, col. 4) $8a/3L'$ for very long tubes. L' is used here in place of L because in Clausing's work the scattering at the wall has been taken to be perfectly diffuse, whereas a proportion of specular reflection reduces the effective length of the tube. Using eqn. (12) for F we obtain an effective thermal conductivity of

$$K_{\text{eff}} = \tfrac{1}{3}\rho C c(2a) \frac{3L}{8a} W\left(\frac{L'}{a}\right) \quad \ldots\ldots\ldots \quad (13)$$

and an effective viscosity of

$$\mu_{\text{eff}} = \frac{1}{32}\rho_{\text{n}} c(2a) \frac{8a}{3L} \frac{1}{W(L'/a)}. \quad \ldots\ldots\ldots \quad (14)$$

The effective mean free path for thermal conduction becomes

$$l_{\text{eff}} = \frac{3L}{8a} W\left(\frac{L'}{a}\right) 2a \quad \ldots\ldots\ldots \quad (15)$$

and that for viscosity becomes

$$l_{\text{eff}} = \frac{8a}{3L} \frac{1}{W(L'/a)} \frac{3}{32}(2a). \quad \ldots\ldots\ldots \quad (16)$$

Provided, now, that the flow in the tube is substantially uniform. i.e. provided that the tube is considerably shorter than a wavelength, we may substitute the modified thermal conductivity (eqn. (13)) in the classical equation of heat conduction,

$$\frac{\partial T}{\partial t} = \frac{K}{\rho C} \frac{\partial^2 T}{\partial t^2}$$

and obtain the velocity and attenuation of temperature waves as

$$c' = \left\{\frac{4}{3}\omega c a \frac{3L}{8a} W\left(\frac{L'}{a}\right)\right\}^{1/2}$$

and

$$\alpha = \left\{\frac{4ca}{3\omega} \frac{3L}{8a} W\left(\frac{L'}{a}\right)\right\}^{-1/2}.$$

Since this is a wave characterized by $\alpha\lambda=2\pi$, the phases and amplitudes predicted by it would be those given by the curve $\alpha/k=0{\cdot}0175$ radian deg.$^{-1}$ in figs. 5 and 6, were it not for the fact that the velocity and attenuation vary with the tube length. This fact necessitates the separate calculation of the predicted phase shift and amplitude as a function of tube length for each frequency used and for a range of possible values of ξ. These curves are then compared with the experimental points (figs. 3 and 4) and the value of ξ is chosen which gives the best agreement between experiment and theory. In making the comparison, the relation between the abscissae is fixed because both the theoretical and experimental points are plotted against actual tube length in centimetres ; the ordinates may however be adjusted to allow for the unknown phase lag and efficiency of the thermometer. For frequencies from 60 c/s to 361 c/s, the experimental amplitudes agree with the theoretical ones within the limits of experimental error, but the errors are such that ξ cannot be determined from these measurements alone. The phase data are however much more accurate and the theoretical curves are more sensitive to the value assumed for ξ. It is possible to obtain an estimate of ξ at each of the six lowest frequencies, and the averaging of these gives the values shown in table 4 where the errors given are the mean deviation of the mean value of ξ

Table 4. Fraction of Phonons Diffusely Reflected

T°K	ξ
0·25	0·26±0·01
0·3	0·29±0·02
0·4	0·35±0·03
0·5	0·28±0·03

The mean wavelength of phonons is of the order of 200Å at 0·5°K, and so may well be comparable with the smoothness of the walls. Values of ξ of the order of 0·3 are therefore not unreasonable, but since the phonon wavelength decreases with increasing temperature it would be expected that the proportion of diffuse scattering would also increase with temperature. For this reason it is believed that this calculation is probably not applicable at 0·5°K because the mean free path is not sufficiently long, although it is thought to be applicable between 0·25°K and 0·4°K.

For reasons already mentioned the foregoing treatment is valid only for low frequencies ; an idea of the limiting behaviour at high frequencies may be obtained by the following device, which is probably capable of giving accurate predictions if suitably developed. If we consider the emission from the heater of a very short pulse of heat, the temperature fluctuation θ at a point distant z from the heater would be given, according to Kramers *et al.* (1954) following Ziman (1954), approximately by

$$\theta(\tau)=\kappa\tau^{-1/2}\exp(-1/\tau)$$

where $\tau=8act/3z^2$ and κ is a constant. This cannot be strictly true since it predicts a temperature which starts to rise immediately the pulse is emitted, whereas there must in reality be a delay of z/c before any phonons can reach the point of observation and before any effect can be observed. As a trial function, we shall assume that a pulse would in fact give rise to a fluctuation

$$\left.\begin{aligned}\theta(\tau)&=\kappa(\tau-\tau_0)^{1/2}\exp\{-1/(\tau-\tau_0)\}\;;\quad \tau>\tau_0\\ \theta(\tau)&=0\qquad\qquad\qquad\qquad\;;\quad \tau\leqslant\tau_0\end{aligned}\right\}\quad . \quad . \quad . \quad (17)$$

where $\tau_0=(8ac/3z^2)(z/c)$. We then regard sine waves of heat emitted from the heater as a succession of pulses of varying amplitude. By adding together the effect of all such pulses preceding the instant of observation we obtain for the resultant temperature fluctuation at distance z from the heater

$$\theta(t,z)=\frac{\kappa}{z}\left(\frac{8ac}{3\omega}\right)^{1/2}\exp\left\{-z\left(\frac{3\omega}{4ac}\right)^{1/2}\right\}\sin\left[\left\{\left(\frac{3\omega}{4ac}\right)^{1/2}+\frac{\omega}{c}\right\}z-\omega t+\frac{\pi}{4}\right].$$

. . . . (18)

At low frequencies the term $\omega z/c$ may be ignored, and the wave velocity and exponential attenuation agree with those previously found. The factor z^{-1} appears to be spurious and has probably arisen because the trial function is not sufficiently accurate, but the expression as a whole works sufficiently well at low frequencies to engender some faith in its predictions for high frequencies. For frequencies so high that

$$\omega/c\gg(3\omega/4ac)^{1/2},$$

the wave velocity is predicted to be simply c, and the transition frequency at which the two terms have equal importance is $f_0=3c/8\pi a=2{\cdot}8$ kc/s. f_0 is such a frequency that its period is comparable with the time taken for a phonon to cross the tube.

The foregoing is to be regarded as strong, although not conclusive, evidence that, if the phonons have a long mean free path and suffer partially diffuse reflection, the velocity of temperature waves will tend to that of ordinary sound at very high frequencies. The curves of fig. 7 show such a tendency at temperatures of 0·4°K and below, but not at higher temperatures. The derivation of these curves is of course only strictly applicable if the continuum theory applies because the end effects become important if the mean free path is long, and the velocity and attenuation then depend on length. It is clear also, however, from direct inspection of the phase difference between the two longest tubes (for which the end corrections are smallest), that the rate of change of phase with length certainly involves a velocity greater than 140 sec^{-1} at frequencies and temperatures where the curves of fig. 7 exceed this value.

From the results in the whole frequency range we conclude, therefore, that the mean free path is substantially longer than the tube diameter at temperatures of 0·4°K and below, but that at and above 0·5°K this is no longer true.

It is to be noted from the earlier part of the above analysis that at low frequencies the ' open gas ' of phonons flows as though it were controlled by a viscosity determined by eqn. (14), implying an effective mean free path given by eqn. (16). With the values of ξ given in table 4, this effective mean free path is about 0·1 cm for the longer tubes. This rather small value accounts for the deceptive self-consistency of the continuum theory when applied at low temperatures where the mean free path is in fact long (see table 3). The mean free paths of table 3 at lower temperatures cannot, however, be quantitatively compared with eqn. (16) because they were deduced from the data at all frequencies whereas eqn. (16) is applicable only to low frequencies ; it can only be said that the agreement in order of magnitude is satisfactory.

§ 8. The Thermometer Response

Throughout the calculations allowance has been made for the fact that the phase and amplitude recorded by the thermometer may differ from those existing in the helium by amounts which will depend on frequency and on temperature but not on tube length. Having established the theoretical interpretation without assuming any values for these unknown quantities, it is now possible to calculate the actual amplitudes and phases which ought to be observed and, by comparing them in absolute magnitude with those actually found, to deduce the phase lag and the efficiency of the thermometer. The latter is defined as the ratio of the temperature amplitude given by the thermometer to that actually existing in the helium.

Table 5. Thermometer Response

Temperature °K	At 60 c/s		At 361 c/s		At 2 kc/s	
	Phase lag (deg.)	Efficiency	Phase lag (deg.)	Efficiency	Phase lag (deg.)	Efficiency
0·25	28	0·8	88	0·14		
0·3	14	0·9	82	0·3		
0·4	4	0·9	64	0·5		
0·5	0	0·8			123	0·4
0·54	0	0·8			125	0·4
0·58	0	(1·1)			118	0·8

The result of this process is shown in table 5. The long mean free path theory which is applicable at the lower temperatures can be applied quantitatively only at frequencies up to about 361 c/s. At the higher temperatures, the continuum theory can readily be applied at 60 c/s and at 2 kc/s, but the calculation of absolute amplitude and phases presents some difficulty in the middle frequency range where the tube is neither ' wide ' nor ' narrow '.

The figures in table 5 apply specifically to the thermometer actually used, consisting of a film of Aquadag on a thin mica substrate, but the same general behaviour may be expected for any carbon thermometer. An increase in frequency or a decrease in temperature tends to reduce the efficiency and to increase the phase lag.

§ 9. Conclusions

(*a*) *The Mean Free Path*

It has been shown in § 6 that only at temperatures above 0·5°K is the mean free path small compared with the size of the apparatus. Because of the trend of mean free path with temperature (table 3) it is thought that the continuum theory is probably valid at 0·58°K and is not far from the truth at 0·54°K. On this basis, the mean free paths are taken to be 0·08 cm at 0·54°K and 0·04 cm at 0·58°K. It has been shown in § 7 that at temperatures of 0·4°K and below the mean free path is long compared with the tube diameter, and that about one-third of the phonons are scattered diffusely at the walls, the remaining two-thirds suffering specular reflection.

Landau and Khalatnikov (1949) have calculated the expected mean free path l of phonons, and for temperatures below 0·8°K they find

$$l=\{1{\cdot}1\times 10^{8}T^{9/2}\exp(-\Delta/\boldsymbol{k}T)+5{\cdot}6\times 10^{2}T^{9}\}^{-1}\text{ cm}, \quad . \quad (19)$$

Fig. 11

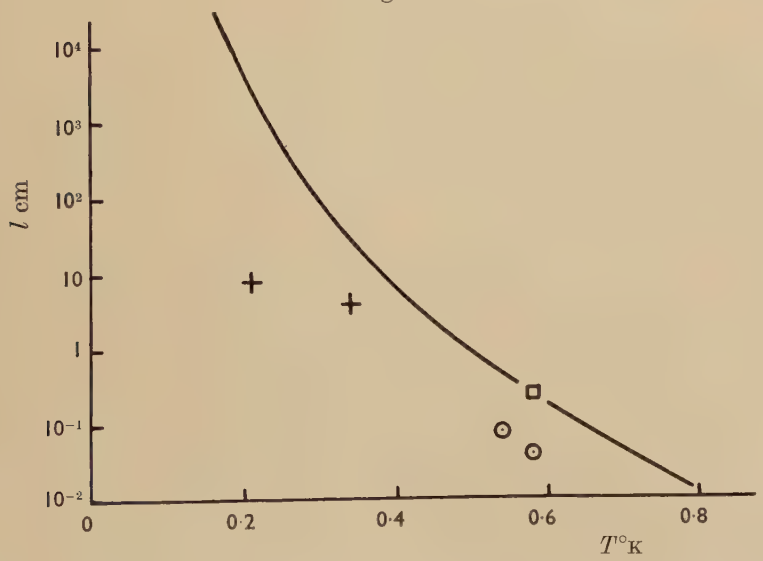

Mean free path of phonons as a function of temperature. Full line, theory of Landau and Khalatnikov (1949); ⊙ experimental points from this paper; □ experimental point of Whitworth (1955); + experimental points of Kramers *et al.* (1954).

where $\Delta/\boldsymbol{k}=9{\cdot}6$ deg. according to Landau (1941, 1947). This function together with the experimental points at 0·54°K and 0·58°K is illustrated in fig. 11. The experimental points are below the curve by a factor of about 6, whereas it is thought that the experimental error is certainly not more than a factor of 2. The experimental points of Whitworth (1955), from measurements of steady heat flow, and of Kramers *et al.* (1954) from measurements on heat pulses are also shown. Neither value is claimed to be accurate, the uncertainty in Whitworth's results being explicitly quoted as a factor of about 4. It should also be remarked that the numerical constants in eqn. (19) must be treated with some reserve since they depend rather sensitively on experimental data which are not very accurately known.

Fairbank and Wilks (1954) have also measured steady heat flow in a tube and they find that their measurements are consistent with a phonon mean free path considerably greater than 0·29 mm, the diameter of their German silver tube, at temperatures below 0·6°K. They find an effective mean free path for thermal conduction of about 0·3 mm at 0·6°K and about 0·4 mm at 0·26°K and they remark that this behaviour suggests an increasing amount of specular reflection as the temperature is reduced. Using eqn. (15) we find from their data $\xi=1$ at 0·6°K and $\xi=0{\cdot}87$ at 0·26°K. Since a quartz tube has been used in the present work and a metal tube was used by Fairbank and Wilks, quantitative agreement about the degree of diffuse reflection is not to be expected, but the trend with temperature is the same in both cases.

(*b*) *Relation to Other Experiments*

Previous work on second sound below 1°K has all been carried out by the pulse method. It might be possible, using the results of the present experiments, to predict what pulse shape ought to be obtained, but this would involve a knowledge of the frequency characteristics of the thermometer and amplifiers used in the pulse work. It is, however, possible to compare the values of c' given in fig. 7 with the velocities derived from pulse experiments by measuring the time of arrival of the beginning of the pulse. The values at 2 kc/s, for example, are in good agreement with the pulse values of de Klerk *et al.* (1953, 1954) at all six temperatures. It seems possible that although higher frequencies were present in their pulses, the adverse effect of falling thermometer sensitivity with increasing frequency (see § 8) prevented frequencies higher than about 2 kc/s from being observed. If in fact c' increases with frequency, the front edge of the received pulse ought to arrive at a time corresponding to the value of c' appropriate to the highest frequency detectable. If this view be correct then at temperatures lower than 0·5°K an ideal thermometer would show a pulse with a front edge occurring at a time corresponding to c, the velocity of ordinary sound. The velocities given by Kramers *et al.* (1954) are larger than those of de Klerk *et al.*, a fact which might be ascribed to a better frequency response of their thermometer.

It seems important that hitherto no interpretation of pulse shapes has taken account of reflection of the waves at the ends of the tube. The present observations are consistent with a reflection coefficient of unity, and the amplitudes observed in the shortest tube can hardly be explained on any other basis. If, therefore, the leading edge of a pulse arrives at the thermometer after a time t, the reflection of this edge will be expected to return there after a further time $2t$. Caution must therefore be exercised in interpreting the shape of that part of a received pulse which arrives after a time $3t$ from the original transmission.

Acknowledgments

I wish to express my thanks to Dr. D. Shoenberg, F.R.S., for his advice and encouragement, to Dr. J. Ashmead for placing at my disposal his ideas for the cryostat and for many subsequent discussions, to Dr. D. ter Haar, Mr. H. E. Hall and Mr. R. W. Whitworth for helpful discussions, to Mr. F. T. Sadler for the construction of the cryostat and for the provision of the relatively large quantities of liquid helium needed for filling it, and to Trinity College, Cambridge, for the award of a Research Fellowship during the tenure of which this work was carried out.

References

Atkins, K. R., 1953, *Phys. Rev.*, **89,** 529.
Atkins, K. R., and Edwards, M. H., 1954, *Phys. Rev.*, **93,** 1416 ; 1955, *Ibid.*, **97,** 1429.
Atkins, K. R., and Osborne, D. V., 1950, *Phil. Mag.*, **41,** 1078.
Berman, R., Simon, F. E., and Ziman, J. M., 1953, *Proc. Roy. Soc.* A, **220,** 176, footnote.
Casimir, H. B. G., 1938, *Physica, 's Grav.*, **5,** 495.
Chase, C. E., 1953, *Proc. Roy. Soc.* A, **220,** 116.
Chase, C. E., and Herlin, M. A., 1955, *Phys. Rev.*, **97,** 1447.
Clausing, P., 1928, *Leiden Dissertation* (Amsterdam : H. J. Paris).
Dingle, R. B., 1950, *Proc. Phys. Soc.* A, **63,** 638 ; 1952, *Physica, 's Grav.*, **18,** 841.
Fairbank, H. A., and Wilks, J., 1954, *Phys. Rev.*, **95,** 277.
Garrett, C. G. B., 1950, *Proc. Roy. Soc.* A, **203,** 375.
Gorter, C. J., 1952, *Phys. Rev.*, **88,** 681.
Helmholtz, H., 1863, *Verhandlungen des Naturhistorisch-medicinschen Vereins zu Heidelberg*, **3,** 16.
Kapitza, P., 1941, *J. Phys., U.S.S.R.*, **4,** 181.
Kennard, E. H., 1938, *Kinetic Theory of Gases* (New York : McGraw-Hill).
Khalatnikov, I. M., 1952, *J. Exp. Theor. Phys., U.S.S.R.*, **23,** 253.
Kirchhoff, G., 1868, *Ann. Phys., Lpz.*, **134,** 177.
de Klerk, D., Hudson, R. P., and Pellam, J. R., 1953, *Phys. Rev.*, **89,** 326, 662 ; 1954, *Ibid.*, **93,** 28.
Kramers, H. C., van den Burg, F. A. W., and Gorter, C. J., 1953, *Phys. Rev.*, **90,** 1117.
Kramers, H. C., van Peski-Tinbergen, T., Wiebes, J., van den Burg, F. A. W., and Gorter, C. J., 1954, *Physica, 's Grav.*, **20,** 743.
Kramers, H. C., Wasscher, J. D., and Gorter, C. J., 1952, *Physica, 's Grav.*, **18,** 329.
Landau, L. D., 1941, *J. Phys., U.S.S.R.*, **5,** 71 ; 1947, *Ibid.*, **11,** 91.

Landau, L. D., and Khalatnikov, I. M., 1949, *J. Exp. Theor. Phys., U.S.S.R.*, **19,** 637, 709.
Maurer, R. D., and Herlin, M. A., 1949, *Phys. Rev.*, **76,** 948.
Mayper, V., and Herlin, M. A., 1953, *Phys. Rev.*, **89,** 523.
Osborne, D. V., 1948, *Nature, Lond.*, **162,** 213 ; 1951, *Proc. Phys. Soc.* A, **64,** 114 ; 1952, *Proc. NBS Symposium on Low Temperature Physics* 1951, 139.
Pellam, J. R., and Scott, R. B., 1949, *Phys. Rev.*, **76,** 869.
Peshkov, V. P., 1948 a, *Rep. Internat. Conf. 'Low Temperatures'* (1946) (London: Physical Society), **2,** 19; 1948 b, *J. Exp. Theor. Phys., U.S.S.R.*, **18,** 951.
Rayleigh, Lord, 1896, *Theory of Sound* (London : Macmillan & Co.), **2,** 319.
Temperley, H. N. V., 1951, *Proc. Phys. Soc.* A, **64,** 105.
Ward, J. C., and Wilks, J., 1952, *Phil. Mag.*, **43,** 48.
Weston, D. E., 1953, *Proc. Phys. Soc.* B, **64,** 695.
Whitworth, R. W., 1955, *Conference on Low Temperature Physics, Paris*, 1955.
Ziman, J. M., 1954, *Phil. Mag.*, **45,** 100.

XXIX. *Collective Effects in Nuclei of Mass* 18 *and* 19

By F. C. Barker
Atomic Energy Research Establishment, Harwell†

[Received November 10, 1955]

In an intermediate coupling shell model calculation for the nuclei of mass 18 and 19, Elliott and Flowers (1955) determined the positions of the low lying levels in the absence of any collective effects. They found, however that certain E2 transition rates in ^{17}O and ^{19}F could not be explained without collective motion and that the introduction of weak coupling of the Bohr and Mottelson (1953) type between the surface and the nucleons outside the ^{16}O core gave simultaneous agreement in ^{17}O and ^{19}F. In this note we consider the effects of such weak coupling, and show that although it enhances the E2 transition rates in ^{19}F by a factor of order 5, the changes in level positions and magnetic moment are negligible.

The condition for validity of the weak coupling approach is

$$x\sqrt{j}=\sqrt{\left(\frac{5}{16\pi}\right)}\frac{k}{\sqrt{(\hbar\omega C)}}\ll 1$$

(cf. BM, eqn. (II.14)). With BM's hydrodynamical estimates of C and $\hbar\omega$ (about 30 and 7 Mev respectively), EF fitted the lifetime of the 0·872 Mev state of ^{17}O, which decays by E2 radiation, using $x\sqrt{j}\approx 0{\cdot}2$. This implies such weak coupling that it is valid to consider only states containing 0 or 1 phonon, and to use perturbation theory to calculate changes in wave functions and energy values.

To fit the quadrupole moment of the ground state of ^{17}O, a much smaller value of $x\sqrt{j}$ is required. This could be attributed to the matrix elements of $k(r)$ between different single particle states being different, contrary to the assumption of BM. This may be due to the single particle states involved being relatively loosely bound (a different reason has been suggested by Blin-Stoyle (private communication)). In order to fit the experimental values for the ^{17}O ground state quadrupole moment and 0·872 Mev state lifetime

$$Q=-0{\cdot}005\times 10^{-24}\ \text{cm}^2,\qquad \tau=2{\cdot}5\times 10^{-10}\ \text{sec},$$

with the nuclear radius $R_0=1{\cdot}44A^{1/3}\ 10^{-13}$ cm, we require (cf. BM eqn. (II.10))

$$\langle 1\text{d}\mid k\mid 1\text{d}\rangle=0{\cdot}033C,\qquad \langle 1\text{d}\mid k\mid 2\text{s}\rangle=0{\cdot}20C$$

† Communicated by B. H. Flowers.

(the matrix elements are assumed to have the same sign). This coupling alters the positions of the levels of ^{17}O, and EF's values for the strength of the spin–orbit force and the d–s level separation are replaced by

$$\xi = 2 \text{ Mev} + 0{\cdot}0010C, \quad \text{d–s} = 1{\cdot}125 \text{ Mev} - 0{\cdot}0052C.$$

For the mass 19 nuclei, the unperturbed wave functions are taken from those determined by EF, with only the maximum orbital symmetry L–S states retained for $T=\frac{1}{2}$, and only the $(\mathrm{d}_{5/2}{}^{3-x}\mathrm{s}^{x})$ j–j states retained for $T=\frac{3}{2}$. The relative changes in the energies E_{TJ} of the lowest states with given T and J are found to be

$$\Delta(E_{1/2,\,5/2}-E_{1/2,\,1/2})=0{\cdot}0016C, \qquad \Delta(E_{1/2,\,3/2}-E_{1/2,\,1/2})=0{\cdot}0018C,$$
$$\Delta(E_{3/2,\,5/2}-E_{1/2,\,1/2})=0{\cdot}0065C, \qquad \Delta(E_{3/2,\,3/2}-E_{1/2,\,1/2})=0{\cdot}0043C,$$
$$\Delta(E_{3/2,\,1/2}-E_{1/2,\,1/2})=0{\cdot}0070C,$$

and the change in the ^{19}F ground state magnetic moment (in units of nuclear magnetons) is

$$\Delta\mu = -0{\cdot}0011\frac{C}{\hbar\omega}.$$

For reasonable values of C and $\hbar\omega$, these changes are negligible.

Recently the magnetic moment of the 0·197 Mev $\frac{5}{2}^{+}$ state of ^{19}F has been measured. The results are

$\mu = 4{\cdot}0 \pm 0{\cdot}9$ (preliminary value, Lehmann *et al.* 1955),

$\mu = 3{\cdot}4 \pm 0{\cdot}9$ (Treacy, private communication).

EF's wave function for this state gives $\mu = 3{\cdot}3$. The change due to surface coupling,

$$\Delta\mu = -0\cdot0016\frac{C}{\hbar\omega},$$

is again negligible.

E2 transitions in ^{19}F are enhanced by the surface coupling by a factor of order 5, but those in competition with M1 transitions between the same states are still unimportant. Even in the $\frac{3}{2}^{+}\rightarrow\frac{1}{2}^{+}$ transition for which EF found an M1 transition rate about 1% of the single particle value, the E2 transition rate is only about one-fifth of this.

References

Bohr, A., and Mottelson, B. R., 1953, *Kgl. Danske Videnskab. Selskab, Mat.-fys. Medd.*, **27**, No. 16 (referred to as BM).

Elliott, J. P., and Flowers, B. H., 1955, *Proc. Roy. Soc.* A, **229**, 526 (referred to as EF).

Lehmann, P., Leveque, A., and Fiehrer, M., 1955, private communication to B. H. Flowers.

XXX. *The Lowering of Fracture-Stress due to Surface Adsorption*

By N. J. Petch
Metallurgy Laboratory, University of Leeds†

[Received September 15, 1955]

Abstract

Gibbs' adsorption equation and the Griffith and dislocation theories of fracture are used to calculate this lowering. The possibility that such adsorption causes the embrittlement of iron by hydrogen is discussed and is shown to be in good agreement with measured fracture stresses.

§ 1. Introduction

The interest in this topic dates from the suggestion (Orowan 1944) that adsorption of atmospheric constituents on surface Griffith cracks in glass lowers the fracture stress and produces the delayed-fracture effect.

The stress σ_f required to enlarge a surface crack of depth c in a solid of surface energy γ and Young's modulus E is

$$\sigma_f=(2E\gamma/\pi c)^{1/2}. \qquad (1)$$

If the surface of the crack is covered by an adsorbed phase, γ is lowered to γ_1 and σ_f is correspondingly lowered, provided the extension of the crack is sufficiently slow to allow the formation of increments of surface that contain the adsorbed phase.

Thus, a knowledge of the surface energy lowering is required for calculation of the new fracture stress.

§ 2. The Surface Energy Lowering

This is, of course, given directly by Gibbs' adsorption equation

$$d\gamma=-\Gamma d\mu,$$

where $d\gamma$ is the change in surface energy produced by a change $d\mu$ in the chemical potential of the adsorbed phase and Γ is the number of molecules adsorbed per unit area.

If the adsorption takes place at temperature T from a gas at pressure p,

$$d\gamma=-\Gamma kT\, d\ln p. \qquad (2)$$

From the Langmuir isotherm,

$$\Gamma=\Gamma_s\frac{Ap}{1+Ap},$$

where Γ_s is the number of molecules adsorbed per unit area at saturation and A is a constant.

† Communicated by the Author.

With a diatomic molecule that dissociates on adsorption, Γ_s is halved and the isotherm becomes

$$\Gamma=\Gamma_s\frac{(Ap)^{1/2}}{1+(Ap)^{1/2}}.$$

Substitution for Γ in (2) and integration gives

$$\gamma_1=\gamma-\Gamma_s kT\ln(1+Ap),$$

or, for a diatomic molecule that dissociates,

$$\gamma_1=\gamma-2\Gamma_s kT\ln(1+(Ap)^{1/2}). \quad . \quad . \quad . \quad . \quad . \quad (3)$$

The lowered fracture stress can then be obtained from (1).

The stronger the adsorption, the greater is A and, as would be expected, the greater is the fracture-stress lowering.

If the Langmuir isotherm is not sufficiently accurate, it may be necessary to use one of the other isotherms or a numerical integration of the experimental one in this calculation.

§ 3. The Fracture of Metals

In this case, we are fairly certainly concerned with the production of cracks ahead of arrays of dislocations held up at some obstacle, rather than with the enlargement of pre-existing Griffith cracks.

Stroh's (1954) criterion for the production of a crack can be put in the form

$$\tau=12\gamma/nb,$$

where the shear stress τ compresses an array of n edge dislocations of Burgers vector b.

From Eshelby, Frank and Nabarro (1951),

$$n=\pi(1-\nu)\tau L/\mu b,$$

where L is the length of the array and μ is the rigidity modulus.

Thus, the tensile stress required at 45° to the plane and length of the array to produce a crack is

$$\sigma=2\tau=2\left(\frac{12\mu\gamma}{\pi(1-\nu)L}\right)^{1/2}. \quad . \quad . \quad . \quad . \quad . \quad (4)$$

With real metals, a considerable stress σ_0 may be necessary merely to move a dislocation in the crystal, so σ_0 must be added to σ in (4) (Hall 1951, Petch 1953, Cracknell and Petch 1955 a). This equation then gives the criterion for the cleavage fracture of polycrystalline specimens, and it seems (Petch 1955) that it will also apply to ductile fracture, at least for α-iron. Thus, the fracture stress is

$$\sigma_f=\sigma_0+4\left(\frac{3\mu\gamma}{\pi(1-\nu)L}\right)^{1/2}. \quad . \quad . \quad . \quad . \quad . \quad (5)$$

It will be appreciated that this calculation assumes isotropy.

If a very mobile solute is present, so that the cracks can form with adsorbed solute on them,

$$\sigma_f=\sigma_0+4\left(\frac{3\mu}{\pi(1-\nu)L}\{\gamma-\Gamma_s kT\ln(1+Ap)\}\right)^{1/2},$$

or, for a diatomic molecule that dissociates on adsorption,

$$\sigma_f=\sigma_0+4\left(\frac{3\mu}{\pi(1-\nu)L}\{\gamma-2\Gamma_s kT\ln(1+(Ap)^{1/2})\}\right)^{1/2}, \quad . \quad (6)$$

where p is the equilibrium pressure of the solute.

For polycrystalline α-iron and zinc, the experimental evidence indicates $L\propto l$, the grain diameter (Petch 1953, Greenwood and Quarrell 1954). In fractures at small plastic deformations, L is probably $l/2$, and, in the case of α-iron, it appears that the effective value of L is not altered by plastic deformation (Petch 1955).

From (6), with $L\propto l$, the lowering of $(\sigma_f-\sigma_0)$ produced by the adsorption depends upon the grain size, being proportional to $l^{-1/2}$.

§ 4. Hydrogen-Embrittlement of Iron

A small quantity of hydrogen in iron markedly lowers the fracture stress. It is quite widely believed (Zapffe and Sims 1941) that the accumulation of hydrogen in small cavities present as defects is the cause ; it is thought that the stress around the cavities initiates premature fracture. The room-temperature equilibrium pressure of hydrogen is certainly very high, even when only small amounts are in solution, and it may well be that these internal stresses do explain the suppression of the yield point that hydrogen can produce (Cracknell and Petch 1955 b), but their role in fracture is less certain. The plastic deformation prior to fracture will tend to homogenize the shear-stress distribution in the metal.

Since an iron fracture surface will be a very strong chemisorber of hydrogen and since hydrogen can diffuse extremely rapidly through iron, Petch and Stables (1952) suggested that adsorption might be the cause of the reduced strength. In keeping with this, hydrogen has no effect on the strength at high strain rates.

The movement of hydrogen involved in the production of a crack at an array should be roughly comparable to the processes of quench- and strain-ageing, so, from the known diffusion rates, it should require $\sim 10^{-5}$ sec at room temperature. This makes it a reasonable possibility in a normal tensile test.

Equation (6) can now be used for a quantitative evaluation of the effect that hydrogen can produce.

The pressure of hydrogen (mm of Hg) in equilibrium with α-iron containing s cm^3 of hydrogen/100 g is given (Sykes, Burton and Gegg 1947) by

$$p^{1/2}=0{\cdot}36s\exp(3650/T).$$

One way of obtaining A in (6) is by noting that it equals $p_{1/2}^{-1}$, where $p_{1/2}$ is the hydrogen pressure for $\Gamma/\Gamma_s=\frac{1}{2}$. This gives $A\sim5\times10^4$ mm^{-1} for hydrogen on nickel at room temperature, and the same value was used for hydrogen on iron, since the two adsorptions are very similar, with practically the same heat of adsorption (Beeck 1940, 1950).

Figure 1 shows the lowering of the surface energy of iron at room temperature calculated from (6) using this data. The effect is large.

Fig. 1

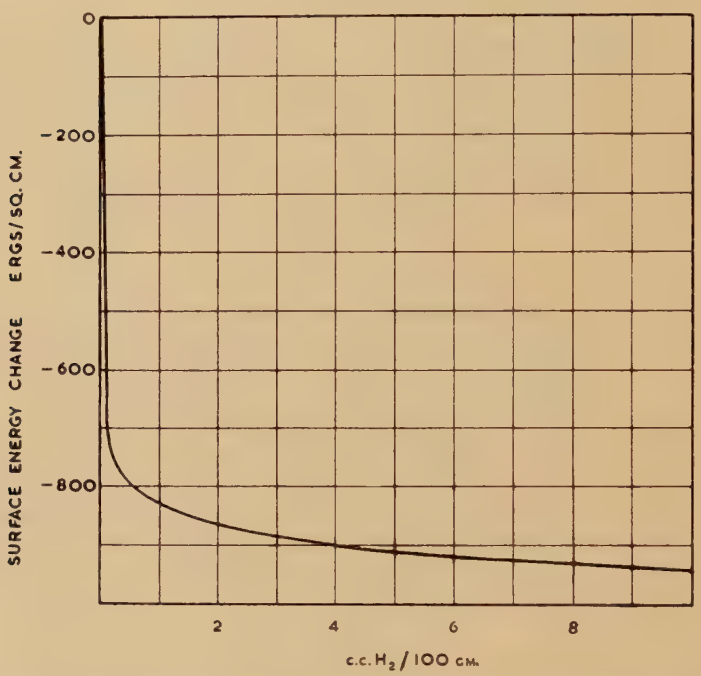

Lowering of the surface energy of iron by adsorption of hydrogen.

To obtain the corresponding values of $(\sigma_f-\sigma_0)$ when hydrogen is present, the initial surface energy is required. A value of 1180 erg/cm^2 was obtained by the application of (5) to previous measurements (Petch 1955) of the fracture stress/grain size relationship for a hydrogen-free mild steel, assuming $L=l/2$. Taking a medium grain size of $l^{-1/2}=5$ mm$^{-1/2}$ as an example, a fall of $(\sigma_f-\sigma_0)$ from 20·5 tons/in.^{2} in the absence of hydrogen to 9·5 tons/in.^{2} at 10 cm^3 H_2/100 g is then indicated.

The influence of temperature on the effect of hydrogen adsorption can be estimated by using the Clausius–Clapyron equation to obtain the adsorption isotherms for other temperatures from the room temperature one. The heat of adsorption is somewhat uncertain. It falls from an initial 33 kilocal/g mole as the fractional coverage θ of the surface increases ; 15 kilocal is reached at 0·1 mm and room temperature, which

probably corresponds to $\theta \sim 0{\cdot}75$, and presumably the value at $\theta \sim 1$ is only a few kilocal (Beeck 1950). A calculation for -115°C using this information suggests that the change from room temperature does not have much effect on the surface energy lowering.

§ 5. Comparison with Experiments

Figure 2 (*a*) shows the dependence of the fracture stress of a polycrystalline mild steel containing ~ 10 cm^3 of hydrogen/100 g upon the grain diameter l at 18°C. Figure 2 (*b*) gives the previously-determined figures for the same steel without hydrogen (Petch 1955).

Fig. 2

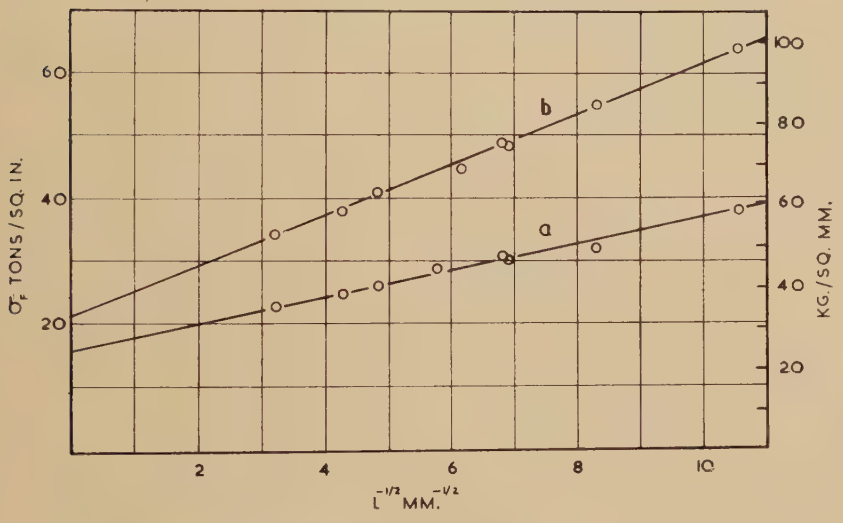

Fracture stress/grain size relationship for a mild steel at 18°C, (*a*) with ~ 10 cm^3 hydrogen/100 g, (*b*) without hydrogen.

In both cases, the relationship is of the form

$$\sigma_f = \sigma_0 + kl^{-1/2},$$

where σ_0 and k are constants. It is apparent that hydrogen causes a reduction in the slope k and in σ_0.

The reduction in k is consistent with a lowering of the surface energy as in (6). At $l^{-1/2} = 5$ mm$^{-1/2}$, the observed value of $(\sigma_f - \sigma_0)$ is 11 tons/in.^{2} in the presence of the hydrogen, compared with the figure of 9·5 tons/in.^{2} obtained using the calculated surface energy lowering.

The reduction in σ_0 by the hydrogen is readily explained as a direct result of the lower strain at fracture, which, in turn, is caused by the reduction in k. The σ_0 term simply represents the stress required to move a dislocation and this movement will be easier if the strain-hardening

is reduced. Thus, σ_0 will fall as the average reduction of area falls from 67% to 21% in the presence of the hydrogen.

Figure 3 shows that lowering the temperature to −115°c has little influence on the hydrogen effect. The average reduction of area is reduced from 61% to 23% by the hydrogen.

Fig. 3

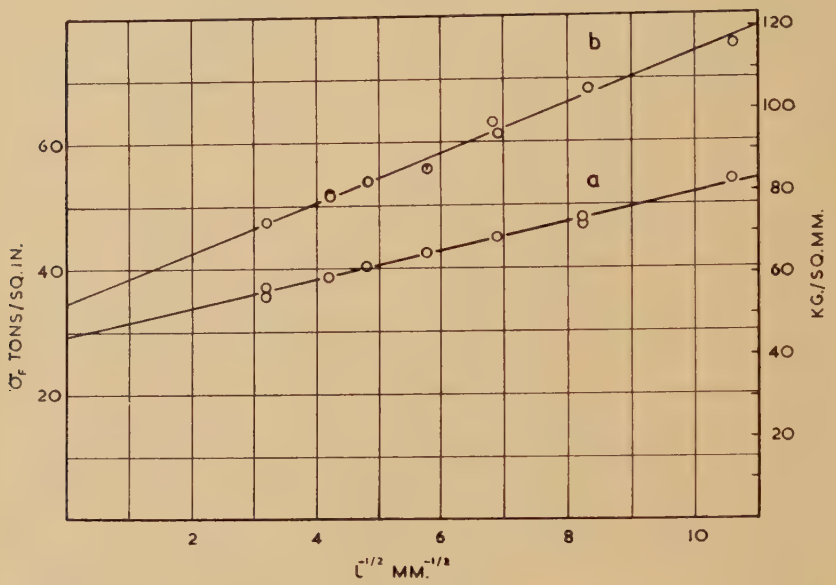

Fracture stress/grain size relationship for a mild steel at −115°c, (*a*) with ~10 cm³ hydrogen/100 g, (*b*) without hydrogen.

All these measurements are in good agreement with the explanation of hydrogen embrittlement in terms of adsorption.

§ 6. Experimental Details

The general procedure followed that used in the measurements on the same mild steel when free from hydrogen (Petch 1955).

In the present case, the tensile specimens were machined to 0·15 in. diameter on the gauge length and annealed at 650°c. The hydrogen was then introduced electrolytically using a 4% H_2SO_4 electrolyte containing a few drops of yellow phosphorus in CS_2 as a poison. The current density was 2 amp/in.², and it was applied for 17 hours. Since electrolytic charging may produce surface blisters, the specimens were turned down to 0·125 in. immediately after charging; 0·001 in. cuts were used and the specimens were oil-cooled during the machining. They were subsequently polished to a 3/0 emery finish and fractured. Some specimens were machined directly to 0·125 in. gauge-length diameter, annealed, hydrogen-charged, polished and tested; the fracture stresses agreed with the previous ones.

Within each series of measurements, there was some variation in the strain at fracture with grain size. Since this introduces a variation in σ_0, a small correction was necessary to bring the results to an average strain. To obtain this correction, σ_0 was plotted against $l^{-1/2}$ without any correction, and the difference in σ_0 between the hydrogen-containing and the hydrogen-free specimens was then used to find the variation of σ_0 with strain.

Acknowledgment

The author wishes to thank Mr. A. Fillingham for his help with the experimental work.

References

Beeck, O., 1950 a, *Faraday Soc. Discussions*, **8**, 118 ; 1950 b, *Ibid.*, **8**, 314.
Beeck, O., Smith, A. E., and Wheeler, A., 1940, *Proc. Roy. Soc.* A, **177**, 62.
Cracknell, A., and Petch, N. J., 1955 a, *Acta Met.*, **3**, 186 ; 1955 b, *Ibid.*, **3**, 200.
Eshelby, J. D., Frank, F. C., and Nabarro, F. R. N., 1951, *Phil. Mag.*, **42**, 351.
Greenwood, G. W., and Quarrell, A. G., 1954, *J. Inst. Metals*, **82**, 551.
Hall, E. O., 1951, *Proc. Phys. Soc.* B, **64**, 747.
Orowan, E., 1944, *Nature, Lond.*, **154**, 341.
Petch, N. J., 1953, *J. Iron Steel Inst.*, **173**, 25 ; 1955, *Phil. Mag.*, in the press.
Petch, N. J., and Stables, P., 1952, *Nature, Lond.*, **169**, 842.
Stroh, A. N., 1954, *Proc. Roy. Soc.* A, **223**, 404.
Sykes, C., Burton, H. H., and Gegg, C. C., 1947, *J. Iron Steel Inst.*, **156**, 155.
Zapffe, C. A., and Sims, C. E., 1941, *Trans. Amer. Inst. Min. Met. Engrs.*, **145**, 255.

XXXI. *The S-matrix for Neutral PS–PV Meson–Nucleon Interaction*

By J. S. R. Chisholm
University College, Cardiff†

[Received October 28, 1955]

Summary

Nucleon and neutral meson fields with an exponential interaction, derived from the PS–PV interaction by the Dyson transformation, are studied. A new system of graphs called 'skeletons' is described; the S-matrix for any process is the sum of terms corresponding to skeletons with the appropriate external lines.

§ 1. Introduction

R. J. Glauber (1951) has investigated neutral meson theories in which an exponential of the meson field occurs in the interaction Hamiltonian. This paper generalizes Glauber's results by deriving the S-matrix for an exponential interaction with fermion and neutral meson fields both quantized. The meson field considered is pseudoscalar, and the interaction Lagrangian is derived from the neutral PS–PV Lagrangian by the Dyson transformation (1948); the transformation is given in § 2, and involves a mass renormalization. In §§ 3 and 4 a graphical theory of the interaction is developed, and in § 5 it is shown that the renormalized S-matrix is a sum of terms corresponding to a new system of graphs called 'skeletons'. The fermion and meson propagators in the skeletons contain $\sinh \Delta_F(x)$ and $\cosh \Delta_F(x)$, and correspond to the propagation of an arbitrarily large number of mesons. Section 6 consists of a discussion of a further renormalization required to eliminate fermion lines which begin and end at the same vertex. Section 7 consists of a brief discussion of possible interactions.

§ 2. The Transformation of the Lagrangian

The Lagrangian density for neutral meson and nucleon fields with PS–PV interaction is

$$L = L_1 + L_2 + L_3 + L_4,$$

where

$$L_1 = \bar{\psi}(x)\gamma_\mu \partial_\mu \psi(x),$$

$$L_2 = M\bar{\psi}(x)\psi(x)$$

$$L_3 = -\tfrac{1}{2}[(\partial_\mu \phi)^2 + m^2\phi^2],$$

$$L_4 = ig\bar{\psi}(x)\gamma_5\gamma_\mu \psi(x)(\partial_\mu \phi),$$

with

$$\bar{\psi}(x) = \psi^*(x)\gamma_4.$$

† Communicated by the Author.

We perform a unitary transformation (Dyson 1948) on the system by putting

$$\left.\begin{aligned}\psi(x)&=\exp\,[iG\gamma_5\phi(x)]\zeta(x)\\ \text{and}\qquad \psi^*(x)&=\zeta^*(x)\exp\,[-iG\gamma_5\phi(x)]\end{aligned}\right\}\quad\ldots\ldots\quad(1)$$

the γ_5 operating on the spinors.

This transformation leaves L_3 unchanged, but affects L_1, L_2 and L_4:

$$L_1=\zeta^*(x)\exp\,[-iG\gamma_5\phi(x)]\gamma_4(\gamma_\mu\partial_\mu)\exp\,[iG\gamma_5\phi(x)]\zeta(x).$$

Now

$$\begin{aligned}\partial_\mu\exp\,[iG\gamma_5\phi]&=\sum_n\frac{(iG\gamma_5)^n}{n\,!}\sum_r\phi^r(\partial_\mu\phi)\phi^{n-r-1}\\ &=iG\gamma_5\exp\,[iG\phi\gamma_5](\partial_\mu\phi)-\tfrac{1}{2}G^2[\phi,\partial_\mu\phi]\exp\,[iG\phi\gamma_5];\end{aligned}$$

the quantity $[\phi,\partial_\mu\phi]$ is infinite for $\mu=4$, as it contains a δ-function with zero argument. We have

$$\begin{aligned}L_1=&\zeta^*(x)\gamma_4\gamma_\mu\{iG\gamma_5(\partial_\mu\phi)-\tfrac{1}{2}G^2[\phi,\partial_\mu\phi]\}\zeta(x)\\ &+\bar{\zeta}(x)\gamma_\mu\partial_\mu\zeta(x);\qquad\ldots\ldots\qquad(2)\end{aligned}$$

also

$$L_4=ig\zeta^*(x)\gamma_4\gamma_5\gamma_\mu\zeta(x)(\partial_\mu\phi),$$

which is cancelled by the first term in (2) if $G=g$. The second term in (2) is an infinite mass renormalization term of the type discussed by R. J. N. Phillips (1954), and is dropped, as is usual for renormalization terms. Then L_1 and L_4 reduce to

$$L_1'=\bar{\zeta}(x)\gamma_\mu\partial_\mu\zeta(x).\qquad\ldots\ldots\qquad(3)$$

Now

$$\begin{aligned}L_2&=M\zeta^*(x)\exp\,[-iG\gamma_5\phi]\gamma_4\exp\,[iG\gamma_5\phi]\zeta(x)\\ &=L_2'+M\bar{\zeta}(x)\{\exp\,[2ig\gamma_5\phi(x)]-1\}\zeta(x)\end{aligned}$$

where $L_2'=M\bar{\zeta}(x)\zeta(x)$.

Thus $L=L_1'+L_2'+L_4'+L_3$

where $L_4'=M\bar{\zeta}(x)[\exp\,(2ig\gamma_5\phi)-1]\zeta(x);\qquad\ldots\ldots\qquad(4\,a)$

L_4' is the transformed interaction Lagrangian.

§ 3. Graphical Representation

The new interaction term (4 *a*) is expressible as a power series in $\phi(x)$:

$$\begin{aligned}L_4'&=M\bar{\zeta}(x)\sum_{n=1}^{\infty}[2ig\gamma_5\phi(x)]^n\zeta(x)/n\,!\\ &=M\bar{\zeta}(x)\zeta(x)\sum_{l=1}^{\infty}[2ig\phi(x)]^{2l}/(2l)\,!\\ &\quad+M\bar{\zeta}(x)\gamma_5\zeta(x)\sum_{l=1}^{\infty}[2ig\phi(x)]^{2l-1}/(2l-1)\,!.\qquad\ldots\qquad(4\,b)\end{aligned}$$

We can use the familiar graphical concepts of perturbation field theory to treat the series of perturbation terms (4 *b*). A term containing $[\phi(x)]^n$ corresponds to a vertex with an incoming and an outgoing fermion

line, representing $\zeta(x)$ and $\bar{\zeta}(x)$, plus n meson lines. These vertices fall into two classes, ' vertices of odd parity ' with $n=2l-1$, in which a factor γ_5 occurs at a vertex, and ' vertices of even parity ' with $n=2l$, in which no such factor occurs. Pairs of operators $2ig\phi(x_i)$, $2ig\phi(x_j)$, and $\zeta(x_i)$, $\bar{\zeta}(x_j)$ from vertices at x_i and x_j can be associated together in P-brackets, giving rise to multiples $-4g^2\Delta_F(x_i, x_j)$ and $S_F(x_i, x_j)$ of the usual Feynman propagators, and we can draw graphs in which vertices are connected by internal meson and fermion lines, these lines being associated with the appropriate propagators. In addition there occur vertex factors $M(\gamma_5)^n/n!$. Clearly two vertices with a large number of meson lines emanating from each may well be joined by many meson lines, and we must also remember that meson lines may begin and end at the same vertex. As in the simpler theories with scalar interactions, the S-matrix element for any process is the sum of terms corresponding to all graphs with the appropriate external lines ; but the system of graphs is very complex as any number of meson lines may connect each pair of vertices. In order to classify the system of graphs we introduce the concept of the ' skeleton ' of a graph. Consider any graph ; in general there will be more than one line (meson or nucleon) connecting any two vertices. The ' skeleton ' of the graph considered is formed by rubbing out internal meson lines until only one line (meson or nucleon) joins each pair of vertices that were joined originally. The set of all graphs with the same skeleton will often be considered together in the following work ; two or more graphs with the same skeleton will be called ' similar graphs '.

§ 4. Enumeration of Graphs

Corresponding to each graph there will generally be many similar terms in the S-matrix, since there are many ways of selecting the pairs $\phi(x_i)$, $\phi(x_j)$ from the nth and pth terms $[\phi(x_i)]^n$ and $[\phi(x_j)]^p$ of $L_4'(x_i)$ and $L_4'(x_j)$. We shall now evaluate the weight of any graph, that is, the number of terms in the S-matrix which correspond to it.

Consider a vertex in any graph with n meson lines emanating from it. Let these lines be grouped as follows :

(a) a group of $2q$ lines which join up in pairs to form ' loop lines ' at the vertex ;

(b) a group of n_1 lines which are external meson lines ;

(c) $(m-1)$ groups of n_r lines $(r=2, \ldots, m)$ which proceed in these groups to $(m-1)$ other vertices.

Then $2q+\sum_{r=1}^{m} n_r=n$.

Regarding each line within a group as indistinguishable, the number of ways of choosing the grouping of the n lines is

$$\frac{n!}{(2q)!\,\Pi n_r!}. \qquad \ldots\ldots\ldots \quad (5)$$

The number of ways of joining up n_r internal lines which leave one vertex and n_r lines which leave another, or of arranging n_1 external lines, is

$$n_r\,! \qquad \ldots\ldots\ldots\ldots \quad (6)$$

the number of ways of joining up $2q$ lines in pairs is

$$\frac{(2q)\,!}{2^q q\,!} \qquad \ldots\ldots\ldots\ldots \quad (7)$$

The product of a factor (5) for each vertex, a factor (6) for each group of n_r meson lines ($r=1, \ldots, \mathrm{m}$), a factor (7) for each vertex, and a factor $(n\,!)^{-1}$ for each vertex from (4 *b*), gives rise to the following product of factors : (i) $(n_r\,!)^{-1}$ for each group of n_r internal meson lines ; (ii) $(2^q)^{-1}$ for a vertex with q loop lines.

There are also in the matrix element factors (iii) $M(\gamma_5)^n$ for a vertex with n meson lines ; (iv) $[-4g^2\Delta_F(x_i, x_j)]^{n_r}$ for each group of n_r meson lines joining vertices at x_i and x_j ; (v) $[-4g^2\Delta_F(x_i, x_i)]^q$ for q loop lines at a vertex ; (vi) $S_F(x_i, x_j)$ for a fermion line joining vertices at x_i and x_j ; (vii) external line factors of the form $\zeta(x)$, $\bar{\zeta}(x)$ and $\phi(x)$; (viii) a factor $(-1)^k$, where k is the sum of the number of vertices in a graph and the number of polygonal fermion arcs (open or closed) ; this factor is due to anticommutation of the fermion operators, and is the same for all graphs with the same skeleton.

§ 5. Multi-Meson Propagators

We are now in a position to sum over S-matrix terms corresponding to similar graphs ; this is equivalent to summing over all possible n_r for each group of internal lines. For the moment we ignore the factors (ii) and (v), which merely give rise to a renormalization. At first sight the factors (i) and (iv) above give rise to meson propagators something like $\exp[-4g^2\Delta_F(x_i, x_j)]$. However the factors (iii) depend on

$$n=n_1+\ldots+n_m+2q\,;$$

that is, they depend on the number of meson lines in each group at the vertex. It is therefore necessary to distinguish between terms in the meson propagators with n_r even and those with n_r odd. We define odd and even meson propagators $d_o(x_i, x_j)$ and $d_e(x_i, x_j)$ by summing over odd and even n_r respectively :

$$d_o(x_i, x_j) = \sum_{l=1}^{\infty} [-4g^2\Delta_F(x_i, x_j)]^{2l-1}/(2l-1)\,!$$
$$= \sinh[-4g^2\Delta_F(x_i, x_j)], \qquad \ldots\ldots \quad (8\,a)$$

$$d_e(x_i, x_j) = \sum_{l=1}^{\infty} [-4g^2\Delta_F(x_i, x_j)^2/(2l)\,!$$
$$= \cosh[-4g^2\Delta_F(x_i, x_j)]\,; \qquad \ldots\ldots \quad (8\,b)$$

likewise we define odd and even fermion propagators

$$s_o(x_i, x_j) = \sinh\,[-4g^2 \Delta_F(x_i, x_j)] \,.\, S_F(x_i, x_j) \quad . \quad . \quad . \quad (9\,a)$$

and $$s_e(x_i, x_j) = \cosh\,[-4g^2 \Delta_F(x_i, x_j)] \,.\, S_F(x_i, x_j). \quad . \quad . \quad . \quad (9\,b)$$

Skeletons can be drawn in which any number of fermion lines are joined end to end. To take account of this iteration of fermion lines, we should replace s_e and s_σ by 'iterated propagators' S_e and S_σ, defined by a Bethe–Salpeter equation. In momentum representation, S_e and S_σ are simple algebraic functions of s_e and s_σ. However, the Fourier transforms of $s_e\,(x)$ and $s_\sigma\,(x)$ are infinite; this difficulty must be overcome before S_e and S_σ can be properly defined.

Now take all terms formed from the skeleton by writing (*a*) d_o *or* d_e for each meson line; (*b*) s_o *or* s_e for each fermion line; (*c*) M or $M\gamma_5$ for each vertex (according to the parity of the vertex, as discussed below); (*d*) $\bar{\zeta}$, ζ and ϕ for the appropriate external lines; then the sum of all such terms is the sum over all graphs with the same skeleton, apart from the factor $(-1)^k$, as it takes into account all possible values of the n_r for each group of meson lines. It remains for us to specify the factor (*c*) more clearly; a factor γ_5 occurs at a vertex when $\sum_{r=1}^{m} n_r$ at the vertex is odd. If we are evaluating a particular term with various odd and even propagators corresponding to lines in the skeleton, it is best to label the lines with minus (odd) and plus (even) signs, giving each a parity. The parity of a vertex in the skeleton is then the product of the parities of the lines arriving at the vertex; then it is easy to insert the correct factors $M\gamma_5$ and M for the odd and even parity vertices respectively.

The factors (ii) and (v) have so far been left out of account. They can be treated separately, since the numbers q occur only in these factors, $(\gamma_5)^{2q}$ in factor (iii) being equal to unity always. These factors, summed over q at a vertex, give a term

$$\sum_{q=0}^{\infty} (q\,!)^{-1}[-8g^2 \Delta_F(x_i, x_i)]^q = \exp\,[-8g^2 \Delta_F(x_i, x_i)]. \quad . \quad . \quad (10)$$

Since $\Delta_F(x, x)$ possesses a δ-function infinity, the vertex factor (10) is a zero of a high order. It is however just a renormalization factor which appears at every vertex. Without any more justification than is provided by similar situations in simpler theories, we omit these vertex factors.

§ 6. Fermion Loop Lines

A further type of divergence is encountered when we consider vertices in skeletons which have several meson lines (either external or connecting with other vertices) and a fermion 'loop line' which begins and ends at the vertex. The cloud of mesons which usually accompanies the fermion line has been eliminated already by the meson loop line renormalization; so the fermion loop line contributes a factor

$$\int \frac{dp}{i\gamma p + M}$$

to the matrix element ; this is a divergent integral which is also encountered as a vacuum polarization term. It is independent of the number and the nature of the meson lines at the vertex, and it can be subtracted out completely by introducing a term

$$-M \operatorname{Tr}\left[\frac{(2ig\phi\gamma_5)^n}{n\,!}\int\frac{dp}{i\gamma p+M}\right]$$

into the Lagrangian, where n is the number of meson lines at the vertex in the *graph* considered. Summing over n, we see that all skeletons containing fermion loop lines are entirely eliminated by adding to the Lagrangian a term

$$-M \operatorname{Tr}\left[\exp\,(2ig\gamma_5\phi)\int\frac{dp}{i\gamma p+M}\right].$$

This further renormalization enables us to omit skeletons containing fermion loop lines.

§ 7. Examples

First we shall demonstrate by a simple example the type of graph and skeleton that can occur. The example is what we might term a third-order nucleon–nucleon interaction. The graph (*a*) represents the type of graph we are considering, with a cloud of mesons passing between each pair of vertices. The skeleton of all such graphs is shown in diagram (*b*). the vertices being labelled 1, 2, 3, for convenience. Each line can have parity + or −, so that there are eight possible labellings of the line parities ; we have labelled diagram (*b*) with one of the eight labellings. Diagram (*c*) shows the corresponding vertex parities. From the skeleton

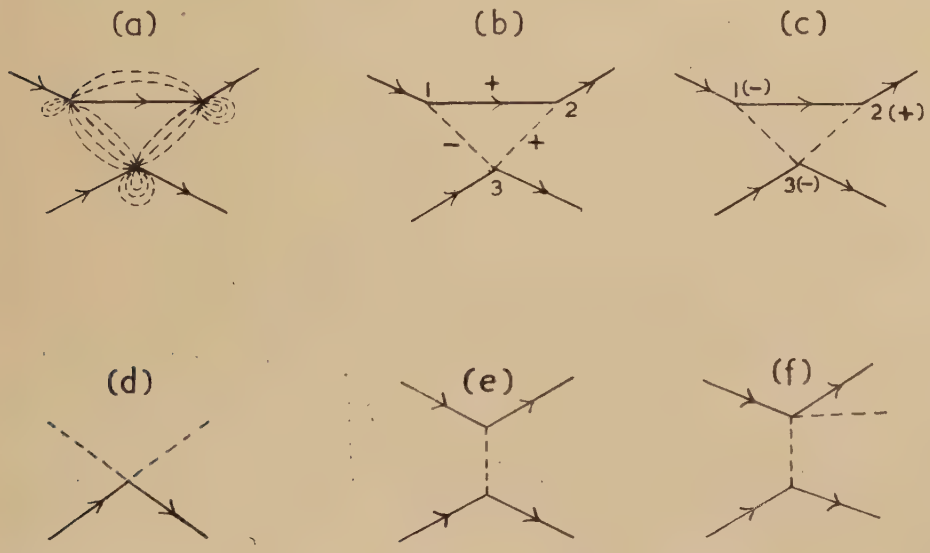

we can write down the matrix element ; it is a multiple of

$$\iiint dx_1\, dx_2\, dx_3[\bar{\zeta}(x_2)Ms_e(x_2, x_1)M\gamma_5\zeta(x_1)]$$

$$\times[\zeta(x_3)M\gamma_5\zeta(x_3)]\, d_e(x_2, x_3)\, d_o(x_3, x_1). \quad . \quad . \quad . \quad . \quad (11)$$

The questions of convergence and evaluation of integrals such as (11) are complex, and no attempt is made here to discuss them.

As in electrodynamics and other weak-coupling theories the simplest processes (represented by the simplest skeletons) do not involve evaluation of integrals in momentum space of the type which occur in (11). The simplest process we can consider is meson–nucleon scattering in first order, with skeleton (*d*) ; we do not even have to deal with the new propagators to work out this term. The simplest nucleon–nucleon scattering process has skeleton (*e*) ; at low energies we may expect only the even propagator to contribute to this term, because of the γ_5 factors occurring with the odd propagator. The simplest meson production skeleton (*f*) is very similar to (*e*) ; skeletons of this type also give rise to multiple meson production. Glauber (1951) has already discussed physical effects corresponding to the simplest graphs.

§ 8. Conclusion

This method of dealing with gradient interaction is not readily extended to charged and symmetric meson theories ; the Dyson transformation does not apply to these theories, due to the non-commutative properties of the τ-matrices. It may be possible however to define a new symmetric theory by generalizing the interaction Lagrangian (4 *a*).

Since this paper was submitted for publication, some work by R. Arnowitt and S. Deser (1955) has come to the notice of the author. This work covers much the same ground as the present paper, and the two pieces of work have been done simultaneously.

The author is very grateful for much help and constructive criticism given by Dr. K. Burton, Dr. A. H. de Borde and Dr. R. G. Moorhouse, and for the constant encouragement of Professor J. L. B. Cooper.

References

Arnowitt, R. and Deser, S., 1955, *Phys. Rev.*, **100,** 349.
Dyson, F. J., 1948, *Phys. Rev.*, **73,** 929.
Glauber, R. J., 1951, *Phys. Rev.*, **84,** 395.
Phillips, R. J. N., 1954, *Phys. Rev.*, **96,** 1678.

XXXII. *On the Steady Flow past a Sphere at High Reynolds Number using Oseen's Approximation*

By K. Stewartson
Department of Mathematics, The University, Bristol †

[Received October 27, 1955]

Summary

The flow of a viscous fluid past a sphere at high Reynolds number as given by Oseen's approximation, in which the inertia terms of the equations of motion are linearized, is discussed. It is found that a boundary layer is formed on the forward side and a wake extending to infinity on the rearward side. Inside the wake, which is bounded by a circular cylinder with its generators parallel to the undisturbed direction of the streamlines, the fluid at infinity is moving towards the sphere, while outside it is moving away with the undisturbed velocity, and there is a shear layer at the cylinder.

§ 1. Introduction

Recently in two papers (Pearcey and McHugh 1955, Tomotika and Aoi 1950) the steady flow past a sphere at low Reynolds number R according to Oseen's approximation has been discussed. In the first of these Tomotika and Aoi (1950) consider the flow at $R \equiv 2aU/\nu = 1$, where U is the velocity of the undisturbed stream, a is the radius of the sphere and ν is the kinematic viscosity, and announce the presence of a small vortex behind the sphere. Their calculations are extended in the second paper, by Pearcey and McHugh (1955), who however do not find such a vortex even when $R = 10$. There is thus some doubt whether Oseen's equations of motion will reveal the presence of a vortex at any Reynolds number. Since a solution of these approximate equations is useful as a guide to the solution of the full Navier Stokes equations it is of interest to examine it at high Reynolds number to see if the vortex is present.

A full discussion of Oseen's equations at high Reynolds number was first given by Oseen himself (1927) who obtained the conditions satisfied by the inviscid part of the flow in general and obtained the explicit solution for the steady flow past a circular cylinder for which there is such a vortex and a thin plate. His discussion is in some ways a little involved and so here in § 2 a shorter derivation of his principal results is given. In § 3 these are applied to the sphere in a uniform flow.

Let C be a circular cylinder circumscribing the sphere and extending downstream of it, and with its generators parallel to the x-axis which is

† Communicated by the Author.

the direction of the stream. It is then found that inside C the fluid is moving with vorticity, and with a speed of never more than about a quarter of the mainstream velocity, towards the sphere and C. It reaches C first and there the velocity component parallel to the x-direction is discontinuous so that outside C the fluid moves away from the sphere with a velocity which is ultimately constant. Beyond this fluid moving in an infinitely long vortex is fluid which has come directly from an infinite distance upstream and whose motion is irrotational except in the immediate neighbourhood of the forward side of the sphere where there is a boundary layer. The thickness of the boundary layer is $O(\nu)$ as against $O(\nu^{1/2})$ for a boundary layer derived from the Navier Stokes equations. Of course the discontinuity on C is the limit of a shear layer whose thickness is $O(\nu^{1/2})$ and it may be regarded as an extension of the boundary layer on the forward side of the sphere. The presence of the boundary layer on the forward side of the sphere confirms the trend indicated by Pearcey and McHugh (1955) but they did not find the vortex and from their diagrams there were only the barest of hints that it would ultimately appear.

It is interesting to consider whether the approximate solution at large values of R throws any light on the exact (although unstable) solution of the full Navier Stokes equations. For this purpose we must bear in mind first that the basic assumption of the approximate theory is that any transportable quantity such as vorticity is carried not with the fluid but parallel to the x-axis with the undisturbed velocity of the fluid. Thus it is seriously in error in the boundary layer on the forward side of the sphere leading to the wrong order of magnitude for its thickness, and in the wake where the direction of motion of the fluid is almost reversed. Second the approximate equations being linear there is no breakdown in the derived boundary layer equations when the skin friction vanishes and in fact the only restriction on the boundary layer is that it is confined to the forward side of the sphere. For a fluid satisfying the Navier Stokes equations a paper of Goldstein (1948) indicates that when the skin friction vanishes the conventional boundary layer probably comes to an end and there is ample evidence from observations to confirm it. The main stream then leaves the body. With these two differences in mind it is inferred from the approximate solution that near the front stagnation point there is a boundary layer which separates from the sphere when the skin friction vanishes. Outside the stream tube which leaves the sphere here is the main body of the fluid moving irrotationally; inside the flow is vortex like and *may* satisfy the no slip condition on the sphere without any necessity for a boundary layer.

The simplest solution of this type is that in which the fluid inside the breakaway stream tube is at rest (Kirchhoff flow) and for a circular cylinder the corresponding flow has already been suggested as being appropriate (Imai 1953, Kawaguti 1953, Squire 1934). However such a conclusion has a grave objection for the two dimensional flow. The argument in favour is briefly as follows. Let us suppose that breakaway

occurs at an angular distance α from the front stagnation point. Then Schmieden (1932) has shown that if $\alpha<55°$ there is a contradiction because the free streamline crosses the cylinder. If $\alpha>55°$ the free streamline has an infinite curvature at breakaway which means an infinite pressure gradient so that the skin friction vanishes at an angular distance $\beta<\alpha$ from the front stagnation point, which is also a contradiction. Further as $\alpha\to 55°+$, $\beta\to 55°+$ and so it is concluded that the correct value of α is 55°. The objection to this is that if $\alpha=55°$ the pressure gradient upstream of separation is always favourable so that at 55° the skin friction is certainly not zero. Although it has not been proved that breakaway cannot occur before the skin friction vanishes (so that it would be discontinuous there) no evidence in support is forthcoming and it is unlikely. In that case the limiting argument given above is misleading and irrelevant once it is established that the limit flow does not satisfy the condition required.

Another solution of this type which is unacceptable is that given by Lighthill (1953) for the flow over a step on a flat plate. He assumed that separation occurred at a distance x from the leading edge of the plate and calculated the resulting Kirchhoff flow. The value of x was then found by an approximate boundary layer theory. The objection to this is that whatever value of x is chosen the pressure gradient is singular at x so that separation must occur at a distance $y<x$ from the leading edge. Thus if the flow is of the Kirchhoff type separation must occur at or very near to the leading edge of the plate.

A second possible type of flow at infinite Reynolds number may be inferred from some recent work of Southwell and Allen (1955) who obtained a numerical solution of the steady flow past a circular cylinder at Reynolds numbers of 1, 10, 100, and 1000. A study of the streamlines they display suggests that the flow at infinite Reynolds number may consist of a potential flow together with a pair of vortices. This interpretation of their work leads to a difficulty also, for such a solution would involve breakaway at a stagnation point. However in all known instances of a main stream accelerating from one stagnation point and then slowing down to another the skin friction vanishes well before the rear stagnation point. Further numerical work seems called for to elucidate the behaviour of the vortices and to ascertain whether perhaps more are formed at higher Reynolds number.

§ 2. Flow at Large Reynolds Number

The body is taken to be at rest and at an infinite distance upstream the fluid moves in the direction of the x-axis (x increasing) with uniform velocity U. In the form of Oseen's approximation which we shall use here the non-linear terms ($\mathbf{u}$. grad) $\mathbf{u}$, where $\mathbf{u}$ is the fluid velocity with components (u, v, w), in the Navier Stokes equations are replaced by $U(\partial\mathbf{u}/\partial x)$ reducing them to

$$U\frac{\partial \mathbf{u}}{\partial x}=-\frac{1}{\rho}\mathbf{grad}\ p+\nu\nabla^2\mathbf{u},\ \text{div}\ \mathbf{u}=0 \quad . \quad . \quad . \quad . \quad . \quad (2.1)$$

where ρ is the constant density of the fluid, p is the pressure and ν the kinematic viscosity. It is noted that Oseen (1927) preferred a slightly different form for (2.1) in which p is replaced by $q=p+\frac{1}{2}\rho\mathbf{u}^2$. The difference in physical terms is that (2.1) assumes that the perturbation of the velocity is small compared with its undisturbed value whereas Oseen's form assumes only that the product of the perturbation of the velocity and the vorticity is negligible. If the motion is irrotational or nearly so it is clear that Oseen's form is more acceptable and would give a more accurate estimation of the pressure. However, such irrotational flows are always adjacent to boundary layers in which the velocity changes rapidly so that Oseen's form is bound to lead to pressure discontinuities at infinite Reynolds number which are known not to occur in practice. In the form which we choose however the pressure is always continuous and so it is felt that a more realistic overall picture is obtained. In any case it is only the pressure which is involved in the difference and we cannot expect too close an agreement with the correct solution whichever point of view we take.

The boundary conditions to be satisfied are that at an infinite distance upstream

$$\mathbf{u}=(U, 0, 0) \quad . \quad . \quad . \quad . \quad . \quad . \quad . \quad . \quad . \quad (2.2)$$

and on the body $\mathbf{u}=0$.

In the usual way we write

$$p=-\rho U(\partial\phi/\partial x) \quad \text{where} \quad \nabla^2\phi=0 \quad . \quad . \quad . \quad . \quad (2.3)$$

whence

$$\mathbf{u}=\mathbf{grad}\ \phi+\mathbf{u}^* \quad . \quad . \quad . \quad . \quad . \quad . \quad . \quad . \quad (2.4)$$

with

$$\nabla^2\mathbf{u}^*=2k\frac{\partial\mathbf{u}^*}{\partial x}, \quad \text{div}\ \mathbf{u}^*=0 \quad \text{and} \quad k=U/2\nu.. \quad . \quad . \quad . \quad . \quad (2.5)$$

The principal result we wish to establish in this section is that if (x_0, y, z) is a point on the body and (x_1, y, z) a neighbouring point outside it

$$\mathbf{u}^*(x_1, y, z)=\mathbf{u}^*(x_0, y, z) \quad \text{if } x_1>x_0$$

and

$$\mathbf{u}^*(x_1, y, z)=0 \quad \text{if } x_1<x_0 \quad . \quad . \quad . \quad . \quad . \quad . \quad (2.6)$$

in the limit as $k\to\infty$. Thus on the side of the body facing the oncoming stream there is a boundary layer at large values of the Reynolds number (i.e. k) in which $\mathbf{u}^*$ rapidly falls from its value on the body to zero just outside, while on the rear side $\mathbf{u}^*$ is independent of x and so a wake is formed. These results may be proved fairly easily as follows. Let us consider a finite value of k. Then at infinity $\mathbf{u}^*=0$ and $\phi=Ux$ to satisfy the boundary conditions there. We suppose that the equation of the body is $x=f(y, z)$ and α represents distance from the body along the outward drawn normal which has direction cosines (l, m, n) relative to the orthogonal frame of reference. If, on the body,

$$\mathbf{u}^*=\mathbf{A}(y, z), \quad \frac{\partial}{\partial\alpha}[\mathbf{u}^*\exp(-kx)]=k\mathbf{B}(y, z)\exp(-kx) \quad . \quad . \quad (2.7)$$

then at any external point

$$4\pi\mathbf{u}^*=\int_S\int\frac{dy'dz'}{l}\exp(kx)\Big\{k\mathbf{B}(y',z')\frac{\exp(-kx'-kR)}{R}$$
$$-\exp(-kx')\mathbf{A}(y',z')\frac{\partial}{\partial\alpha}\left[\frac{\exp(-kR)}{R}\right]\Big\} \quad . \quad . \quad . \quad (2.8)$$

where $R^2=(x-x')^2+(y-y')^2+(z-z')^2$ the integral being taken over the surface of the body. The behaviour of the integral is required when k is large it being assumed and proved *a posteriori* that **A** and **B** do not vary rapidly with y' and z' except possibly at isolated points. No evidence for such a possibility is present in the solutions at small values of k and as we shall see below a complete solution may be found in which **A** and **B** do not vary rapidly.

It is sufficient to consider the contribution $\mathbf{u}_1^*$ to $\mathbf{u}^*$ where

$$4\pi\mathbf{u}_1^*=\int_S\int\frac{dy'dz'}{l}k\mathbf{B}\frac{\exp[k(x-x'-R)]}{R} \quad . \quad . \quad . \quad . \quad . \quad (2.9)$$

corresponding to a surface distribution of sources, for the effect of **A** which corresponds to a surface distribution of doublets may then be deduced from it. It is also sufficient to assume that any line parallel to the x-axis cuts the body in at most two points. The integrand of (2.9) is exponentially small when k is large unless $y-y'$ and $z-z'$ are both vanishingly small so that if the line through (x, y, z) parallel to the x-axis does not meet the body at all $\mathbf{u}_1^*\to0$ as $k\to\infty$. If it does let one of the points of intersection be (ξ, y, z). Then in (2.9) $\mathbf{B}(y', z')$ may be replaced by $\mathbf{B}(y, z)$ and taken outside the sign of integration and for the contribution to $\mathbf{u}_1^*$, from the neighbourhood of (ξ, y, z) we must evaluate

$$k\mathbf{B}(y,z)\int\int\frac{dy'dz'}{lR}\exp[k(x-x'-R)] \quad . \quad . \quad . \quad . \quad (2.10)$$

taken over the infinite plane $lx'+my'+nz'=l\xi+my+nz$.

Write

$$(y-y')(1-l^2)^{1/2}=lmr\cos\theta+nr\sin\theta+lm(x-\xi)(1-l^2)^{1/2},$$
$$(z-z')(1-l^2)^{1/2}=lnr\cos\theta-mr\sin\theta+ln(x-\xi)(1-l^2)^{1/2}$$

and (2.10) becomes

$$k\mathbf{B}\int_0^\infty\frac{rdr}{[r^2+l^2(x-\xi)^2]^{1/2}}\int_0^{2\pi}d\theta\exp k[kl^2(x-\xi)-(1-l^2)^{1/2}r\cos\theta$$
$$-(r^2-l^2(x-\xi)^2)^{1/2}]$$
$$=\pi k\mathbf{B}\int_0^\infty\frac{rdr}{[r^2+l^2(x-\xi)^2]^{1/2}}I_0(kr(1-l^2)^{1/2})\exp k[l^2(x-\xi)$$
$$-(r^2+l^2(x-\xi)^2)^{1/2}]. \quad (2.11)$$

$$\left.\begin{aligned}&=2\pi k\mathbf{B} \quad \text{if } x>\xi\\&=2\pi k\mathbf{B}\exp[2kl^2(x-\xi)] \quad \text{if } x<\xi\end{aligned}\right\} \quad . \quad . \quad . \quad . \quad . \quad . \quad . \quad . \quad . \quad (2.12)$$

(Doetsch 1943). Similar results hold for the second point of intersection between the line and the body and also for **A**. It is concluded therefore

that (2.12) is the limiting value $\mathbf{u}^*$ where now $\mathbf{B}$ is a function of y and z to be determined and ξ is that intersection of the line $y=y'$, $z=z'$ with the body nearer to (x, y, z). The results may also be written as

$$\left.\begin{aligned} &\frac{\partial \mathbf{u}^*}{\partial \alpha} \to \infty \quad \text{as } k \to \infty \text{ on the front side of the body,} \\ \text{and} \quad &\frac{\partial \mathbf{u}^*}{\partial x} \to 0 \quad \text{as } k \to \infty \text{ on the rear side.} \end{aligned}\right\} \quad . \quad . \quad (2.13)$$

The boundary conditions on ϕ as $k \to \infty$ may now be determined. On the front side of the body

$$0 = \operatorname{div} \mathbf{u}^* = 2\pi\left(\frac{\partial B_y}{\partial y} + \frac{\partial B_z}{\partial z}\right) + 4\pi l^2 k\left(u^* - \frac{\partial \xi}{\partial y} v^* - \frac{\partial \xi}{\partial z} w^*\right). \quad . \quad . \quad (2.14)$$

Since the first term is finite the last terms on the right hand must remain finite as $k \to \infty$ and so

$$u^* - \frac{\partial \xi}{\partial y} v^* - \frac{\partial \xi}{\partial z} w^* \to 0. \quad . \quad . \quad . \quad . \quad . \quad (2.15)$$

Then the normal component of $\mathbf{u}^* \to 0$ as $k \to \infty$ and therefore so also does the normal component of **grad** ϕ.

On the rear side when k is large,

$$0 = \operatorname{div} \mathbf{u}^* = \left(\frac{\partial v^*}{\partial y}\right)_{x,z} + \left(\frac{\partial w^*}{\partial z}\right)_{x,y}. \quad . \quad . \quad . \quad . \quad (2.16)$$

Introducing a new coordinate $\beta = x - \xi$ instead of x (2.16) implies that

$$\left(\frac{\partial v^*}{\partial y}\right)_{\beta,z} + \left(\frac{\partial w^*}{\partial z}\right)_{\beta,y} = 0 \quad \text{at } \beta = 0 \quad . \quad . \quad . \quad . \quad . \quad . \quad (2.17)$$

and since $\mathbf{u}^* = -$**grad** ϕ on the body

$$\frac{\partial^2 \phi}{\partial x \partial y}\frac{\partial \xi}{\partial y} + \frac{\partial^2 \phi}{\partial y^2} + \frac{\partial^2 \phi}{\partial x \partial z}\frac{\partial \xi}{\partial z} + \frac{\partial^2 \phi}{\partial z^2} = 0, \quad . \quad . \quad . \quad (2.18)$$

ϕ being regarded as a function of x, y, z. Since ϕ is harmonic (2.18) reduces to

$$0 = \left(\frac{\partial}{\partial x} - \frac{\partial \xi}{\partial y}\frac{\partial}{\partial y} - \frac{\partial \xi}{\partial z}\frac{\partial}{\partial z}\right)\frac{\partial \phi}{\partial x} = \frac{\partial}{\partial \alpha}\left(\frac{\partial \phi}{\partial x}\right). \quad . \quad . \quad . \quad (2.19)$$

Thus on the rear side of the derivative $\partial\phi/\partial x$ along the normal is zero in the limit $k \to \infty$.

In a two-dimensional flow (i.e. independent of z) (2.16) simplifies immediately to $v^* = $ constant. Since $\phi = Ux$ at an infinite distance downstream and $\mathbf{u}^* = 0$ outside the wake (bounded by C) the integrated form of the equation of continuity shows that the constant must be zero. Hence $\partial\phi/\partial y = 0$ on the rear side of the body.

If there is symmetry about the x-axis and r denotes distance from it a similar argument shows that $\partial\phi/\partial r = 0$ on the rear side.

The boundary conditions which have been obtained above are all originally due to Oseen (1927).

At infinite Reynolds number therefore the ultimate flow is irrotational except in the wake which is bounded by the cylindrical surface C touching and extending downstream of the body and with generators parallel to the x-axis. This potential flow involves slip past the front side of the body which is reduced to rest by a boundary layer whose thickness is $0(\nu)$ from (2.12). This may be contrasted with the boundary layers in the full Navier Stokes equations whose thicknesses are $0(\nu^{1/2})$ in comparable cases. In the wake a flow with velocity components independent of x and which is rotational is added to the potential flow. This means that in the wake the fluid velocities do not tend to the uniform flow at infinity.

§ 3. Application to a Sphere

The results of § 2 are now applied to the flow past a sphere, using a method originally given by Burgers (1921) for the flow past a circular cylinder. For that problem however Zeilon (1923) was later able to obtain the solution in closed form using a theorem of Hilbert.

First we must find ϕ. Let r denote distance from the axis of symmetry and write $x=aR\cos\theta$, $r=aR\sin\theta$, $|\theta|\leqslant\pi$ where a is the radius of the sphere. Then ϕ is harmonic and satisfies

$$\left.\begin{aligned} &\partial\phi/\partial R=0 \quad \text{if } R=1 \quad \text{and} \quad \pi=|\theta|\leqslant\pi/2 \\ &\partial\phi/\partial r=0 \quad \text{if } R=1 \quad \text{and} \quad |\theta|\leqslant\pi/2 \end{aligned}\right\} \qquad . \quad . \quad . \quad . \quad (3.1)$$

and $\phi\sim UaR\cos\theta$ when R is large.
Further we write

$$\phi=UaRP_1(\mu)+Ua\sum_{n=0}^{\infty}\frac{A_n}{(n+1)R^{n+1}}P_n(\mu) \qquad . \quad . \quad . \quad . \quad (3.2)$$

where the P_n are Legendre polynomials with $\mu=\cos\theta$ and the A_n are constants to be determined in the course of the analysis. The third condition of (3.1) is automatically satisfied and so are the others if

$$\left.\begin{aligned} &L(\mu)\equiv P_1-\sum_{n=0}^{\infty}A_nP_n=0 \qquad -1\leqslant\mu\leqslant 0 \\ &\text{and} \\ &M(\mu)\equiv-\sin\theta\sum_{n=0}^{\infty}\frac{A_nP'_{n+1}}{n+1}=0 \qquad 0\leqslant\mu\leqslant 1. \end{aligned}\right\} \quad . \quad . \quad . \quad (3.3)$$

Following Burgers we solve these equations by the method of least squares minimizing

$$X\equiv\int_{-1}^{0}L^2(\mu)d\mu+\int_{0}^{1}M^2(\mu)d\mu. \qquad . \quad . \quad . \quad (3.4)$$

For this purpose we make use of the following results which are either given or may be deduced from formulae in Modern Analysis (Whittaker and Watson 1927)

$$\int_{-1}^{0}P_iP_jd\mu=\int_{0}^{1}(1-\mu^2)P_i'P_j'd\mu=0$$

if $i-j$ is even and not zero; and if i is odd j is even

$$\int_{-1}^{0}P_iP_jd\mu=-\frac{1}{j(j+1)}\int_{0}^{1}(1-\mu^2)P_i'P_i'd\mu=\frac{P_j(0)P_i'(0)}{(j-i)(j+i+1)} \quad . \quad . \quad (3.5)$$

Then
$$X\equiv\sum_{n=0}^{\infty}A_n^2\left(\frac{1}{2n+1}+\frac{n+2}{(n+1)(2n+3)}\right)-2\sum_{\substack{n\text{ even}\\ m\text{ odd}}}A_nA_m\times\frac{(n-m)P_n(0)P_m'(0)}{(n-m)(n+m+1)(m+1)(n+m+3)}$$
$$-\tfrac{2}{3}A_1-2\sum_{n\text{ even}}\frac{A_nP_n(0)}{(n-1)(n+2)}+\tfrac{1}{3}. \qquad (3.6)$$

For X to be a minimum $\partial X/\partial A_n=0$ for all A_n and so we can set up an infinite set of simultaneous linear equations for the A_n with solution

$$\left.\begin{aligned}&A_0=-0{\cdot}2645,\ A_1=+0{\cdot}4745,\ A_2=-0{\cdot}3201,\ A_3=+0{\cdot}011\\&A_4=+0{\cdot}100,\ A_5=-0{\cdot}006,\ A_6=-0{\cdot}054,\ A_7=+0{\cdot}004,\\&A_8=+0{\cdot}033,\ A_9=-0{\cdot}004,\ A_{10}=-0{\cdot}024\end{aligned}\right\} \qquad (3.7)$$

while for higher values of n

$$A_n\sim(-)^{n/2-1}\left(\frac{2}{\pi n^3}\right)^{1/2} \quad \text{if } n \text{ is even}$$
$$\sim(-)^{\frac{1}{2}(n+1)}\frac{1}{q}\left(\frac{2}{\pi n^3}\right)^{1/2} \quad \text{if } n \text{ is odd where } q\approx 10.$$

If now a stream function $\psi=\psi_0+\psi_1$ is introduced, defined by

$$\partial\psi/\partial r=ru, \quad -\partial\psi/\partial x=rv$$

where $(u\ v)$ are the components of $\mathbf{u}$ in the axial and radial directions, ψ_0 is the contribution from ϕ and ψ_1 is the contribution from $\mathbf{u}^*$ it follows from (3.2) that

$$\psi_0=\tfrac{1}{2}Ua(1-\mu^2)R^2-Ua(1-\mu^2)\sum_1^{\infty}\frac{A_nP_n'(\mu)}{n(n+1)R^n}+UaA_0(1+\mu). \qquad (3.8)$$

Further $\psi_1=0$ except inside C where

$$\frac{\partial\psi_1}{\partial r}=-\frac{\partial\phi}{\partial x} \quad \text{on } R=1$$

since $\mathbf{u}=0$ there. Since $\dfrac{\partial\psi}{\partial r}=\dfrac{\partial\psi}{\partial x}=0$ on $R=1$, $0\leqslant\mu\leqslant1$ and $\psi=0$ on $R=1$, $-1\leqslant\mu\leqslant0$, $\psi=0$ on $R=1$, $0\leqslant\mu\leqslant1$.

Therefore since ψ_1 is independent of x

$$\psi_1=-\tfrac{1}{2}Ua(1-\mu_1^2)+Ua(1-\mu_1^2)\sum_1^{\infty}\frac{A_nP_n'(\mu_1)}{n(n+1)}-UaA_0(1+\mu_1) \qquad (3.9)$$

where $a^2(1-\mu_1^2)=r^2$, if $0\leqslant\mu_1\leqslant1$ and is zero otherwise.

The streamlines are sketched in fig. 1 and their most striking feature is the slow inflow throughout the wake ($r\leqslant a$, $x>0$). As each streamline reaches C its direction abruptly changes because of the discontinuity in u at $r=a$, $x>0$ and it moves outward to infinity. At large but not infinite Reynolds number there will be a shear layer along this surface and a boundary layer along the front side of the sphere. Further the wake will be closed and its length of order a^2U/ν so that the streamlines on which ψ is negative are also closed.

The pressure on the sphere is given by

$$p=-\rho U\partial\phi/\partial x=\rho U^2\sum_0^\infty A_nP_{n+1}(\mu) \quad . \quad . \quad . \quad (3.10)$$

Fig. 1

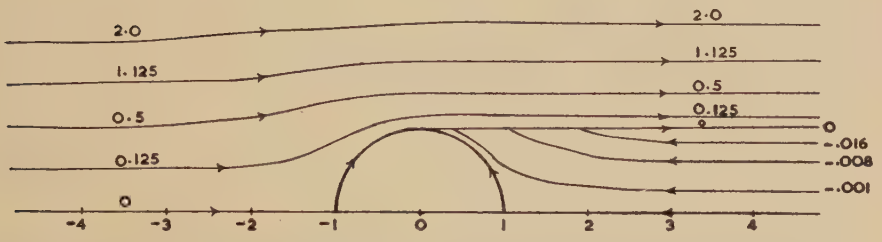

Streamlines of flow past a sphere at high Reynolds number according to Oseen's approximation. The value of ψ on each streamline is marked on the figure.

Fig. 2

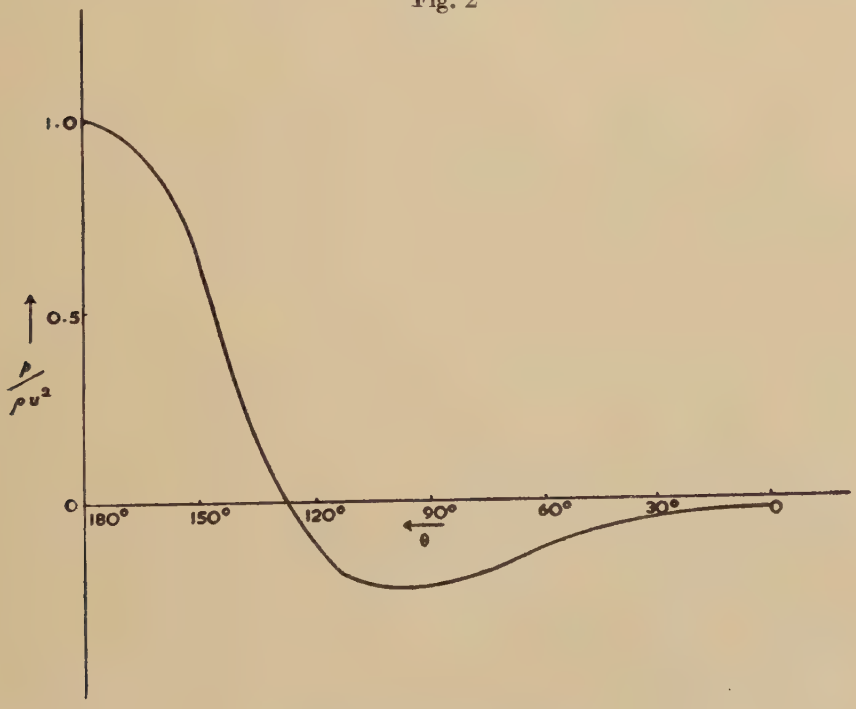

Pressure on the sphere.

and is displayed in fig. 2. It is noted that the wake velocity at infinity which is in the direction of x, is given by $p'/\rho U$ in the range $0\leqslant|\theta|\leqslant\pi/2$ with $r=a\sin\theta$. The contribution D_p from the pressure to the drag D on the sphere is

$$D_p=-\int_0^\pi 2\pi a^2\sin\theta\cos\theta p d\theta=-\frac{4}{3}\pi\rho U^2a^2A_0. \quad . \quad . \quad (3.11)$$

so that the contribution from the pressure to the drag coefficient is

$$C_p = \frac{D_p}{\pi a^2 \rho U^2} = 0{\cdot}35.$$

In addition to the pressure a strict interpretation of Oseen's theory means that there will also be a contribution from the skin friction, for the normal derivative of $\mathbf{u}^*$ is $0(k)$ on the forward side and so when multiplied by the coefficient of viscosity a density of order one is obtained for the skin friction. With the full Navier Stokes equation the skin friction density would be $0(\nu^{1/2})$ when ν is small. Tomotika and Aoi (1950) have shown that on a sphere the skin friction contributes twice as much the pressure to the drag for all k and so in the limiting case $k \to \infty$ we have

$$D = 3D_p = 1{\cdot}06\pi a^2 U^2 \rho$$

and

$$C_D = 1{\cdot}06.$$

This result may be compared with the values of C_D, namely 2·85 at $R=10$ and 2·08 at $R=20$, obtained by Goldstein (1929).

Acknowledgments

The author is indebted to Professor P. A. Lagerstrom and Dr. S. Kaplun for long and stimulating discussions on flow at high Reynolds number during 1953–4 when he was a Research Fellow at the California Institute of Technology. He is also grateful to Professor L. Howarth for his continued interest and advice.

References

Burgers, J. M., 1921, *Kon. Ak. v. Wetenschappen te Amsterdam*, Deel 29.
Doetsch, G., 1943, *Laplace Transformation* (Dover), p. 403.
Goldstein, S., 1929, *Proc. Roy. Soc.* A, **123**, 226 ; 1948, *Quart. J. Mech. and Appl. Math.*, **1**, 42.
Imai, Isao., 1953, *J. Phys. Soc., Japan*, **8**, 399.
Kawaguti, M., 1953, *J. Phys. Soc., Japan*, **8**, 403.
Lighthill, M. J., 1953, *Proc. Roy. Soc.* A, **217**, 344.
Oseen, C. W., 1927, *Neuere Methoden und Ergebnisse in der Hydrodynamik* (Leipzig : Akademische Verlagsgesellschaft M.B.H. Leipzig).
Pearcey, T., and McHugh, B., 1955, *Phil. Mag.*, **46**, 783.
Schmieden, C., 1932, *Ing. Arch.*, **3**, 356.
Southwell, R. J., and Allen, D. N. de G., 1955, *Quart. J. Mech. and Appl. Math.*, **8**, 129.
Squire, H. B., 1934, *Phil. Mag.*, **17**, 1150.
Tomotika, S., and Aoi, I., 1950, *Quart. J. Mech. and Appl. Math.*, **3**, 140.
Whittaker, E. J., and Watson, G. N., 1927, *Modern Analysis* (Cambridge : University Press), Chap. 15.
Zeilon, N., 1923 *K. Sv. Vetenskapsakademiens Handlinger*. Ser. 3, Band 1.

XXXIII. ^{8}Li *Emission from Proton Induced Disintegrations at* 950 Mev

By B. A. Munir
Department of Physics, University of Birmingham†

[Received November 8, 1955]

Summary

G5 plates exposed to 950 Mev protons were are ascanned and fifty ^{8}Li ' Hammer stars ' discovered. They were divided into stars representing light and heavy nuclei disintegrations. In the case of light element stars the energy and angular distributions of the ^{8}Li fragment indicate that it is the residual nucleus after a light element breakup. For heavy nuclei stars the mechanisms of direct knock-on and evaporation can be excluded. The simplest hypothesis is that the fragments are ejected as part of the cascade process.

§ 1. Introduction

A T-shaped track associated with a cosmic ray star was first reported by Occhialini and Powell (1947) and was thought to be due to a ^{8}Li fragment coming out of a nuclear disintegration and decaying at rest into two alpha particles and an electron. This was later confirmed by Franzinetti and Payne (1948) and Pickup and Voyvodic (1949). Alvarez (1950) pointed out that $^{8}_{5}$B should also give a similar ' Hammer track ', though ^{8}Li emission should be more common due to a smaller potential barrier facmg a ^{8}Li nucleus.

Studies of ^{8}Li fragments coming out of nuclear disintegrations have been made by several workers. Wright (1950) measured the cross sections for ^{8}Li production in light and heavy elements by bombarding them with 340 Mev protons and 190 Mev deuterons. He found a sharp discontinuity in the production cross sections in light and heavy elements. Hodgson (1951) analysed ^{8}Li fragments associated with cosmic ray stars and compared his results with predictions of the ' Evaporation theory '. Titterton (1951) analysed the ejected ^{8}Li fragments from neutron induced stars at 150 Mev. He failed to see any ^{8}Li fragment associated with a heavy element breakup. The results available so far, however, are not conclusive. In the previous analyses either the incident energy was not fixed or the direction of the incident primary was not uniquely defined. An attempt has therefore been made to investigate the ejected ^{8}Li fragments in proton induced stars at 950 Mev. The direction and energy of the primary being both fixed, it is hoped that the data may throw some further light on the mechanism of heavy fragment emission from nuclear explosions.

† Communicated by Professor P. B. Moon, F.R.S.

§ 2. Experimental Procedure

G5 plates 400 microns thick were exposed to the 950 mev proton beam of the Birmingham Proton Synchrotron, scattered out from the inflector tip (Moon, Riddiford and Symonds 1955). The beam was allowed to pass through the plates parallel to one edge and in the plane of the emulsion so that almost horizontal proton tracks were obtained. The plates were subsequently area scanned for stars under a $\times 10$ objective and $\times 15$ eye pieces. Each star with more than three prongs was closely scrutinized under a $\times 45$ objective and the prong number noted for stars having an incident minimum track in the general beam direction so that only proton induced stars were recorded. All black tracks from the proton induced stars were followed to their end in order to avoid losing very energetic ^{8}Li fragments.

Stars near to the surfaces of the emulsion were not examined to minimize the loss factor due to the number of fragments passing out of the emulsion before coming to rest.

A small percentage of the ' hammer ' fragments may well be due to $^{8}_{5}$B (Alvarez 1950) but in what follows it is assumed that all the ' hammer ' fragments are $^{8}_{3}$Li nuclei.

The stars with ' hammer ' tracks were divided into those due to heavy elements (Ag, Br) and those due to light elements (C, N, O). This was done because different mechanisms have been thought to be responsible for the emission of ^{8}Li from light and heavy nuclei (e.g. Wright 1950). It can be shown that stars due to light element breakup and having an associated ^{8}Li fragment can only have a prong number between four and seven.

$$^{12}_{6}\mathrm{C}+^{1}_{1}\mathrm{H}\longrightarrow {}^{8}_{3}\mathrm{Li}+{}^{3}_{2}\mathrm{He}+2{}^{1}_{1}\mathrm{H} \qquad \text{(four prongs)}$$

$$^{16}_{8}\mathrm{O}+^{1}_{1}\mathrm{H}\longrightarrow {}^{8}_{3}\mathrm{Li}+6{}^{1}_{1}\mathrm{H}+3{}^{1}\mathrm{n} \qquad \text{(seven prongs).}$$

In the case of seven-pronged stars, all the prongs except the ^{8}Li fragment must be due to singly charged particles. Thus all the stars with prong number greater than seven were classified as heavy element stars. In case of seven pronged stars, if any one prong other than the ^{8}Li was identified as due to a doubly charged particle the star was included in the heavy element class. All stars with a short recoil were included in the heavy element category. The stars with prongs between four and seven, if not otherwise identified as being due to heavy nuclei were classified as light element disintegrations. Some uncertainty is possible in the above classification due to increase in prong number due to meson production but the energy distributions for ^{8}Li fragments from light and heavy elements (fig. 1(*a*) and 1(*b*)) suggest that the above classification is largely correct.

§ 3. Experimental Results

A total of 25 200 stars of four or more prongs were examined and 50 examples of the ejection of ^{8}Li fragments were found. Of these 28 came from heavy element disintegrations and 22 from light element disintegrations. The energy and angular distributions of the fragments are given

in figs. 1 and 2. In the latter figure the angle θ is the true angle in space between the ejected fragment and the direction of motion of the primary particle. The range–energy relation for the ^{8}Li fragments was calculated from that for protons as given by Rotblat (1950).

Fig. 1

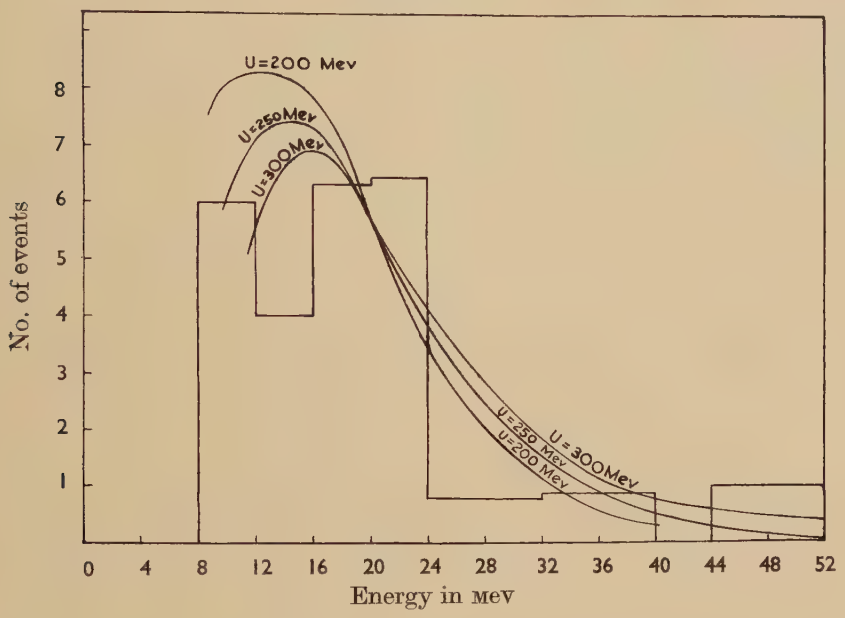

(*a*)

Energy spectrum of the ^{8}Li fragments ejected from heavy nuclei disintegrations.

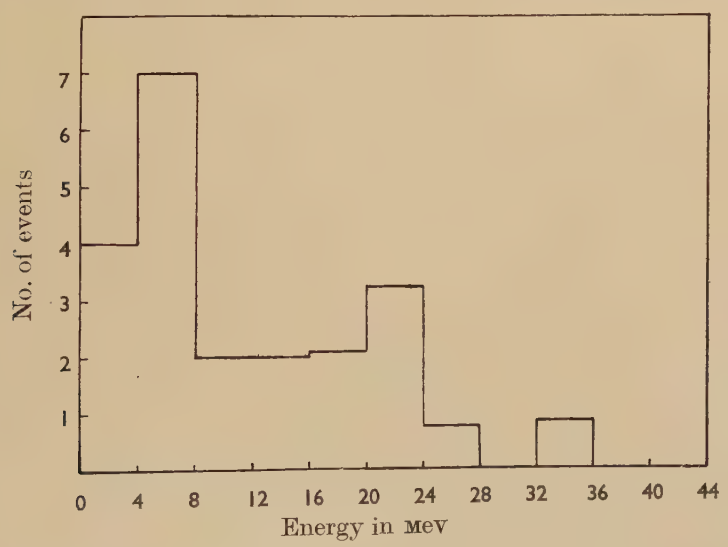

(*b*)

Energy spectrum of the ^{8}Li fragments ejected from light nuclei disintegrations.

Fig. 2

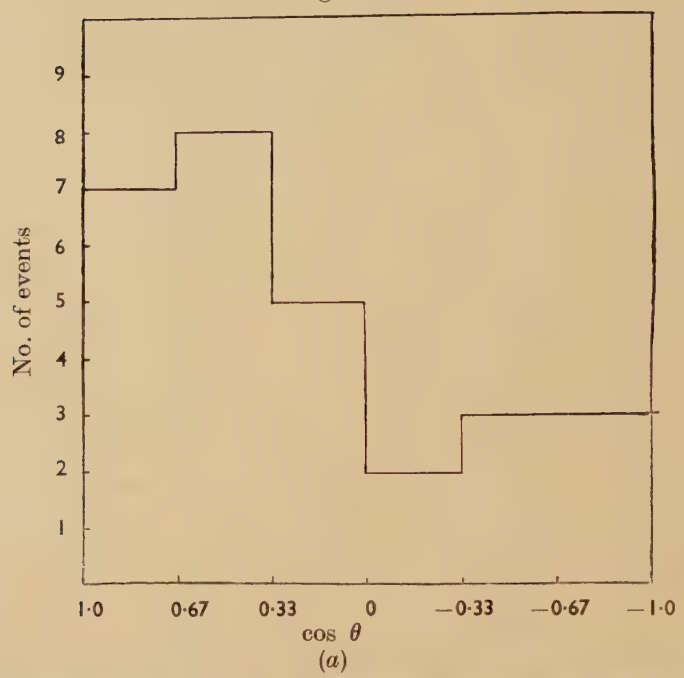

(*a*)

Angular distribution of the ^{8}Li fragments ejected from heavy nuclei disintegrations, with respect to the projected primary direction.

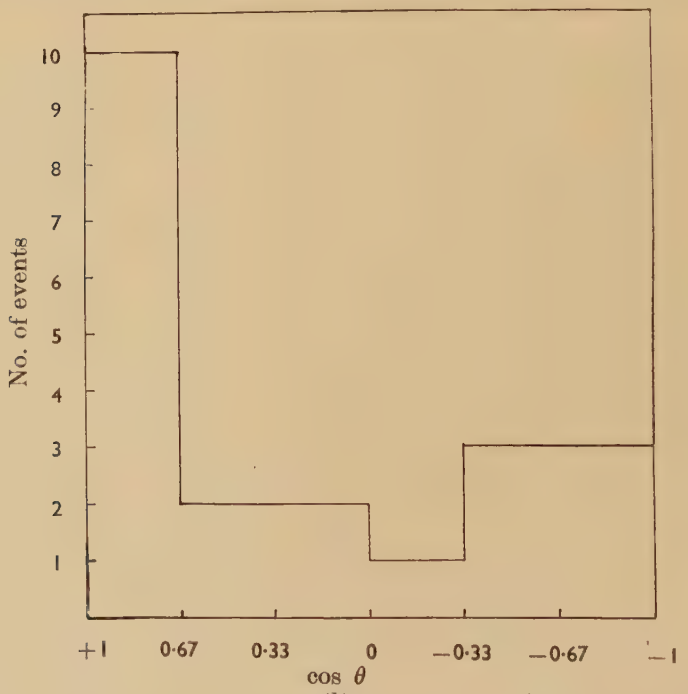

(*b*)

Angular distribution of the ^{8}Li fragments from light nuclei disintegrations.

The energy spectrum of the α-particles from the decay of the ^{8}Be shows a peak near 3 MEV and agrees with the results of Baxter, Burcham and Paul (1950). All but six of the events had associated decay electrons ; the loss is probably due to observational inefficiency which arises from the finite thickness of the emulsions used.

Heavy Element Disintegrations

The energy distribution of the fragments (which has been corrected for loss in the usual way) shown in fig. 1 (*a*), has a cut-off at 8 MEV indicating that the potential barrier facing ^{8}Li in a heavy nucleus is of this order of magnitude. The most energetic fragment observed was ejected with 51 MEV.

The angular distribution (fig. 2 (*a*)) shows a pronounced forward peak. the forward to backward ratio being 2·5 : 1.

Of the 25 200 stars examined, 21 800 correspond to disintegration of heavy nuclei (see Lock, March and McKeague 1955). Correcting for loss the number of ^{8}Li nuclei ejected from these stars is 30, corresponding to a production cross section of $1{\cdot}1 \pm 0{\cdot}3$ mb.

Light Element Disintegrations

The energy spectrum of the ^{8}Li fragments (fig. 1 (*b*)) has a peak between 4 and 8 MEV, the average energy is 12 MEV. The angular distribution (fig. 2 (*b*)) shows a forward to backward ratio of 2 : 1.

Correcting for loss the number of ^{8}Li nuclei ejected from the 3400 light element disintegrations with four or more prongs is 22·5, corresponding to a production cross section of $0{\cdot}5 \pm 0{\cdot}2$ mb.

§ 4. INTERPRETATION

^{8}Li *Emission from Light Elements*

The analysis of Titterton (1951) favoured the hypothesis that ^{8}Li is left as a residual nucleus in a light element breakup. Wright (1950) and Hodgson (1951) reached a similar conclusion. This recoil nucleus should, in general, come out with a small amount of energy and its angular distribution should be isotropic in the centre-of-mass system.

The present results strengthen the above hypothesis. The fragments are emitted with a small amount of energy ; the angular distribution is anisotropic in the laboratory system, but at such high incident momentum the centre-of-mass velocity is not negligible. In the present experiment the incident momentum is 1650 MEV/*c*. In an encounter with a light nucleus, only a fraction of this momentum is transferred say, 300 MEV/*c*. This momentum given to an $^{16}_{8}$O nucleus corresponds to an energy of 0·13 MEV per nucleon. This nucleus will be in a highly excited state after the impact and one can assume it to fly to pieces instantaneously, leaving a ^{8}Li nucleus as a residue, which recoils with a small energy. For the

average recoil energy of 12 Mev, an isotropic angular distribution in the C-system will appear to be 1·8 : 1 in the forward direction on considerations of the centre of mass velocity. This agrees with the observed distribution of 2 : 1 in the forward direction. Thus, the present results are compatible with the hypothesis that the ^{8}Li is a recoil nucleus from the light element disintegration.

^{8}Li *Emission from Heavy Elements*

The simplest hypothesis to explain the emission of ^{8}Li fragments from heavy nuclei is that they are emitted during the evaporation process. If this is the case then their angular distribution should be isotropic, their energy spectrum of Maxwellian form and their frequency in agreement with that calculated by Le Couteur (1955).

The experimental results do not seem to exhibit these characteristics in any striking way. The angular distribution is strongly peaked forward, with a forward to backward ratio of 2·5 : 1 ; for heavy nuclei disintegrations the centre of mass velocity is small and the correction to the angular distribution is negligible. The expected energy spectrum $N(E)dE$ can be calculated using the relation

$$N(E)dE = \frac{(E-V)}{T^2}\exp-\frac{(E-V)}{T}\,dE \qquad \text{(Le Couteur 1950)}$$

where the potential barrier V is taken to be 8 Mev and T is the nuclear temperature. The mean number of tracks in heavy element stars with ejected ^{8}Li fragments is 9. On the average the number of shower and grey tracks per star is 2 (this agrees with the figures given by Lock *et al.* 1955). It is reasonable to assume that 0·5 tracks per star are the low energy component of ' cascade ' particles. Then the mean number of evaporation prongs per star is 6·5, including a ^{8}Li prong. This corresponds roughly to an excitation energy of 250 Mev and to an initial value of $T \simeq 6$ Mev. The energy spectrum calculated with these values is shown in fig. 2 (*b*) together with the spectra corresponding to 200 and 300 Mev excitation energies. It can be seen that the experimental distribution does not show good agreement with any of the calculated spectra.

The frequencies of ejection of ^{8}Li fragments calculated by Le Couteur (1955) on the basis of evaporation theory are 0·0005 and 0·003 fragments per star for excitation energies of 150 and 250 Mev respectively. The experimental figure is $0{\cdot}0014 \pm 0{\cdot}0002$, in poor agreement with the calculated value for an excitation energy of 250 Mev. The agreement with the value for 200 Mev excitation energy is better but such an excitation energy is inconsistent with the average size of the disintegrations from which the fragments are ejected.

Therefore, on the basis of the evidence discussed above, one may conclude that it is unlikely that the ^{8}Li fragments are ejected during the evaporation process.

The results of Hodgson (1951) seemed to favour the evaporation mechanism for ^{8}Li ejection from cosmic ray induced stars but his statistics were poor and he gave no quantitative measurements on the angular distribution. The results of workers on heavy fragments in general do not favour the evaporation hypothesis (see Perkins 1950, Camerini, Lock and Perkins 1952).

The opposite extreme to the evaporation hypothesis is to assume that the ^{8}Li fragment is directly ejected by the incident proton. The maximum energy of the ^{8}Li in such a collision would be 475 MEV which is far in excess of the observed maximum energy of 51 MEV. This suggests that direct ejection does not often occur, if at all. It appears more reasonable to assume that the ^{8}Li fragment is ejected in some manner during the cascade process. Such a hypothesis is intermediate between the evaporation picture and direct ejection. The angular distribution is then readily explained since it is well known that the angular distribution of ' cascade ' particles is peaked forward. The exact manner in which the ^{8}Li is ejected remains to be solved, as does the question of how such an aggregate of 3 protons and 5 neutrons keeps together even when ejected with energy up to 50 MEV. Presumably higher energy fragments are unstable and disintegrate immediately after leaving the nucleus.

§ 5. EJECTION OF ^{9}Li FROM A DISINTEGRATING NUCLEUS

During the scanning for ^{8}Li fragments, an event was discovered similar to a hammer but the alpha-particles were inclined at an angle of 140°. The event may be interpreted as the emission from a heavy nucleus of ^{9}Li which decays according to the scheme

$$^9\mathrm{Li} \xrightarrow{e^-} {}^9{}^*\mathrm{Be} \longrightarrow {}^1\mathrm{n} + 2\,{}^4\mathrm{He}.$$

Due to simultaneous ejection of a neutron and two alpha particles from the excited ^{9}Be nucleus, the alpha particles do not come out exactly in the opposite directions. The momenta of the alpha particles in this case are 122 MEV/c and 88 MEV/c and the angle between them 140°. The energy of the neutron can be easily calculated from this and is 3·5 MEV. Thus the disintegration energy of the ^{9}*Be is 6·5 MEV. Thus the event observed could be due to the decay of ^{9}Li to an excited state of ^{9}Be near 8 MEV, which subsequently gave two alpha particles and a neutron with a total energy of 6·5 MEV.

A similar event has been observed by Fry (1953) in plates exposed to a μ^- meson beam, which appeared to be due to a breakup of ^{9}*Be from the 6·8 MEV level.

§ 6. CONCLUSIONS

It seems probable that the explanation of Titterton (1951) is correct for ^{8}Li emission from light elements. When a fast proton strikes a light nucleus, it transfers to it a part of its momentum, the remaining being carried away by fast knock-on particles or the incident proton itself.

The residual nucleus is in a highly excited state and almost spontaneously breaks up into pieces, not always charged, leaving ^{8}Li as a residual nucleus, which then recoils with a small amount of energy. The recoil energy should be in general higher, if a larger portion of the incident energy is transferred to the nucleus. Both the energy and angular distributions substantiate this assumption. The situation in the case of ^{8}Li emission from heavy nuclei is not so clear. The 'evaporation' and 'direct knock-on' hypotheses appear to be excluded by the experimental data. The observations can best be explained by assuming that the ^{8}Li fragments are ejected during the 'cascade' process by some mechanism not yet understood.

Acknowledgments.

I wish to express my thanks to Dr. H. Muirhead of the University of Glasgow for kindly allowing me to use the data on ^{8}Li fragments found at Glasgow, Dr. S. J. Goldsack for several useful discussions, Dr. W. O. Lock for his guidance during the course of this work, and Professors W. E. Burcham and P. B. Moon for their interest and encouragement.

References

Alvarez, L. W., 1950, *Phys. Rev.*, **80,** 519.
Baxter, A. S., Burcham, W. E., and Paul, E. B., 1950, *Phil. Mag.*, **41,** 937.
Camerini, U., Lock, W. O., and Perkins, D. H., 1952, *Progress in Cosmic Ray Physics* (Amsterdam: North Holland Publishing Company), **1,** 1.
Franzinetti, C., and Payne, R. M., 1948, *Nature, Lond.*, **161,** 735.
Fry, W. F., 1953, *Phys. Rev.*, **89,** 325.
Hodgson, P. E., 1951, *Phil. Mag.*, **42,** 207.
Le Couteur, K. J., 1950, *Proc. Phys. Soc.* A, **63,** 259; 1955, private communication.
Lock, W. O., March, P. V., and McKeague, R., 1955, *Proc. Roy. Soc.* A, **231,** 368.
Moon, P. B., Riddiford, L., and Symonds, J. L., 1955, *Proc. Roy. Soc.* A, **230,** 204.
Occhialini, G. P. S., and Powell, C. F., 1947, *Nature, Lond.*, **159,** 93.
Perkins, D. H., 1950, *Proc. Roy. Soc.* A, **203,** 399.
Pickup, E., and Voyvodic, L., 1949, *Phys. Rev.*, **76,** 1534.
Rotblat, J., 1950, *Nature. Lond.*, **165,** 387.
Titterton, E. W., 1951, *Phil. Mag.*, **42,** 109.
Wright, S. C., 1950, *Phys. Rev.*, **79,** 838.

XXXIV. *The Decay of* ^{58}Co *and* ^{57}Co

By M. A. Grace,† G. A. Jones‡ and J. O. Newton
Atomic Energy Research Establishment, Harwell, Berks §

[Received November 5, 1955]

Abstract

The single channel ^{58}Co gamma-ray spectrum and the spectrum in coincidence with K-x-rays have been studied with scintillation counters and a proportional counter and show no evidence for radiation other than the well-established 805 kev gamma-ray. Our results accord well with the decay scheme of Deutsch and Elliott. An upper limit of $2{\cdot}5\times10^{-3}$ per disintegration was set on the intensity of 29 kev gamma radiation which, according to a recent suggestion, follows the decay of ^{57}Co.

§ 1. Introduction

The intention of the experiments described in this paper is to resolve some of the uncertainties in the decay schemes of ^{58}Co and ^{57}Co which have arisen following a recent study of these isotopes by Cork, Brice and Schmid (1955) who find evidence for new gamma-rays in their decays.

The situation regarding ^{58}Co prior to their paper is embodied in the decay scheme presented in fig. 1 (*a*) which incorporates work reported by a number of authors. Livingood and Seaborg (1941) detected positrons of maximum energy 500 kev (approximately) and gamma-rays of about 800 kev. Deutsch and Elliott (1944) and Good, Peaslee and Deutsch (1946), using a beta-ray spectrometer, measured the end point of the positron spectrum and the converted electron groups from 507 and 805 kev gamma-radiation. They also studied coincidences between Fe K-x-rays and gamma-rays and arrived at the branching ratio of positron emission and K-capture leading to the 805 kev level. Strauch (1950) determined the internal conversion coefficient for the 805 kev radiation, as also did Cheng, Dick and Kurbatov (1954). Daniels *et al.* (1952) measured the angular distribution of the 805 kev radiation from oriented ^{58}Co and on the basis of the decay scheme given in fig. 1 (*a*), were able to assign spins to the levels.

The recent work of Cork *et al.* however favours the decay scheme given in fig. 1 (*b*). They arrive at this conclusion from gamma–gamma

† On leave from the Clarendon Laboratory, Oxford.
‡ On leave from the Cavendish Laboratory, Cambridge.
§ Communicated by the Authors.

coincidence studies under conditions in which annihilation radiation alone is unlikely to give coincidences. Using scintillation counters they measured the pulse height distribution due to gamma radiation in coincidence with pulses attributed to the ' photo-peak ' of the 500 kev radiation and found that it was similar to the ungated spectrum. From this they have inferred the existence of a genuine 500 kev gamma-ray in the decay of ^{58}Co.

Fig. 1

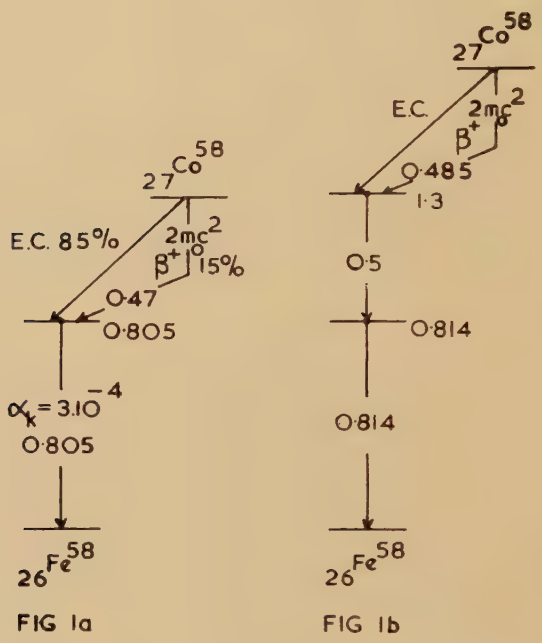

(*a*) Decay scheme of Deutsch and Elliott (1944).
(*b*) Decay scheme of Cork, Brice and Schmid (1955).

For ^{57}Co, in addition to the three well known gamma-rays of 14·4, 123·0 and 137·4 kev (see Lemmer, Sagaert and Grace 1955 for references), Cork *et al.* have proposed further gamma-rays of 29, 99·8 and 700 kev.

§ 2. Source Preparation

The cobalt 58 source was prepared through the ^{58}Ni(n, p)^{58}Co reaction by irradiating natural nickel in the fast neutron flux of the pile. In this way effectively carrier free ^{58}Co can be separated without detectable amounts of other cobalt activities. This was then evaporated down on a sheet of thin cellophane. The cobalt 57 source was that used in earlier experiments and was deposited on 0·001 in. aluminium foil. Its preparation has been described elsewhere (Lemmer *et al.* 1955).

§ 3. Cobalt 58

Two tests were made to distinguish between the two decay schemes. Firstly the ratio of the intensities of the 500 kev to 805 kev radiations was estimated from the pulse height spectrum in a scintillation counter : for decay scheme 1 (*a*) this should be 0·3 compared with 1·3 for 1 (*b*). Secondly the spectrum of gamma radiation in coincidence with x-radiation was determined : the x-rays arise almost solely from K-capture transitions, the internal conversion of the 500 and 805 kev radiations being known from previous evidence to be small. For decay scheme 1 (*a*) this should show only 805 kev radiation while for 1 (*b*) both 805 and 500 kev radiations should appear.

The gamma-ray spectra have been taken with two NaI crystals both of $1\frac{3}{4}$ in. diameter and having lengths of 2 in. and $\frac{1}{2}$ in. respectively. The spectrum taken in the 2 in. crystal is shown in fig. 2 (*a*). In order to determine the ' photo-peak ' intensities of the 500 and 805 kev lines, the spectrum of a single gamma-ray of energy 845 kev from the decay of ^{54}Mn was taken for comparison ; this spectrum is presented in the same figure after suitable scaling and adjustment in order to resemble more closely a gamma-ray of energy 805 kev. The ' photo-peak ' has been normalized to fit the ^{58}Co ' photo-peak ' and displaced by approximately 5% in energy ; the Compton spectrum has been decreased in height relative to the ' photo-peak ' by 4%, this being the value predicted simply from the relative efficiencies of the two processes at these gamma-ray energies. The discrepancy, in the region below 400 kev, between the ' adjusted ' 805 kev curve and the experimental points of figs. 2 (*a*), (*b*) can probably be attributed to the effect of external scattering ; the ^{54}Mn source was further away from the detector than was the ^{58}Co source. Even so it is possible to determine the ratio of the counting rates in the ' photo-peaks ' with an accuracy of 10%.

To determine the true intensity ratio from this measured value, the total absorption of the two gamma-rays in the crystals was determined by numerical integration over the geometrical arrangement, the fractions of the counts in the photo-peaks being estimated from the shapes of the single line spectra ; a cross-check for this estimate is provided by the results of Maeder, Muller and Wintersteiger (1954). In this way the ratio of intensities of 500 kev to 805 kev radiation is found to be 0·29 using the $\frac{1}{2}$ in. crystal and 0·23 using the 2 in. crystal, giving a mean value of 0·26 with about 10% accuracy.

Coincidences were observed between Fe K-x-rays and gamma-rays, the latter being detected with the 2 in. crystal and the former, through a 0·0015 in. mica window, by a krypton filled proportional counter of the Maze type (West 1953). The source was placed between the two detectors, the sodium iodide crystal being covered by a thin lead sheet ; this prevented the 28 kev iodine K-x-rays or degraded gamma-radiation produced in the crystal from reaching the proportional counter.

By means of coincidence and anticoincidence units coincidences were recorded only when the pulses in the x-ray channel lay in or near the

Fig. 2

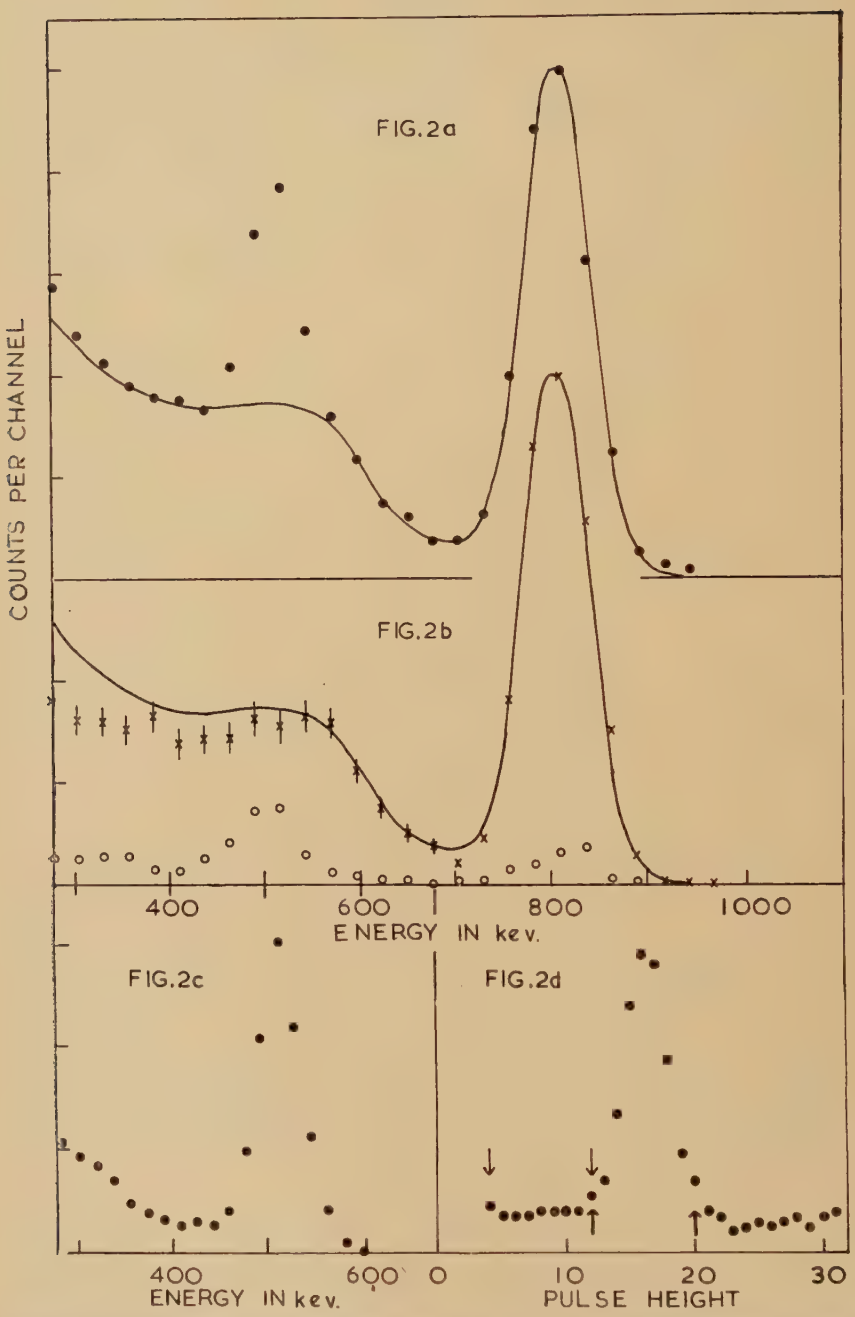

(*a*) Gamma-ray spectrum from the decay of ^{58}Co. Dots: experimental results. Full line: 'adjusted' spectrum from the decay of ^{54}Mn (see text).

(*b*) ^{58}Co gamma-ray spectrum taken in coincidence with the K-x-rays. Crosses: spectrum with background subtracted. Circles: background spectrum. Full line: 'adjusted' ^{54}Mn spectrum.

(*c*) Spectrum of annihilation radiation from a ^{22}Na source.

(*d*) K-x-ray spectrum from ^{58}Co decay. The arrows show the bias limits for two 'window positions'.

peak. The coincidences were then made to open the kicksorter gate through which the pulses from the gamma-ray channel were fed. The resulting spectrum, after subtracting a calculated random background and a genuine background, is shown in fig. 2 (*b*) in which the genuine background spectrum is also plotted. Since the genuine background seems to account for all the coincidences in the 500 kev peak much importance was attached to its correct assessment.

Figure 2 (*d*) gives the x-ray spectrum in the neighbourhood of the peak ; it will be seen that the peak is superimposed upon a slowly falling background, thought to arise from detection of the positrons and gamma-radiation with incomplete absorption of the ionizing particle within the counter. Insertion of a thin aluminium foil between counter and source removed the x-ray peak completely and produced a reduction of the background in the neighbourhood of this peak, presumably by partial absorption of the positrons. The coincidence spectrum under these conditions was compared with that obtained with no absorber but with the x-ray channel ' window ' moved below the peak. The two spectra were not significantly different, since both positron–gamma and gamma–gamma coincidences are expected to enhance the 500 kev peak relative to that at 805 kev. The statistical accuracy was not good enough to recognize small differences between these two sources of background. This comparison indicates that the coincidence spectrum due to background in the proportional counter is unlikely to change appreciably when the ' window ' is moved just below the x-ray peak. The genuine background in fig. 2 (*b*) was obtained under the latter conditions.

In fig. 2 (*b*) the adjusted Mn spectrum is also shown for comparison with the coincidence spectrum after removal of random events and background. It is seen that there is no significant peak due to 500 kev radiation and that certainly less than 10% of the 500 kev radiation is in coincidence with x-radiation.

These results cannot be reconciled with the decay scheme presented in fig. 1 (*b*). Even if the assessment of the background coincidence spectrum be completely in error, in which case up to 25% of the 500 kev radiation could be in coincidence with x-radiation, only 6% of the 805 kev radiation could be part of the 500–805 kev cascade ; in fact we consider that our results give no significant indication of the presence of a cascade and further that not more than $2\frac{1}{2}$% of the 805 kev radiation could arise from such a cascade.

In addition we have attempted to confirm more quantitatively the original decay scheme—fig. 1 (*a*). Our measurements on the intensity ratio of the 500 and 805 kev radiations are in agreement with this scheme, leading to a value of $13 \pm 1{\cdot}3$% for the proportion of nuclei decaying by positron emission.

As a confirmation of previous measurements on the positron spectrum we showed that coincidences occurred between the 805 kev and 500 kev radiations ; sodium iodide crystals were used as detectors and one

channel was biased just below the 805 kev ' photo-peak '. It follows from the coincidence and single channel counting rates that the predominant part of the 500 kev radiation is in coincidence with 805 kev radiation.

§ 4. Cobalt 57

We have examined the gamma-ray spectrum of ^{57}Co with the krypton filled proportional counter in the energy range 9–48 kev. No evidence was found for any radiation other than that at 14·4 kev and in particular we can set an upper limit to the intensity of any 29 kev gamma-ray as 3% of that of the 14·4 kev gamma-ray; this corresponds to an upper limit of $2{\cdot}5\times10^{-3}$ per disintegration.

§ 5. Discussion and Conclusions

The measurements on the decay of ^{58}Co reported here are consistent with the generally accepted decay scheme (fig. 1 (*a*)) and not consistent with the decay scheme proposed by Cork, Brice and Schmid (1955). It is suggested that it may be possible to reconcile their data with the accepted decay scheme in the following way. They observed coincidences between two sodium iodide scintillation detectors one of which was gated on the 500 kev ' photo-peak '. The counters were arranged so that coincidences between annihilation radiation would not occur. Since they obtained in their coincidence spectrum a 500 kev peak having approximately the same intensity ratio to the 805 kev peak as occurred in the singles spectrum, they assumed that there must be a 500 kev gamma-ray in cascade with the 805 kev gamma-ray. However, it is clear that there must be some pulses under the 500 kev ' photo-peak ' which are due to the Compton distribution of the 805 kev radiation. Moreover the peak of the 805 kev Compton distribution occurs at approximately 500 kev (see for example fig. 2 (*a*)). Therefore a 500 kev peak will appear in the coincidence spectrum due to coincidences with 805 kev radiation, each 805 kev quantum being associated with two annihilation quanta. It is easy to show that a result similar to that obtained by Cork, Brice and Schmid could be obtained by this mechanism.

Our upper limit of $2{\cdot}5\times10^{-3}$ for the number of 29 kev gamma-rays per disintegration of ^{57}Co makes it unlikely that the gamma-ray exists: although Cork, Brice and Schmid give no value for its intensity it seems doubtful whether they could have observed a radiation as weak as this with a sodium iodide crystal.

Acknowledgments

We are most grateful to Dr. C. E. Mellish of the Isotope Division, A.E.R.E., Harwell, for supplying us with the source of cobalt 58. Two of us (G. A. J. and M. A. G.) are indebted to the Director of A.E.R.E. for the generous hospitality afforded to them.

References

Cheng, L. S., Dick, J. L., and Kurbatov, J. D., 1952, *Phys. Rev.*, **88**, 887.
Cork, J. M., Brice, M. K., and Schmid, L. C., 1955, *Phys. Rev.*, **99**, 703.
Daniels, J. M., Grace, M. A., Halban, H., Kurti, N., and Robinson, F. N. H., 1952, *Phil. Mag.*, **43**, 1297.
Deutsch, M., and Elliott, L. G., 1944, *Phys. Rev.*, **65**, 211.
Good, W. M., Peaslee, D., and Deutsch, M., 1946, *Phys. Rev.*, **69**, 313.
Lemmer, H. R., Segaert, J. A., and Grace, M. A., 1955, *Proc. Phys. Soc.* A, **68**, 701.
Livingood, J. J., and Seaborg, G. T., 1941, *Phys. Rev.*, **60**, 913.
Maeder, D., Miller, R., and Wintersteiger, V., 1954, *Helvetica Physica Acta*, **27**, 3.
Strauch, K., 1950, *Phys. Rev.*, **81**, 973.
West, D., 1953, *Progress in Nuclear Physics*, **3**, 18.

XXXV. CORRESPONDENCE

Direct Observation of Static Nuclear Susceptibilities at Room Temperature

By D. F. Evans
Physical Chemistry Laboratory, Oxford

[Received November 9, 1955]

When a substance containing nuclei with spin I is placed in a magnetic field, the nuclei occupy $2I+1$ energy levels, corresponding to the different orientations of the nuclear magnets with respect to the field. As a result of the Boltzmann distribution between these energy levels, they will not be occupied equally, and accordingly the substance has a resultant nuclear paramagnetic susceptibility χ_0 given by the expression

$$\chi_0 = \frac{N\mu^2}{3kT}\left(\frac{I+1}{I}\right)$$

where N is the number of nuclei per cm^3, and μ is their magnetic moment (Smith 1953, Ramsey 1953). Nuclear susceptibilities at ordinary temperatures are extremely small; thus for water at 20°C, since the proton has a spin of $\frac{1}{2}$ and a magnetic moment of $1{\cdot}41\times10^{-23}$ erg gauss, the calculated nuclear susceptibility is $3{\cdot}3\times10^{-10}$ c.g.s. units, as compared with a diamagnetic susceptibility of $0{\cdot}72\times10^{-6}$. The only direct determination of a static nuclear susceptibility was made by Lasarew and Schubnikow (1930), who measured the susceptibility of solid hydrogen at 4·22°, 2·18° and 1·76° K. At these temperatures, the nuclear susceptibility is an appreciable fraction of the normal diamagnetic susceptibility, and the observed (diamagnetic) susceptibility decreased as the temperature was lowered.

Nuclear magnetic resonance, which was discovered independently by Purcell *et al.* (1946) and Bloch *et al.* (1946), involves the detection of transitions between these energy levels of a nucleus in a uniform magnetic field H_0, as the result of the application of a small radio-frequency field H_1 at the resonant frequency $\mu H_0/Ih$. At resonance, the real and imaginary parts of the nuclear susceptibility χ' (dispersion) and χ'' (absorption) are both very much greater than the static susceptibility χ_0.

The direct detection of the static susceptibility of nuclei at room temperature by the method of Lasarew and Schubnikow would clearly be extremely difficult. However, there is an alternative method available which involves the removal of this static susceptibility by means of a strong radio-frequency field at the resonant frequency. If the field is sufficiently strong, ' saturation ' occurs, i.e. as a result of the absorption of radio-frequency energy the populations of the energy levels are equalized,

and the nuclear susceptibility vanishes. The experimental problem is, therefore, to detect an increase of about 0·05% in the diamagnetic susceptibility of a suitable substance when a relatively strong radio-frequency field at the appropriate resonant frequency is applied.

The apparatus used was a modification of that previously constructed for work on photomagnetism (Evans 1955). Two thin glass tubes (~1 mm diameter, 9 mm long) containing solid hexaethylbenzene were suspended from a 20μ quartz fibre in an inhomogeneous magnetic field (fig. 1).

Fig. 1

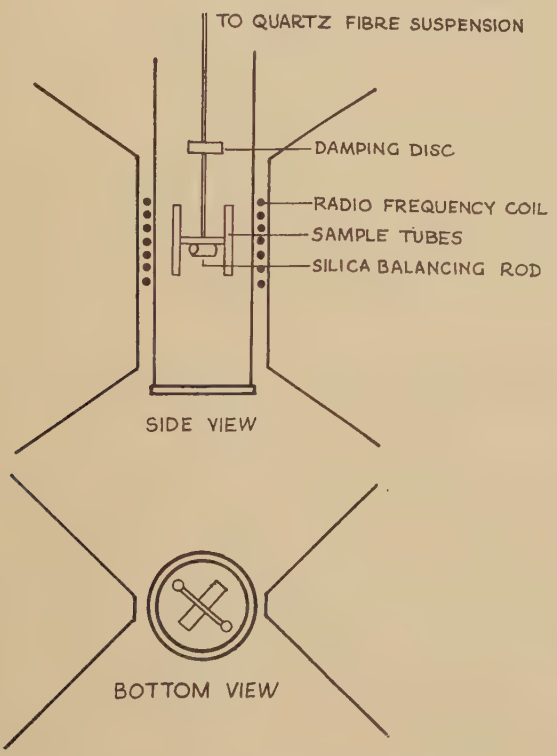

Experimental arrangement.

Hexaethylbenzene was chosen since it has a relatively high proportion of protons, and also in the hope that its relaxation time would not be unduly short (which would necessitate relatively high radio-frequency power levels to attain ' saturation '). The size of the silica balancing rod was such that, by suitable adjustment of the torsion head carrying the quartz fibre, the system took up a position similar to that shown in the figure, both with the field on and off. A Hartley oscillator supplied up to about 100 volts across the radio-frequency coil. Since the samples are in an inhomogeneous field it is necessary to use a relatively broad frequency band to bring all the protons to resonance. This was obtained by sweeping the frequency (~40 times per second) over a range of 5–10% by means of a

subsidiary condenser driven by a motor. At the resonant frequency the hexaethylbenzene becomes slightly more diamagnetic, and accordingly the system swings in a clockwise direction (as seen from below). This motion was amplified and recorded as described previously (Evans 1955).

Fig. 2

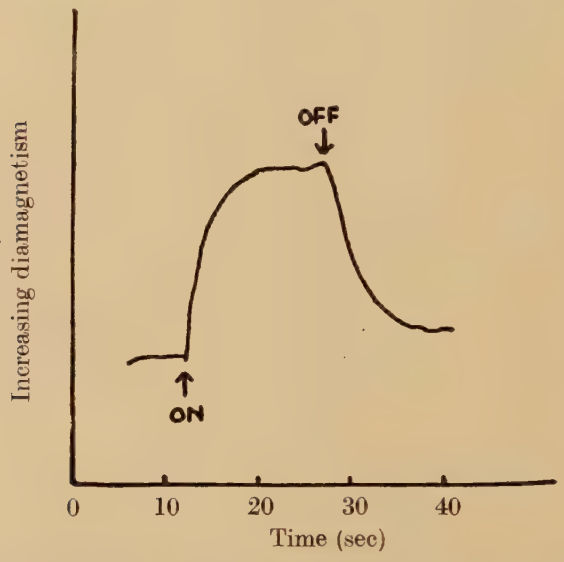

The static nuclear susceptibility of the protons in solid hexaethylbenzene at room temperature. The arrow at the left indicates when the radio-frequency field was switched on, and that at the right when the field was switched off. The theoretical change in the diamagnetic susceptibility of the hexaethylbenzene (assuming complete saturation, which was probably not quite attained) is 0·04%. The small zero drift is probably due to radio-frequency heating of the apparatus.

A signal obtained in this way is shown in fig. 2. A mean frequency of about 30 Mc/s was employed, which was about that expected from a very rough measurement of the magnetic field. The effect of varying the magnetic field and the frequency clearly showed that the signals obtained were, in fact, due to the nuclear susceptibility of the protons in the sample. Thus, when the magnetic field was increased, the effect virtually disappeared, but could be restored by increasing the frequency of the oscillator. Furthermore, if the oscillator motor was stopped, so that a very narrow frequency band was generated, only a negligible effect was observed. At frequencies and magnetic fields not corresponding to resonance, no effect was observed immediately after switching on the oscillator. However, if the oscillator was not quickly switched off, slow drifts were always obtained after a lag of about 10 seconds (probably due to radio-frequency heating of the system). As a result of the fairly long

period of the suspension, and the fact that the system was slightly overdamped, it is not possible to make an estimate of the relaxation time of hexaethylbenzene, although it must be less than about 3 seconds.

It may be noted that the sensitivity of the above method of studying nuclear susceptibilities is not very much less than that of the conventional nuclear magnetic resonance technique (only about 15 mg of hexaethylbenzene were used, and the limit set by Brownian fluctuations had not been reached in the present apparatus). However, it is unlikely to have any practical importance, since an inhomogeneous field is necessary and therefore the resolution is excessively low. Nevertheless, the experiment does demonstrate in a very direct manner both the existence of nuclear susceptibilities and the phenomenon of 'saturation'. An even more direct method (suggested to the author by Dr. R. E. Richards) is to dispense with the radio-frequency field, and merely measure the magnetic susceptibility as a function of time immediately after switching on the main magnetic field. Some substances, such as lithium fluoride, have very long relaxation times, and accordingly the diamagnetic susceptibility would gradually decrease to a constant value as the nuclear susceptibility was excited by the magnetic field. An attempt to detect this effect was unsuccessful, due (at least in part) to the instability of the apparatus immediately after switching on the field. A system with a carefully balanced taut suspension (as in a galvanometer) would almost certainly be more suitable.

The author wishes to thank Dr. R. E. Richards for helpful discussions, and the University of Oxford for an I.C.I. Research Fellowship.

References

Bloch, F., Hansen, W. W., and Packard, M. E., 1946, *Phys. Rev.*, **70**, 474.
Evans, D. F., 1955, *Nature, Lond.*, **176**, 777.
Lasarew, B. G., and Schubnikow, L. W., 1937, *Phys. Z. Sowjet*, **11**, 445.
Purcell, E. M., Torrey, H. C., and Pound, R. V., 1946, *Phys. Rev.*, **69**, 37.
Ramsey, N. F., 1953, *Nuclear Moments* (John Wiley and Sons, Inc.).
Smith, J. A. S., 1953, *Quart. Revs.*, **7**, 279.

The Photoneutron Yields from ^{208}Pb

By J. D. Prentice and K. G. McNeill
Department of Natural Philosophy, The University, Glasgow

[Received December 10, 1955]

The relative photoneutron yields from ^{208}Pb and natural lead have been measured at 22 Mev maximum bremsstrahlung x-ray energy, using the technique for determining (γn) yields developed by McNeill (1955). In the present work a specimen of lead enriched in the isotope of mass 208, isolated by Professor F. Soddy in his work on isotopes (Soddy 1916), and generously lent to us, was placed in the collimated beam of the Glasgow

22 MeV synchrotron, and above a large NaI crystal. The photoneutrons created in the lead caused (n,γ) reactions in the iodine of the crystal, producing ^{128}I, which decays by beta emission with a half life of 25 minutes. The intensity of the activity thus produced was compared with the corresponding activity produced when the enriched lead was replaced by a geometrically identical specimen of ordinary lead. After subtraction of 'cosmic' background and the beam background produced when there is no target in position, the ratio of the activities produced by the enriched specimen and the ordinary lead sample is the ratio of the photoneutron yields in the two cases. This ratio was found to be $Y_{\text{enriched}} : Y_{\text{ordinary}} = 1{\cdot}09 \pm 0{\cdot}16$. The relatively high error is due to the small amount of enriched lead available, for the background was comparable with the activity produced by the photoneutrons from the lead samples.

As the enriched sample contains 80% of ^{208}Pb, with approximately 10% each of ^{206}Pb and ^{207}Pb, this result indicates that the ratio of the total photoneutron yield from lead 208 to the yield from ordinary lead is $1{\cdot}15 \pm 0{\cdot}24$.

The opportunity has been taken to increase the accuracy of the order of magnitude measurement made by Reid and McNeill (1953) on the 22 MeV yield for the photoproduction from natural lead of the 0·8 second isomer. It is concluded that the ratio of this yield to the 22 MeV yield of ^{62}Cu produced by ^{63}Cu(γn)^{62}Cu, written $Y_{207^*}/Y_{^{62}\text{Cu}}$, is 0·27, which is somewhat higher than the original estimate.

In conjunction with other known photoneutron yields, the present results can be used to find the proportion of photoneutron events in ^{208}Pb which lead to the isomeric state of ^{207}Pb, that is, Y_{207^*}/Y_{207}. For, as was shown by the use of enriched isotopes (Reid and McNeill 1954) the 0·8 second isomer is produced by a photoneutron reaction in ^{208}Pb, and the 22 MeV photoneutron yields from ^{62}Cu and ordinary lead are well established.

Then $(Y_{207^*}/Y_{207}) = (Y_{207^*}/Y_{^{62}\text{Cu}}) \times (Y_{^{62}\text{Cu}}/Y_{\text{Pb}}) \times (Y_{\text{Pb}}/Y_{207})$ where the subscripts refer to the product of the photoneutron reaction, and Y_{Pb} refers to the neutron yield from natural lead.

As stated above, $Y_{207^*}/Y_{^{62}\text{Cu}}$ has been found to be 0·27, and $Y_{^{62}\text{Cu}}/Y_{\text{Pb}}$ is 2·8 27 (Katz and Cameron 1951, and Montalbetti *et al.* 1953). The present work shows that the final term is $0{\cdot}87 \pm 0{\cdot}18$, giving a final result of $Y_{207^*}/Y_{207} = 0{\cdot}025$. It may be concluded that about 25 in every 1000 photoneutron events induced in ^{208}Pb by bremsstrahlung x-rays of 22 MeV maximum energy lead to the 0·8 second isomeric state in ^{207}Pb.

References.

Katz, L., and Cameron, A. G. W., 1951, *Can. J. Phys.*, **29**, 518.

McNeill, K. G., 1955, *Phil. Mag.*, **46**, 321.

Montalbetti, R., Katz, L., and Goldemburg, J., 1953, *Phys. Rev.*, **91**, 659.

Reid, J. M., and McNeill, K. G., 1953, *Proc. Phys. Soc.* A, **66**, 1179; 1954, *Phil. Mag.*, **45**, 957.

Soddy, F., 1916, *Ann. Rep. Chem. Soc.*, **13**, 247, 272.

XXXVI. REVIEWS OF BOOKS

Meteors. Edited by T. R. Kaiser. (London: Pergamon Press Ltd.) [Pp. 204.] Price 55*s*.

This work consists of 39 papers by authors from some ten countries, presented at a symposium on meteor physics held at the Jodrell Bank Experimental Station in July 1954. It forms also a special supplement (Vol. II) to the *Journal of Atmospheric and Terrestrial Physics.*

Static and Dynamic Electron Optics. By P. A. Sturrock. (Cambridge: University Press.) [Pp. x+240.] Price 30*s*.

A brief explanation of the title is needed. Sturrock deals with mathematical techniques which originated from the study of electron microscopes where electrons move in static fields. But the scope of these techniques goes far beyond electron microscopy. In particular, in the second part of his book, entitled *Dynamic electron optics* Sturrock extends them to accelerators, with time-varying orbits: he succeeds in bringing two subjects under one roof.

Indeed, the book teaches the mathematical craft of tracing charged particles through quite general electromagnetic fields in a meaningful manner, i.e. giving the relevant information in each case, such as focus, quality of picture, stability, beam width, etc. Thus the book is useful to anyone working, say, in electron tube design, electron microscopy, mass-spectroscopy, high-energy accelerator physics, cosmic-ray physics. It ought to be consulted *before* calculations are begun on the instrument or situation in hand.

For Sturrock's methods are analytical, general and powerful. He exploits fully the beautiful theories of Hamilton, Lagrange and Poincaré and takes these beyond the realm of aesthetic mathematical pastimes and tripos exercises. In many respects, the book is an apt successor to Synge's *Geometrical Optics and De Broglie Waves* of the same series of monographs. The variational method, ' perturbation characteristic functions ' and invariants are the basic tools. In all cases the establishment of an axial (unperturbed) ray is followed by the discussion of the paraxial (linear) approximation which is then improved upon by the calculation of aberrations or ' non-linear ' effects.

In this age of mechanization, it is gratifying to find that Sturrock has banished numerical drudgery from his calculations. By demonstrating the power of the analytical method, he has rescued the subject from being devoured wholesale by computing machines to whom orbit integrations are very digestible fare. Indeed, a problem would have to be of a very special and highly non-linear kind before Sturrock's perturbation methods failed and had to be complemented by computing effort. The successful handling of non-linear effects in accelerators in the last chapter of this book demonstrates the superiority of his methods.

He is able to generalize static electron-optical methods to the ' dynamic ' accelerator problem with such ease because, throughout, he observes relativistic accuracy—a comforting thought in all applications—so that time, to him, is " just another coordinate ". In fact, the only remaining distinction between ' static ' and ' dynamic ' electron optics lies in the different interpretations of the term ' focusing '. The book is not ' easy '. The arguments are condensed and the mathematics, although not beyond the range of an average physicist, is not ' elementary '. It therefore remains a specialists' book. One has the

feeling that a little expansion here and there would render the book readable to a wider public. Some changes in notation are called for : the letter ' p ' is used in too many senses, albeit in different type. Some of the formulae could be symmetrized : equations which are in principle covariant (especially the fundamental equations) are not manifestly so.

But these are minor criticisms which should not deter the serious student of the subject from reading this highly commendable book. O. B.

Thermodynamics and Physics of Matter. (Volume I of a Series on High Speed Aerodynamics and Jet Propulsion.) Edited by F. D. Rossini. (Oxford : University Press ; Princeton : University Press.) [Pp. xviii+812.] Price 100*s*. ($15.00).

High speed flight and propulsion have now advanced to a stage where the designer or research worker needs to understand and apply a very wide range of information, embracing applied mechanics, physics and chemistry. This situation has prompted an eminent American committee to begin the compilation of a comprehensive series of twelve volumes designed to present all the fundamental information conceivably needed by modern flight and propulsion engineers and, in the later volumes, to indicate its utility and application. This encyclopaedic aim has necessitated the division of not only the series but also each individual volume among serveral specialist authors. One danger of this arrangement is that the marshalling of the sections in logical order and with uniform notation without omissions or undue repetition may prove too difficult. On the whole the material has been well organized in the volume under review. Another danger is that the specialist authors may lack the space or the enthusiasm to treat their topic fully and instead refer the reader to publications elsewhere. When this happens, as it does occasionally in Volume I of the series, one begins to doubt the desirability of such compendious publications, since they are evidently not a substitute for specialist works. If space is at a premium in these volumes, the allotment of space to introductory elementary thermodynamics can only be attributed to the need to counteract the wide distribution of engineering thermodynamical texts which treat the subject in a form ill-suited to more advanced development. In contrast the sudden, if inevitable, introduction of statistical mechanics without preamble in the first section on thermodynamic fundamentals is not calculated to encourage the reader with the normal engineering background. A more thorough study of the implications of statistical mechanics occurs in later parts of the book.

There are comprehensive chapters on gaseous, liquid and solid state theory and on transfer processes and reaction rates in the fluid states, and a very detailed study of the behaviour of fluids near the critical point. It is obvious by this stage that the book is aimed at a wider public than workers on high speed flight and propulsion. The section by Beattie on the properties of real substances and mixtures will however prove invaluable to aerodynamicists and engineers. The relaxation phenomena important in severe shockwaves and elsewhere receive very adequate treatment. A section on gases of such low density that continuous fluid theory is inapplicable paves the way for aerodynamics at high altitude, presumably to be discussed in later volumes. The volume ends with a brief study of the thermodynamics of irreversible processes. Nearly all the chapters end abruptly and would have been improved by the addition of general remarks summarizing the important points and indicating their relevance to high speed flight and propulsion. J. A. S.

Spectroscopy at Radio and Microwave Frequencies. By D. J. E. Ingram. (London : Butterworths Scientific Publications.) [Pp. xii+332.] Price 45*s*.

Although spectroscopy at radio and microwave frequencies was almost unknown ten years ago, the subject has developed rapidly and this review of the main applications and techniques is welcome both to the research worker in the field and to the non-specialist who requires an idea of methods and possibilities.

After discussing the relation between microwave and ordinary spectroscopy and indicating the scope of the subject, the author devotes the first three chapters to the production and measurement of microwave power, frequency measurement, waveguide techniques, and the design and construction of different types of microwave spectroscope.

The following four chapters are concerned with the theory and the experimental results for the three main branches of the subject, gaseous microwave spectroscopy, paramagnetic resonance and radiofrequency spectroscopy. In each case the theory is stated in a clear and concise manner without detailed mathematical treatment and well illustrated by reference to the experimental results which are given in considerable detail.

The final chapter is devoted to a very useful discussion of the applications of microwave and radiofrequency spectroscopic techniques. The inclusion of these topics and the large number of references to original papers at the end of each chapter should make this book of considerable interest to those engaged in both pure and applied research. K. S.

ADDENDUM

Two omissions in the bibliography of " The Thermal Instability of a Fluid Sphere Heated Within ", *Phil. Mag.*, **46**, 1310, have come to the attention of its author. They are :

MALURKHAR, S. L., 1937, *Proc. Ind. Acad. Sci.*, **7**, No. 1, Sec. A.
JEFFREYS, H., and JEFFREYS, B. S., 1950, *Methods of Mathematical Physics* (Cambridge : University Press), p. 442.

ERRATUM

The Magnetic Susceptibilities of some Diamagnetic Alloys, by W. G. HENRY and J. L. ROGERS, 1956, *Phil. Mag.*, **1**, 246.

The denominator in eqn. (4.9) should read $4mc^2$ not $8mc^2$.